NACA TN 3030

# NATIONAL ADVISORY COMMITTEE
# FOR AERONAUTICS

**TECHNICAL NOTE 3030**

A METHOD FOR CALCULATING THE SUBSONIC STEADY-STATE

LOADING ON AN AIRPLANE WITH A WING OF ARBITRARY

PLAN FORM AND STIFFNESS

By W. L. Gray and K. M. Schenk

Boeing Airplane Company
Seattle, Wash.

NACA

Washington
December 1953

H

# CONTENTS

Page

NATIONAL ADVISORY COMMITTEE FOR AERONAUTICS

TECHNICAL NOTE 3030

A METHOD FOR CALCULATING THE SUBSONIC STEADY-STATE

LOADING ON AN AIRPLANE WITH A WING OF ARBITRARY

PLAN FORM AND STIFFNESS[1]

By W. L. Gray and K. M. Schenk

SUMMARY

A method for computing the steady-state span load distribution on
an elastic airplane wing for specified airplane weights and load factors
is given.  The method is based on a modification of the Weissinger
L-method and applies at subcritical Mach numbers.  It includes the
effects of external stores and fuselage on the spanwise loading.  Modi-
fications are outlined for treating tail-boom and tailless airplane con-
figurations and for calculating the divergence dynamic pressure of a
swept wing with a large external store.  A method is also outlined for
reducing wind-tunnel data to obtain effective aerodynamic coefficients
which are free of model flexibility effects.  The effects of Mach num-
ber can readily be evaluated from the aerodynamic coefficients thus
obtained.

INTRODUCTION

The inclusion of the effects of flexibility in the solution of the
spanwise airload distribution applied to a wing of arbitrary plan form
and stiffness distribution has increased the complexity of analysis over
that for a rigid wing.  The methods that are available at the present
time are generally concerned with the calculation of loading on an iso-
lated flexible wing rather than the more practical case not only where
the effects of fuselage and nacelles on the spanwise loading must be
taken into account but also where the total lift on each of the major
components must be considered simultaneously in order to determine the
wing loading at a specified load factor.  A method for including such
effects without recourse to iterative procedures for steady-state flight
conditions and subcritical Mach numbers is presented in this paper.  The

_____

[1]Based on Boeing Airplane Company Document No. D-10624, "A Matrix
Solution for the Subsonic Steady State Aeroelastic Loading on Airplanes"
by W. L. Gray and K. M. Schenk, June 1, 1951.  Acknowledgement is made
to Messrs. Paul W. Harper and John B. Garvin of the NACA for extensive
work in editing and revising this document.

equations are derived so that the spanwise airload distribution can be expressed in matrix form in terms of influence coefficients for aerodynamic induction and structural deflection in a manner similar to that employed in reference 1.

The basic method is outlined in the body of the paper. Included in appendixes are details of the various derivations, the expansion of the basic equations to include fuselage interference and store load effects, the modifications for tail-boom and tailless configurations, a method for determining divergence dynamic pressures for swept wings with large external stores, a method for reducing wind-tunnel data to obtain effective aerodynamic coefficients which are free of model flexibility effects, and a method for obtaining compressibility corrections.

## SYMBOLS

The following symbols appear in the body of this report. Additional symbols which appear only in the appendixes are defined as they are introduced.

| | |
|---|---|
| $b$ | wing span, in. |
| $C_{L_{F_0}}$ | fuselage lift coefficient in presence of wing at $\alpha_r = 0$, $L_F/qS$ |
| $C_{m_{F_0}}$ | fuselage pitching-moment coefficient about $\bar{c}/4$ point in presence of wing at $\alpha_r = 0$, $M_F/qS\bar{c}$ |
| $\left(C_{L_F}\right)_\alpha$ | rate of change of fuselage lift coefficient with $\alpha_r$, per radian |
| $\left(C_{m_F}\right)_\alpha$ | rate of change of fuselage pitching-moment coefficient with $\alpha_r$, per radian |
| $c$ | local chord parallel to plane of symmetry, in. |
| $\bar{c}$ | wing mean geometric chord, in. |
| $c_{m_0}$ | wing section pitching-moment coefficient |
| $EI$ | effective value of product of modulus of elasticity and wing section beam bending moment of inertia, lb-in.$^2$ |
| $GJ$ | effective value of product of shear modulus of elasticity and wing section polar moment of inertia, lb-in.$^2$ |

| | |
|---|---|
| $h$ | semispan of horseshoe vortex, in. |
| $I_X$ | airplane rolling moment of inertia, lb-in.$^2$ |
| $I_Y$ | airplane pitching moment of inertia, lb-in.$^2$ |
| $L_F$ | fuselage lift in presence of wing, $\left[C_{L_{F_0}} + \left(C_{L_F}\right)_\alpha \alpha_r\right] qS$, lb |
| $l$ | wing running lift per inch of span perpendicular to plane of symmetry, lb/in. |
| $M_F$ | fuselage pitching moment about $\bar{c}/4$ point in presence of wing, $\left[C_{m_{F_0}} + \left(C_{m_F}\right)_\alpha \alpha_r\right] qS\bar{c}$, in-lb |
| $M_X$ | airplane rolling moment, in-lb |
| $M_{X_{a_1}}$ | elastic-airplane rolling moment caused by unit aileron deflection, in-lb |
| $M_{X_{p_1}}$ | elastic-airplane damping moment in roll caused by unit wing-tip helix angle $(pb/2V)_1$, in-lb |
| $M_{X_{\dot{p}_1}}$ | elastic-airplane rolling moment caused by unit rolling angular acceleration acting on the wing distributed inertia, in-lb |
| $M_{X_{s_1}}$ | elastic-airplane rolling moment caused by unit spoiler deflection, in-lb |
| $m_0$ | two-dimensional lift-curve slope per radian, including compressibility effects, for sections parallel to plane of symmetry |
| $n$ | airplane load factor, positive when inertia loads are downward |
| $P_T$ | balancing tail load, positive upward, lb |
| $p$ | airplane rolling velocity, radians/sec |
| $\dot{p}$ | airplane rolling angular acceleration, radians/sec$^2$ |
| $q$ | dynamic pressure, lb/sq in., $\rho V^2/2$ |
| $r$ | radial distance from vortex core, in. |
| $S$ | wing area, sq in. |

$V$      true free-stream velocity, in./sec

$W$      airplane gross weight, lb

$w_r$      wash velocity induced by line vortex at perpendicular distance $r$ from vortex line, positive for downwash, in./sec

$\left(\dfrac{w}{V}\right)_{3c/4}$      downwash angle at three-quarter-chord point induced by vortex system representing wing and its spanwise lift distribution

$x$      streamwise distance from pitch reference axis to bound portion of horseshoe vortex, positive when vortex is to rear of pitch reference axis, in.

$\bar{x}$      streamwise distance from pitch reference axis to $\bar{c}/4$ line, positive when $\bar{c}/4$ line is to rear of pitch reference axis, in.

$x_A$      streamwise distance from pitch reference axis to airplane center of gravity, positive when center of gravity is to rear of pitch reference axis, in.

$x_T$      streamwise distance from pitch reference axis to center of pressure of balancing tail load, positive when center of pressure is to rear of pitch reference axis, in.

$y$      lateral distance from wing center line, in.

$\alpha_f$      final angle of attack of section zero-lift line with respect to local free-stream direction, $\alpha_r + \alpha_g + \alpha_s$, radians (see fig. 1)

$\alpha_g$      change in section angle of attack due to aerodynamic twists and due to all structural twists associated with a flexible wing which are not accounted for by the $\alpha_s$ term, radians (see fig. 1)

$\alpha_r$      angle of attack of root-section zero-lift line, radians (see fig. 1)

$\alpha_s$      change in section angle of attack due to wing lift distribution acting on a flexible wing $\left(\alpha_s = 0 \text{ for a rigid wing}\right)$, radians (see fig. 1)

$\Gamma$      strength of line vortex, in.$^2$/sec

$\delta_a$      aileron deflection, radians

$\delta_s$      spoiler deflection

$\eta$      dimensionless spanwise station, $y / \frac{b}{2}$

$\ddot{\theta}$      airplane pitching angular acceleration, positive for nose up, radians/sec$^2$

$\Lambda$      local sweep angle of elastic axis, radians

$\Lambda_M$      equivalent local sweep angle including compressibility effects, radians

$\rho$      mass density of ambient atmosphere, slugs/cu in. $\left( \rho = 0.114679 \times 10^{-6} \text{ lb-sec}^2/\text{in.}^4 \text{ at standard sea-level conditions} \right)$

Matrix notation:

$[\;\;]$      square matrix, elements of which are designated by use of subscripts; for example, element $a_{ij}$ is in ith row and jth column

$\lfloor\;\;\rfloor$      row matrix

$\{\;\;\}$      column matrix

$\begin{bmatrix} \cdot \\ \; \end{bmatrix}$      diagonal matrix, which is a square matrix in which all elements are zeros except those on the principal diagonal $a_{11}$, $a_{22}$, $a_{33}$, $\cdots a_{nn}$

$[S_1]$      aerodynamic-induction or downwash matrix in which elements $a_{ij}$ relate downwash angle at station $i$ to unit running lift at station $j$ on wing

$[S_2]$      elasticity matrix in which elements $a_{ij}$ relate changes in streamwise angle of attack at station $i$ to unit running lift at station $j$ on wing

$[\bar{S}_1]$      fuselage image-vortex matrix relating image downwash effects at station control points to unit running lifts (see appendix E)

$\begin{bmatrix} \cdot \\ \bar{S}_0 \end{bmatrix}$      fuselage "overvelocity" matrix (see appendix E)

$\left[\text{I}\right]$          identity matrix; that is, diagonal matrix in which
diagonal elements are equal to unity

## PRESENTATION OF METHOD

In this section of the report the basic equations necessary to the method are outlined and discussed in a general way.  Details of the derivations are contained in the various appendixes.

### Assumptions

In the development of the method certain assumptions that are common to airfoil theory apply, namely:

(1) The flow is potential; that is, boundary-layer effects, separation, and compressibility shocks are absent or negligible.

(2) The wing thickness is small.

(3) A stagnation point exists at the wing trailing edge.

(4) The angles of attack $\alpha$ are small so that $\tan \alpha \approx \sin \alpha \approx \alpha$ (where $\alpha$ is measured in radians) and $\cos \alpha \approx 1$.

(5) All drag-load effects except those due to nacelles and stores are neglected entirely in determining the deformations of the wing used in obtaining the equilibrium spanwise airload distribution.

With regard to the structure the following assumptions are made:

(1) Camber changes arising from twisting and bending of the wing are neglected entirely.

(2) The elastic twist of the control surface is the same as that of the adjoining wing structure.

(3) The angles of structural deflection $\theta$ are small so that $\tan \theta \approx \sin \theta \approx \theta$ (where $\theta$ is measured in radians) and $\cos \theta \approx 1$.

(4) Although the angle-of-attack changes, including those due to bending and torsional deformations of the wing, are accounted for in the determination of the equilibrium spanwise airload distribution on the wing, this final airload distribution is applied to the geometry of the undeflected wing in computing the bending and torsional moments.

## Basic Equations

*Symmetrical flight conditions.*- The fundamental problem involved is the development of a series of equations which relate the spanwise lift distribution for an arbitrary wing plan form in a given flight condition to the properties and attitudes of the individual sections that form the wing.

If the two-dimensional wing is considered first, the following relationships for lift and downwash behind an airfoil are available from most standard textbooks on aerodynamics:

$$l = \rho V \Gamma \tag{1}$$

$$l = m_0 \rho \alpha_f \frac{V^2}{2} c \tag{2}$$

$$w_r = \frac{\Gamma}{2\pi r} \tag{3}$$

The circulation $\Gamma$ is taken to be such that, at a specified distance $r$ behind the lifting line, the resultant of the downwash velocity $w_r$ and the flight velocity $V$ is parallel to the section zero-lift line; that is, no flow exists normal to the zero-lift line at this point. Then,

$$\frac{w_r}{V} = \alpha_f \tag{4}$$

and from equations (1) and (2),

$$\Gamma = m_0 \alpha_f \frac{V}{2} c \tag{5}$$

Substituting equation (5) into equation (3) results in

$$w_r = \frac{m_0}{2\pi} \frac{c/2}{r} \alpha_f V \tag{6}$$

or

$$\frac{w_r}{V} = \frac{m_0}{2\pi} \frac{c/2}{r} \alpha_r \qquad (7)$$

In order to satisfy equation (4), the expression $\frac{m_0}{2\pi} \frac{c/2}{r}$ in equation (7) must be equal to 1.0. Since the theoretical section two-dimensional lift-curve slope is equal to $2\pi$, $r$ must equal $c/2$, which is the distance between the lifting line and the three-quarter-chord point.

In the development of the method presented in this report, equation (7) is always used in the form

$$\left(\frac{w}{V}\right)_{3c/4} = \frac{m_0}{2\pi} \alpha_r \qquad (8)$$

This simplification requires that the section lift-curve slope $m_0$ be the two-dimensional value (i.e., the value of the lift-curve slope for an unswept two-dimensional wing) and that the location of the downwash control point $D$ (see fig. 2) be one-half of the local streamwise chord to the rear of the quarter-chord point, or at $3c/4$.

The essential difference between a two-dimensional wing and a wing of finite aspect ratio arises from the nonuniform spanwise loading which produces the trailing vortices of the finite-aspect-ratio wing. The equations presented thus far are considered to apply to the finite-aspect-ratio wing when the effects of all the vortices, both bound and trailing, have been taken into account.

Equation (8) in matrix form is

$$\left\{\frac{w}{V}\right\}_{3c/4} = \left[\overset{0}{\frac{m_0}{2\pi}}\right] \left\{\alpha_r\right\} \qquad (9)$$

This matrix relation represents a series of equations, each applicable to a particular station on the semispan of the wing. The values of $\left(\frac{w}{V}\right)_{3c/4}$, every one of which is affected by the bound and trailing

vortices at all of the wing stations, can be evaluated from

$$\left\{\frac{w}{V}\right\}_{3c/4} = \frac{1}{4\pi V}\left[S_1\right]\left\{\Gamma\right\}$$

which, in combination with equation (1), results in

$$\left\{\frac{w}{V}\right\}_{3c/4} = \frac{1}{8\pi q}\left[S_1\right]\left\{l\right\} \tag{10}$$

The $\left[S_1\right]$ matrix in these equations is the aerodynamic-induction or downwash matrix which is derived in appendix A.

Combining equations (9) and (10) gives

$$\left\{\frac{w}{V}\right\}_{3c/4} = \frac{1}{8\pi q}\left[S_1\right]\left\{l\right\} = \left[\overset{o}{\frac{m_o}{2\pi}}\right]\left\{\alpha_f\right\} \tag{11}$$

or

$$\left[\overset{o}{\frac{1}{4qm_o}}\right]\left[S_1\right]\left\{l\right\} = \left\{\alpha_f\right\} \tag{12}$$

The series of equations represented by the matrix equation (12) expresses, for any given dynamic pressure, the relationship between the spanwise variation of running lift $\left\{l\right\}$, the final section angles of attack $\left\{\alpha_f\right\}$, and the spanwise variation of the two-dimensional section lift-curve slope $\left[\overset{o}{m_o}\right]$. The effects of wing plan-form geometry are accounted for through the elements of the $\left[S_1\right]$ matrix. The section lift-curve slope is expressed in the general form $m_o$ rather than $2\pi$ to permit substitution of actual values when available from scaled-model tests or to permit correction for compressibility effects as described in appendix A.

The final angle-of-attack variation across the span $\{\alpha_f\}$ can be considered to be composed of three essential parts (see fig. 1)

$$\{\alpha_f\} = \{\alpha_r\} + \{\alpha_g\} + \{\alpha_s\} \tag{13}$$

For a wing free of external stores, the angle of attack $\{\alpha_s\}$ caused by structural deflection of a flexible wing due to the section lifts acting at the section aerodynamic centers is linearly related to the matrix $\{l\}$ by an expression derived in appendix B as

$$\{\alpha_s\} = [S_2]\{l\} \tag{14}$$

The wing geometry and stiffness are accounted for in the structural-deflection matrix $[S_2]$. This matrix is based on loadings associated with stations which are parallel to the airplane plane of symmetry. In a swept wing, however, the structure is usually arranged such that the wing boxes are formed between stations approximately perpendicular to the elastic axis. In order to obtain a closer representation of the loadings and deflections on this actual wing, an $[S_2{}']$ matrix was also derived (see appendix B) and may be substituted for the $[S_2]$ matrix in equation (14) when desirable.

The $\{\alpha_g\}$ matrix of equation (13), as described in detail in appendix C, is composed of built-in twist, apparent or aerodynamic twists such as those due to interference, control deflection, and angular velocities, and all structural twists of an elastic wing which are not accounted for in the $\{\alpha_s\}$ matrix.

Although equation (12) is perfectly general, it is not useful in the form given for determining the lift distribution on a flexible wing since a component of the $\{\alpha_f\}$ matrix is itself a function of the lift. If $\{\alpha_s\}$ is therefore expressed as in equation (14), equations (12)

and (13) may be combined so as to express the load distribution on a flexible wing in terms of wing root angle of attack and any combination of the $\{\alpha_g\}$ twists as

$$\left[\frac{\overset{\circ}{1}}{4qm_0}\right]\left[S_1\right]\{l\} = \{\alpha_r\} + \{\alpha_g\} + \left[S_2\right]\{l\} \tag{15}$$

or

$$\left[\left[\frac{\overset{\circ}{1}}{4qm_0}\right]\left[S_1\right] - \left[S_2\right]\right]\{l\} = \{\alpha_r\} + \{\alpha_g\} \tag{16}$$

Design conditions, however, are usually specified in terms of gross weight and load factor rather than root angle of attack. The inclusion of these two additional independent variables requires two additional equations. By considering that the airplane must be in equilibrium as regards vertical forces and pitching moments, the two additional equations may be written as

$$2\lfloor 2h \rfloor\{l\} + P_T - nW = 0 \tag{17}$$

for equilibrium of vertical forces and

$$-2\lfloor 2hx \rfloor\{l\} + 2q\lfloor 2hc^2 \rfloor\{c_{m_0}\} - P_T x_T + nW x_A = 0 \tag{18}$$

for equilibrium of pitching moments about the pitch axis.

Equations (16), (17), and (18) are the basic equations for a flexible-wing airplane. They may be solved simultaneously for $\{l\}$, $\alpha_r$, and $P_T$ as functions of any design values of speed, gross weight, and load factor. Equation (16) as written applies to symmetrical flight conditions, but by substitution of an antisymmetrical $\left[S_1\right]$ matrix (see appendix A) it is then applicable to unsymmetrical flight conditions which are considered in greater detail under the following section heading.

Equations (16), (17), and (18) can be altered as shown in the following paragraphs to include (a) the effects of forces on the fuselage, (b) the effects of external stores by the method derived in appendix D, and (c) the interference effects on the exposed-wing loading due to the presence of the fuselage by the method derived in appendix E.

In connection with forces on the fuselage (item (a)), the lift and moment characteristics of the fuselage in the presence of the wing are assumed to be known. The lift and pitching moment of the fuselage may then be written with small error as

$$L_F = qS \left[ C_{L_{F_0}} + \left( C_{L_F} \right)_\alpha \alpha_r \right] \tag{19}$$

$$M_F = qS\overline{c} \left[ C_{m_{F_0}} + \left( C_{m_F} \right)_\alpha \alpha_r \right] \tag{20}$$

in which fuselage up loads and nose-up moments are considered positive. This lift and moment may be appropriately included in equations (16), (17), and (18) to get the following more complete set of equations (see fig. 2):

For the wing load distribution,

$$\left[ \left[ \frac{1}{4qm_0} \right] \left[ S_1 \right] - \left[ S_2 \right] \right] \{l\} - \{\alpha_r\} + P_T\{0\} = \{\alpha_g\} \tag{21}$$

for the summation of vertical forces,

$$2 \lfloor 2h \rfloor \{l\} + qS \left( C_{L_F} \right)_\alpha \alpha_r + P_T = nW - qSC_{L_{F_0}} \tag{22}$$

and for the summation of pitching moments,

$$2\left|\frac{2hx}{x_T}\right|\{l\} + \frac{qS}{x_T}\left[\bar{x}\left(C_{L_F}\right)_\alpha - \bar{c}\left(C_{m_F}\right)_\alpha\right]\alpha_r + P_T =$$

$$nW\frac{x_A}{x_T} + 2q\left|\frac{2hc^2}{x_T}\right|\{c_{m_0}\} + \frac{qS}{x_T}\left(\bar{c}C_{m_{F_0}} - \bar{x}C_{L_{F_0}}\right) \tag{23}$$

The twist term $P_T\{0\}$ appearing in equation (21) has been included at this point to provide for the possibility that tail loads may enter the wing at some point along the span, as for a tail-boom type of configuration, for instance. This $P_T\{0\}$ contribution is otherwise considered to be zero. A method for handling the tail-boom type of airplane as well as the case of the tailless airplane is described in appendix F.

In considering the effects of the external stores (alteration (b)), as in the case of the fuselage, the lift and moment characteristics of the stores in the presence of the wing are assumed to be known so that the lift and moment can be given by expressions similar to equations (19) and (20) for the fuselage.

The lift-distribution equation for the store case derived in appendix D, with the $P_T$ term included as before for generality, is

$$\left[\left[[I] - qS[A]\right]\left[\frac{1}{4qm_0}\right][S_1] - [S_2]\right]\{l\} + P_T\{0\} - \{\alpha_r\} =$$

$$\{\alpha_g\} + qS\{B\} \tag{24}$$

in which the matrices $[A]$ and $\{B\}$ relate an $\alpha_g$ type of twist of the elastic wing to the store lift and moment. This twist is handled in two parts so that the part that varies with the span loading $\{l\}$ may be introduced on the left-hand side of the equation in a manner parallel to that for the $\left[S_2\right]$ matrix.

The vertical-force and pitching-moment equations (22) and (23) are modified to include store lift and moment in a manner similar to that in which the fuselage lift and moment were previously included. In the notation introduced in appendix D these equations for one or more stores become

$$\left[ 2 \lfloor 2h \rfloor + 2qS \left[ \sum \left( C_{L_{E_n}} \right)_\alpha \lfloor E_n \rfloor \right] \left[ \begin{smallmatrix} 0 \\ \frac{1}{4qm_0} \end{smallmatrix} \right] \left[ S_1 \right] \right] \{l\} +$$

$$qS \left( C_{L_F} \right)_\alpha \alpha_r + P_T = nW - qSC_{L_{F_0}} - 2qS \sum C_{L_{E_{0_n}}} \qquad (25)$$

for summation of vertical forces and

$$\left[ 2 \lfloor 2hx \rfloor + 2qS \left[ \sum x_n \left( C_{L_{E_n}} \right)_\alpha \lfloor E_n \rfloor - \sum \bar{c} \left( C_{m_{E_n}} \right)_\alpha \lfloor E_n \rfloor \right] \left[ \begin{smallmatrix} 0 \\ \frac{1}{4qm_0} \end{smallmatrix} \right] \left[ S_1 \right] \right] \{l\} +$$

$$qS\bar{x} \left( C_{L_F} \right)_\alpha \alpha_r - qS\bar{c} \left( C_{m_F} \right)_\alpha \alpha_r + P_T x_T = 2q \lfloor 2hc^2 \rfloor \{c_{m_0}\} -$$

$$2qS \left( \sum x_n C_{L_{E_{0_n}}} - \sum \bar{c} C_{m_{E_{0_n}}} \right) + qS \left( \bar{c} C_{m_{F_0}} - \bar{x} C_{L_{F_0}} \right) + nWx_A - I_Y\ddot{\theta} \qquad (26)$$

for summation of pitching moments. In these equations the subscript n is the store index which, for any particular configuration, has as many values as there are stores on the semispan. The matrix notation $\lfloor E_n \rfloor$ which gives the angle of attack of the store is defined in appendix D.

The third and final alteration (item (c)) to be considered in connection with equations (16), (17), and (18) is the change in span load distribution of the exposed wing due to the presence of the fuselage. This interference effect is derived in appendix E. The over-all fuselage-interference effect is considered to be composed of two parts. The first is that due to the image vortex system within the fuselage which is required to satisfy the condition of zero velocity normal to and at the fuselage surface. This condition is satisfied by adding a correcting

$[S_i]$ matrix (see appendix E) to the $[S_1]$ downwash matrix. The second part of the effect is the increment in vertical velocities over the exposed wing due to the presence of the fuselage at an angle of attack. This effect is calculated as an interference twist of the $\{\alpha_g\}$ type and is expressed as a function of fuselage angle of attack times the "overvelocity" matrix $\overset{o}{[S_o]}$. (See appendix E.) The lift distribution (eq. (21)) when altered to include these fuselage-interference effects becomes

$$\left[\left[\frac{1}{4qm_o}\right]\left[\overset{o}{[S_1]} + [S_i]\right] - [S_2]\right]\{l\} - \alpha_T\left[[I] + \overset{o}{[S_o]}\right]\{1\} + P_T\{0\} =$$

$$\{\alpha_g\} - \alpha_i\overset{o}{[S_o]}\{1\} \tag{27}$$

where the elements of the $\overset{o}{[S_o]}$ matrix give the increments in vertical velocities along the span.

The calculation of these fuselage effects would not be required if appropriate data were available from wind-tunnel tests of a scaled model of the subject airplane. A method of determining these and other aerodynamic twists as well as the applicable values of section lift-curve slope from appropriate wind-tunnel data is given in appendix G. The method utilizes equation (12) to obtain aerodynamic coefficients which are free of model wing flexibility effects and which are therefore applicable to the full-scale airplane having a wing flexibility different from that of the model.

Unsymmetrical flight conditions.- In addition to the symmetrical flight conditions already outlined, a number of unsymmetrical flight conditions are usually investigated in structural design. Among the conditions which may readily be investigated by the methods of this report are those which arise through the use of roll-producing devices such as ailerons or spoilers. The load distributions on an elastic wing associated with roll-control deflections may be thought of as the summation of distributions from the following specific loadings:

(1) The symmetrical or pre-roll loading which existed prior to the deflection of the roll-producing device.

(2) The incremental loading resulting from the deflection of the roll-producing device.

(3) The incremental loading associated with a constant rolling velocity with no roll-control deflection, which is usually described as the damping-in-roll loading.

(4) The incremental loading caused by the rolling angular acceleration. This loading results from the structural twists $\{\alpha_g\}$ of the elastic wing when the rolling acceleration $\dot{p}$ acts on the wing mass distribution (see appendix C). Note that the resulting aerodynamic rolling moment will generally be in the same direction as the applied rolling acceleration.

Three flight rolling conditions will be used to outline the procedure for determining unsymmetrical loadings on the wing. These rolling conditions are:

(a) Steady roll at some specified value of wing-tip helix angle $pb/2V$ with no rolling acceleration

(b) Roll initiation resulting from the instantaneous deflection of the roll-control device to the angle required to obtain the specified value of $pb/2V$ but with no rolling velocity

(c) Roll termination, that is, control surfaces deflected in opposition to the steady rolling velocity $pb/2V$

Steady roll: In a steady-roll condition the span load distribution for the elastic wing is given by the summation of the first three loadings enumerated.

The distribution obtained for the first, or pre-roll, loading is described in detail in the section "Symmetrical flight conditions." Equations (16), (17), and (18) or their appropriate equivalents are used together with the symmetrical $[S_1]$ matrix of appendix A.

The distribution of loading and its associated rolling moment $M_{X_{a_1}}$ or $M_{X_{s_1}}$ resulting from a unit antisymmetrical deflection $\delta_{a_1}$ or $\delta_{s_1}$ of the roll-control device are obtained from equation (16), the antisymmetrical matrix $[S_1]$ of appendix A, and the appropriate $\{\alpha_g\}$ matrices which give the aerodynamic and structural twists resulting from a unit deflection of the roll-control device. These $\{\alpha_g\}$ matrices can be written in terms of control-surface deflection by the method described in appendix F or by means of data from wind-tunnel tests, if available.

Similarly, the distribution of loading and the damping moment $M_{X_{p_1}}$ associated with a unit value of the wing-tip helix angle $(pb/2V)_1$ are obtained from equation (16) and the antisymmetrical $\begin{bmatrix} S_1 \end{bmatrix}$ matrix. The $\{\alpha_g\}$ values in this case vary linearly and antisymmetrically across the span from $(pb/2V)_1$ at one tip to $-(pb/2V)_1$ at the other.

These unit load distributions associated with $\delta_{a_1}$ or $\delta_{s_1}$ and $(pb/2V)_1$ must then be scaled up or down according to the amount of control deflection $\delta_a$ or $\delta_s$ required to give the desired value of $pb/2V$. The deflection required is obtained from the equation of equilibrium of the airplane in roll as

$$\delta_a \frac{M_{X_{a_1}}}{\delta_{a_1}} = \frac{pb}{2V} \frac{M_{X_{p_1}}}{(pb/2V)_1} \tag{28a}$$

or

$$\delta_s \frac{M_{X_{s_1}}}{\delta_{s_1}} = \frac{pb}{2V} \frac{M_{X_{p_1}}}{(pb/2V)_1} \tag{28b}$$

where the rolling moment produced by the control deflection balances the rolling moment due to damping in roll in the steady specified rolling condition.

After the unit load distributions have been scaled in the manner just described, they may be added to the pre-roll loading to obtain the load distribution for the specified steady-roll condition.

In this outline the assumption of equal and opposite roll-control deflections is made. If, as is more generally the case, unequal deflections of the ailerons or spoilers are involved, the span loading must be determined in a slightly different way. To illustrate the procedure, a spoiler deflection on only one wing may be considered to be equivalent to a symmetrical and an antisymmetrical deflection with an amplitude

equal to half of the spoiler deflection $\delta_s/2$. The antisymmetrical deflection results in a gain in lift on one wing which is exactly balanced by a loss in lift on the other wing so that a rolling moment is produced without a change in the over-all wing lift. The symmetrical deflection, however, results in a change in total wing lift, and hence load factor, with no rolling moment. In order to compensate for this change, both the vertical-force and the pitching-moment balance equations must be introduced so that the wing load distribution associated with the change in $\alpha_r$ required to compensate for the change in tail load can be determined. Adding the symmetrical and unsymmetrical loading distributions will give the proper lift distribution for the wing with a single spoiler deflection $\delta_s$.

Differentially operated ailerons might be considered in a manner similar to that outlined for the spoiler. A further extension to include the combined deflection of both ailerons and spoilers can also be made in the same way by making use of the proper spoiler-to-aileron gearing ratio.

Roll initiation: In the roll-initiation condition where no rolling velocity is assumed to exist, all the listed loadings occur except that due to damping in roll.

Since the control deflection ($\delta_a$ or $\delta_s$) will already be known from the steady-roll condition, the problem is to determine the initial rolling angular acceleration $\dot{p}$ for instantaneous control deflection. The procedure involved is first to find the wing spanwise airload distribution and its rolling moment $M_{X_{\dot{p}_1}}$ due to a unit rolling angular acceleration $\dot{p}_1$. The values of $M_{X_{\dot{p}_1}}$ depend on the wing mass and stiffness distributions as well as wing aerodynamics. The values are obtained from equation (16), or its equivalent, for antisymmetric flight. With the value of $M_{X_{\dot{p}_1}}$ known, the desired angular acceleration $\dot{p}$ is then found by solving the following equation of motion for the airplane in roll:

$$\dot{p} = \frac{\delta_a \dfrac{M_{X_{a_1}}}{\delta_{a_1}}}{\dfrac{I_X}{386.4} - \dfrac{M_{X_{\dot{p}_1}}}{\dot{p}_1}} \tag{29a}$$

or

$$\dot{p} = \frac{\delta_s \dfrac{M_{X_{s_1}}}{\delta_{s_1}}}{\dfrac{I_X}{386.4} - \dfrac{M_{X_{\dot{p}_1}}}{\dot{p}_1}} \tag{29b}$$

where the moments are given in inch-pounds. The value of $\dot{p}$ obtained from equation (29) is then used to scale the loadings previously found for the unit rolling acceleration to the correct value.

Roll termination: In the roll-termination condition, the airplane is assumed to be rolling with a wing-tip helix angle $pb/2V$ and the roll-control device is moved abruptly in a direction such as to reduce the rolling velocity to zero. As in the roll-initiation condition, the desired airplane rolling acceleration is obtained from the equation expressing the equilibrium of the airload and inertia-load rolling moments, which for aileron control is

$$\dot{p} = \frac{\delta_a \dfrac{M_{X_{a_1}}}{\delta_{a_1}} + \dfrac{pb}{2V} \dfrac{M_{X_{p_1}}}{(pb/2V)_1}}{\dfrac{I_X}{386.4} - \dfrac{M_{X_{\dot{p}_1}}}{\dot{p}_1}}$$

The airloads on the wing are those caused by the pre-roll condition plus the airloads from aileron deflection, damping in roll, and rolling acceleration. The inertia loads are those arising from the pre-roll condition plus the effects of the rolling acceleration $\dot{p}$.

## DISCUSSION

The method outlined in this report not only includes several previously omitted items which are of practical interest in the design of a wing for aeroelastic effects but also is sufficiently extensive in scope that almost any type of airplane configuration may be considered. Because of its length, however, the method is better adapted to the determination of loads on a specific airplane rather than to preliminary design studies of several configurations.

Matrix formulation of the problem has particular merit for such a general treatment since discontinuities in angles or masses due to either special aerodynamic or structural features can readily be included. It also permits future improvements to be made to the details of the separate appendixes without essentially modifying the method which has been outlined. In fact, throughout the paper it is possible that the engineer would modify the method to suit his own needs and draw from the appendixes whatever material would be required to investigate the problem at hand. In such a modification he would of necessity consider the relative merits of ease in computation against the accuracy both of the method and of the data available.

For these reasons, only a few general guides which might be considered for successful application of the method are given.

For $m_0$ equal to $2\pi$, equation (12) will give essentially the same results as those given by the Weissinger L-method of reference 2 which is valid for wings of arbitrary plan form and having flat-plate, circular-arc, or parabolically cambered airfoil sections (refs. 3, 4, and 5). The method would be expected to give the most accurate results when applicable values of $m_0$ are known, such as those obtainable by the method of appendix G for instance, since in general the fuselage, flaps, and external stores will affect the applicable values of $m_0$. In fact, equivalent values of any of the aerodynamic parameters as obtained from experimental data by the method of appendix G are preferable to purely theoretical values and may easily be incorporated.

The treatment of compressibility effects used in this report, wherein each wing section is permitted to have its own compressibility correction, differs from the Prandtl-Glauert method in that the wing plan form is not distorted; instead, the angles of attack are altered as indicated by equation (11). The treatment adopted has the merit of considerable saving in time for equal or better accuracy since only one $[S_1]$ matrix is required for all Mach numbers. The methods of obtaining compressible values of $m_0$ are described in appendixes A and G.

With regard to the number and selection of the horseshoe vortices to be used to represent span loading, it is suggested that the horseshoes be chosen narrower over that portion of the span where large gradients in loading are expected, that is, near the ends of control surfaces, near large changes in sweep, and at the wing tips. At least two vortices should be used with each control surface and a minimum of seven per semispan is suggested for a "clean" wing.

With regard to the structural parameters $EI$ and $GJ$ required, it may be stated that equivalent values which include the stiffnesses contributed by the leading- and trailing-edge structure should be used in preference to the usually conservative values employed in the structural analysis of the wing for shear and bending stresses.

In the design of a simple wing-fuselage combination without external stores or nacelles, it is necessary to study and apply the results of only appendixes A, B, C, and E which describe the $[S_1]$, $[S_2]$, and $\{\alpha_g\}$ matrices as well as the fuselage-interference effects. Effects of store and nacelle loads and moments on the wing load distribution are covered in appendix D. Appendix F outlines the modifications required to adapt the method to the determination of wing loads on flexible tailless and tail-boom airplane configurations. Appendix G indicates a procedure for obtaining equivalent values of section lift-curve slopes, effective compressible section sweep angles, and interference twists from wind-tunnel tests of models which may not be scaled correctly for flexibility. Appendix H deals with the determination of the divergence dynamic pressure of a swept-wing airplane with a large external store. The problem of divergence normally does not occur with a swept wing except that the attachment of a large external store may cause it to diverge. The determination of the divergence dynamic pressure is the only case in this paper which requires iterative procedures.


Boeing Airplane Company,
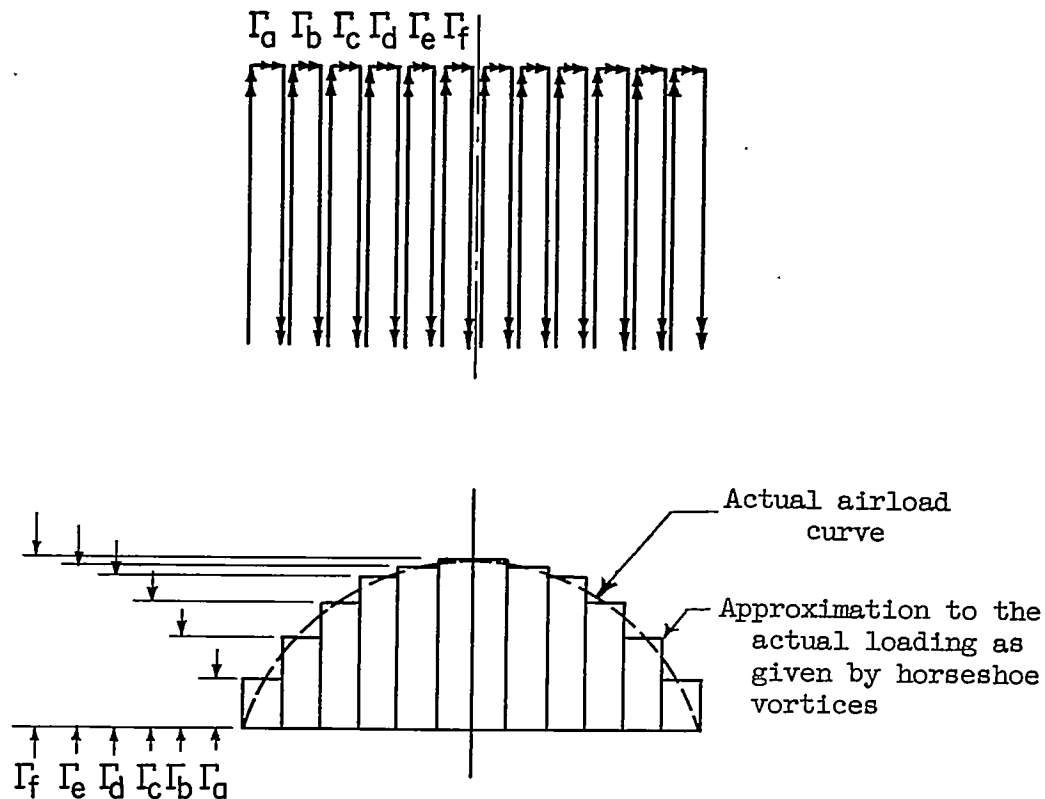      Seattle, Wash., July 8, 1953.

# APPENDIX A

## AERODYNAMIC FUNDAMENTALS

### The $\begin{bmatrix} S_1 \end{bmatrix}$ Matrix

The purpose of this appendix is to explain, in simplified form, the aerodynamics involved in and the steps necessary for the computation of the downwash matrix $\begin{bmatrix} S_1 \end{bmatrix}$ and to develop the correction for compressibility used in this report.

The lift or circulation distribution which varies along the span of a wing can be visualized as resulting from a system of horseshoe vortices, each of which is of constant strength. Such a system of horseshoes is illustrated in the following sketches, in which double arrows are used to indicate that the sense of circulation around each line-vortex segment is given by the right-hand rule:

$$\Gamma_a \ \Gamma_b \ \Gamma_c \ \Gamma_d \ \Gamma_e \ \Gamma_f$$

Actual airload
curve

Approximation to the
actual loading as
given by horseshoe
vortices

$$\Gamma_f \ \Gamma_e \ \Gamma_d \ \Gamma_c \Gamma_b \ \Gamma_a$$

It is obvious from the sketches that the shape of the actual load
distribution may be approximated to any practical degree of accuracy by
a suitable change in the number of horseshoes, each of constant strength.
The point of importance is that the net strength of the trailing vortex
at any point on the span of the wing is numerically equal to the rate
of change of strength of the bound vortex in the spanwise direction.
The strength of the trailing vortices would therefore be greater for
those portions of the wing span over which the more rapid changes in
the spanwise airload distribution occur.

Results of theoretical investigations have shown that little loss
in accuracy with respect to the spanwise airload distribution will be
entailed if:

(1) The total strength of the chordwise system of bound vortices
is concentrated in one bound vortex located at the local streamwise
quarter-chord point.

(2) The downwash angle at each vortex station across the span of
the wing, at a point one-half of the local streamwise chord downstream
of the bound vortex, is equal to the geometric angle of attack. Herein-
after, this point is referred to as the downwash control point D.

The downwash angle at any such control point D is therefore the
total induced downwash velocity at that point, normal to the plane of
the wing and caused by the complete system of bound and trailing vortices,
divided by the flight velocity of the wing.

It should be mentioned that the condition described in paragraph (2)
is true as written only for airfoils having a two-dimensional lift-curve
slope equal to $2\pi$. As is discussed in a subsequent section of this
appendix, the condition described in paragraph (2) is modified to the
following form when the section two-dimensional lift-curve slope is
different from $2\pi$:

$$\left(\frac{w}{V}\right)_{3c/4} = \frac{m_0}{2\pi}\,\alpha_f \qquad\qquad (A1)$$

The downwash velocity at a point due to a single horseshoe which
is composed of a bound vortex and its associated pair of trailing vortices
is known to be proportional to the strength of the circulation of that
horseshoe and, therefore, proportional to the running lift on that por-
tion of wing span represented by the bound vortex of that horseshoe. The
downwash angle at any one downwash control point thus is the sum of the
incremental downwash angles due to each of the horseshoes in the system
of horseshoes which represent the wing and its lift distribution.

Within the limitations which accrue from the use of a limited number
of horseshoe vortices to represent a wing, the elements with which to
solve the following problem are now available:

Given the geometry of a wing plan form, the angle-of-attack varia-
tion, and the section two-dimensional lift-curve-slope variation across
the span, determine the spanwise airload distribution. The unknowns
are, of course, the values of the running lift at each of several points
on the span. A necessary condition to the determination of these unknowns
is that as many independent equations be available as there are unknowns.
This condition can be fulfilled if the angle of attack is known at each
of the wing stations for which the loading is to be determined.

It is obvious that, if the strength of each bound vortex represents
the average airload over its own portion of the wing span, good accuracy
will be obtained if the values of the running load, as determined from
the solution of the simultaneous equations, are considered to be valid
at the midspan point of each bound vortex. The shape and distribution
of the continuously varying airload curve is then obtained by fairing
a curve through all of the points thus obtained, with the restriction
that the loading must drop to zero at the wing tip.

The method for determining the $\begin{bmatrix} S_1 \end{bmatrix}$ matrix is now illustrated for
a typical wing shown in the following sketch, which includes a system
of horseshoe vortices and associated downwash control points:
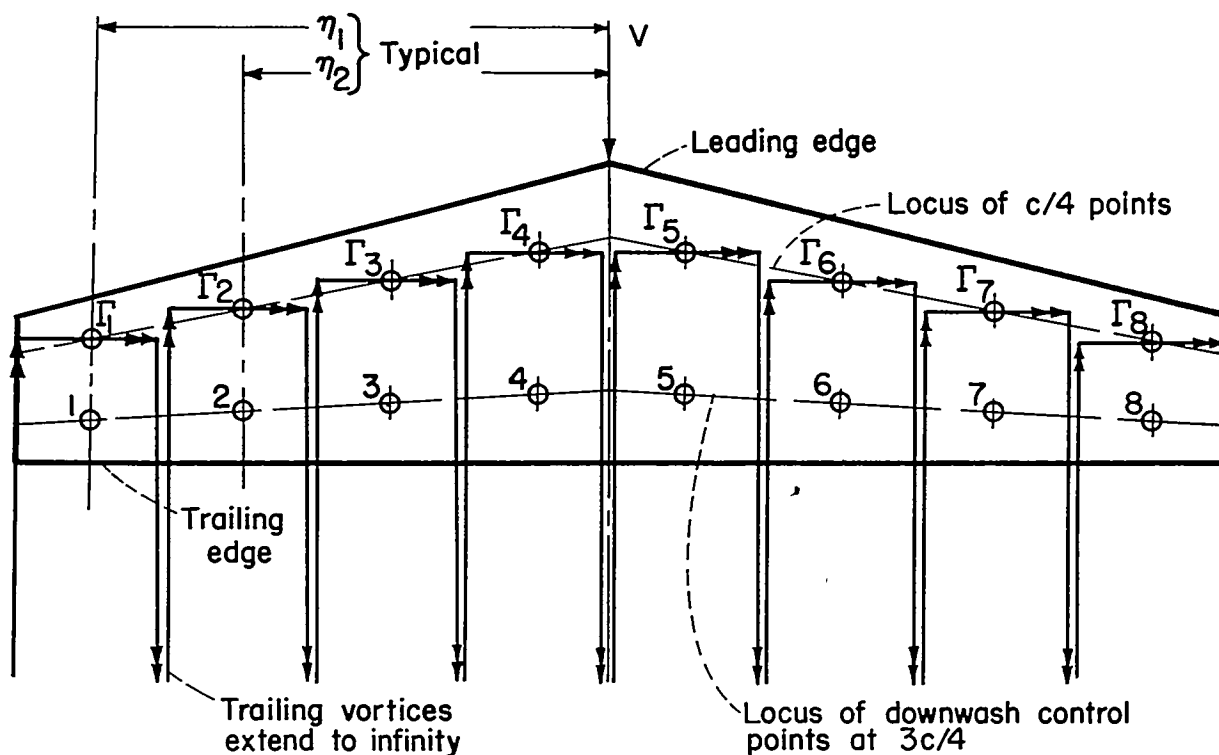
In actual practice it will usually be necessary to use a larger number of horseshoes to represent the wing. Four per semispan are used in the following presentation for convenience only. The following typical information is available at each spanwise station:

The section lift-curve slopes (in two-dimensional flow) at stations $\eta = \eta_1,\ \eta_2,\ \ldots$ are $m_0 = m_1,\ m_2,\ \ldots$. The angles of attack of the section zero-lift line at stations $\eta = \eta_1,\ \eta_2,\ \ldots$ are $\alpha_f = \alpha_1,\ \alpha_2,\ \ldots$.

Since a linear relationship exists between the strength $\Gamma_j$ of a particular horseshoe vortex $j$ and the downwash velocity $w_{ij}$ at a particular point $i$ on the wing plan form due to that horseshoe vortex, the following general equation can be written:

$$w_{ij} = K_{ij}\Gamma_j \tag{A2}$$

where $K$ is a constant. A particular horseshoe vortex, such as $\Gamma_1$, then causes the following values of downwash velocity at control points 1 to 8:

$$
\left.
\begin{aligned}
w_{11} &= K_{11}\Gamma_1 & w_{51} &= K_{51}\Gamma_1 \\
w_{21} &= K_{21}\Gamma_1 & w_{61} &= K_{61}\Gamma_1 \\
w_{31} &= K_{31}\Gamma_1 & w_{71} &= K_{71}\Gamma_1 \\
w_{41} &= K_{41}\Gamma_1 & w_{81} &= K_{81}\Gamma_1
\end{aligned}
\right\} \tag{A3}
$$

Similar relationships exist between $\Gamma_2,\ \Gamma_3,\ \ldots\ \Gamma_8$ and the control points 1 to 8, that is,

$$
\left.
\begin{aligned}
w_{12} &= K_{12}\Gamma_2 & w_{22} &= K_{22}\Gamma_2 & \ldots & & w_{82} &= K_{82}\Gamma_2 \\
w_{13} &= K_{13}\Gamma_3 & w_{23} &= K_{23}\Gamma_3 & \ldots & & w_{83} &= K_{83}\Gamma_3 \\
\ldots & & \ldots & & \ldots & & \ldots & \\
w_{18} &= K_{18}\Gamma_8 & w_{28} &= K_{28}\Gamma_8 & \ldots & & w_{88} &= K_{88}\Gamma_8
\end{aligned}
\right\} \tag{A4}
$$

If the horseshoes are symmetrical with respect to the center line of the wing plan form, the following values of $K$ are equal for the typical wing sketched:

$$
\begin{array}{llll}
K_{11} = K_{88} & K_{12} = K_{87} & K_{13} = K_{86} & K_{14} = K_{85} \\[2ex]
K_{21} = K_{78} & K_{22} = K_{77} & K_{23} = K_{76} & K_{24} = K_{75} \\[2ex]
K_{31} = K_{68} & K_{32} = K_{67} & K_{33} = K_{66} & K_{34} = K_{65} \\[2ex]
K_{41} = K_{58} & K_{42} = K_{57} & K_{43} = K_{56} & K_{44} = K_{55} \\[2ex]
K_{51} = K_{48} & K_{52} = K_{47} & K_{53} = K_{46} & K_{54} = K_{45} \\[2ex]
K_{61} = K_{38} & K_{62} = K_{37} & K_{63} = K_{36} & K_{64} = K_{35} \\[2ex]
K_{71} = K_{28} & K_{72} = K_{27} & K_{73} = K_{26} & K_{74} = K_{25} \\[2ex]
K_{81} = K_{18} & K_{82} = K_{17} & K_{83} = K_{16} & K_{84} = K_{15}
\end{array} \tag{A5}
$$

Further, for symmetrical wing plan forms at zero yaw it is always possible to obtain a spanwise airload distribution which is unsymmetrical with respect to the plan-form center line as the sum of two airload distributions, one of which is symmetrical and the other of which is antisymmetrical with respect to the plan-form center line; for example,
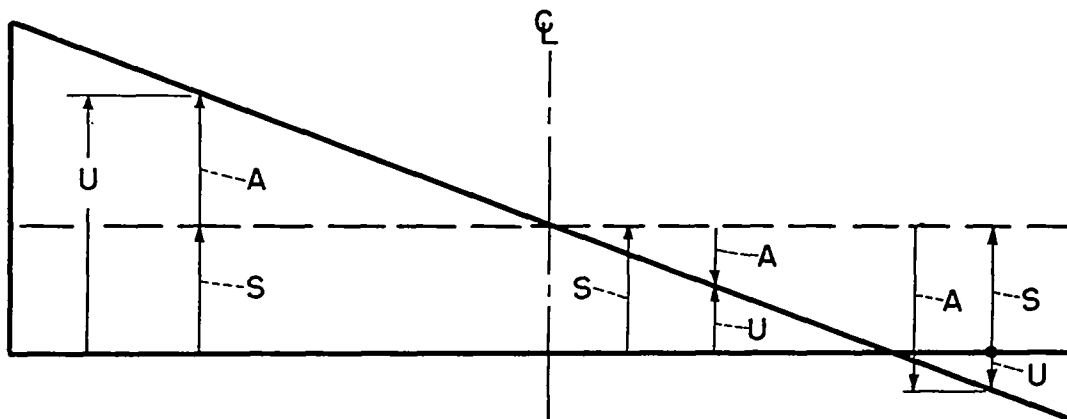
At each spanwise station the  S  component is that due to the symmetrical distribution of load, the  A  component is that due to the antisymmetrical distribution, and the  U  component represents the algebraic sum of the S  and  A  components, that is, the unsymmetrical distribution of load across the span.  This division offers a considerable reduction in the amount of work required in that, for either symmetrical or unsymmetrical flight conditions, airload distributions need be determined on only one-half of the wing, provided, of course, that proper account is taken of the sign of the circulations existing over the other half of the wing.

For a symmetrical distribution of airload over the span

$$\left.\begin{array}{ll} \Gamma_1 = \Gamma_8 & \Gamma_3 = \Gamma_6 \\ \\ \Gamma_2 = \Gamma_7 & \Gamma_4 = \Gamma_5 \end{array}\right\} \tag{A6}$$

and for an antisymmetrical distribution of airload

$$\left.\begin{array}{ll} \Gamma_1 = -\Gamma_8 & \Gamma_3 = -\Gamma_6 \\ \\ \Gamma_2 = -\Gamma_7 & \Gamma_4 = -\Gamma_5 \end{array}\right\} \tag{A7}$$

The total downwash velocity at any control point is the sum of the downwash-velocity contributions at that point that are induced by each of the horseshoe vortices in the system that represents the wing; that is,

$$\left.\begin{array}{l} w_1 = w_{11} + w_{12} + w_{13} + w_{14} + w_{15} + w_{16} + w_{17} + w_{18} \\ \\ w_2 = w_{21} + w_{22} + w_{23} + w_{24} + w_{25} + w_{26} + w_{27} + w_{28} \\ \\ \qquad \cdot \qquad\quad \cdot \qquad \cdot\cdot \qquad\quad \cdot \qquad\quad \cdot \end{array}\right\} \tag{A8}$$

If the equation for the downwash velocity at control point 1 is expanded as an example, the result is

$$w_1 = K_{11}\Gamma_1 + K_{12}\Gamma_2 + K_{13}\Gamma_3 + K_{14}\Gamma_4 + K_{15}\Gamma_5 + K_{16}\Gamma_6 +$$

$$K_{17}\Gamma_7 + K_{18}\Gamma_8 \tag{A9}$$

Alternatively, by use of the relations in equation (A5), equation (A9) can be written as

$$w_1 = K_{11}\Gamma_1 + K_{12}\Gamma_2 + K_{13}\Gamma_3 + K_{14}\Gamma_4 + K_{84}\Gamma_5 + K_{83}\Gamma_6 +$$

$$K_{82}\Gamma_7 + K_{81}\Gamma_8 \tag{A10}$$

In case a symmetrical airload condition is being investigated, substituting equations (A6) into equation (A9) results in

$$w_{1_S} = \Gamma_1(K_{11} + K_{18}) + \Gamma_2(K_{12} + K_{17}) + \Gamma_3(K_{13} + K_{16}) +$$

$$\Gamma_4(K_{14} + K_{15}) \tag{A11}$$

For an antisymmetrical airload distribution, substituting equations (A7) into equation (A9) results in

$$w_{1_A} = \Gamma_1(K_{11} - K_{18}) + \Gamma_2(K_{12} - K_{17}) + \Gamma_3(K_{13} - K_{16}) +$$

$$\Gamma_4(K_{14} - K_{15}) \tag{A12}$$

For the typical horseshoe system assumed, the complete series of equations relating downwash velocities to the circulations are:

For a symmetrical airload distribution,

$$
\begin{aligned}
w_{1_S} &= \Gamma_1\left(K_{11} + K_{18}\right) + \Gamma_2\left(K_{12} + K_{17}\right) + \Gamma_3\left(K_{13} + K_{16}\right) + \\
&\quad \Gamma_4\left(K_{14} + K_{15}\right) \\[6pt]
w_{2_S} &= \Gamma_1\left(K_{21} + K_{28}\right) + \Gamma_2\left(K_{22} + K_{27}\right) + \Gamma_3\left(K_{23} + K_{26}\right) + \\
&\quad \Gamma_4\left(K_{24} + K_{25}\right) \\[6pt]
w_{3_S} &= \Gamma_1\left(K_{31} + K_{38}\right) + \Gamma_2\left(K_{32} + K_{37}\right) + \Gamma_3\left(K_{33} + K_{36}\right) + \\
&\quad \Gamma_4\left(K_{34} + K_{35}\right) \\[6pt]
w_{4_S} &= \Gamma_1\left(K_{41} + K_{48}\right) + \Gamma_2\left(K_{42} + K_{47}\right) + \Gamma_3\left(K_{43} + K_{46}\right) + \\
&\quad \Gamma_4\left(K_{44} + K_{45}\right)
\end{aligned}
\right\} \tag{A13}
$$

and for an antisymmetrical airload distribution,

$$
\begin{aligned}
w_{1_A} &= \Gamma_1\left(K_{11} - K_{18}\right) + \Gamma_2\left(K_{12} - K_{17}\right) + \Gamma_3\left(K_{13} - K_{16}\right) + \\
&\quad \Gamma_4\left(K_{14} - K_{15}\right) \\[6pt]
w_{2_A} &= \Gamma_1\left(K_{21} - K_{28}\right) + \Gamma_2\left(K_{22} - K_{27}\right) + \Gamma_3\left(K_{23} - K_{26}\right) + \\
&\quad \Gamma_4\left(K_{24} - K_{25}\right) \\[6pt]
w_{3_A} &= \Gamma_1\left(K_{31} - K_{38}\right) + \Gamma_2\left(K_{32} - K_{37}\right) + \Gamma_3\left(K_{33} - K_{36}\right) + \\
&\quad \Gamma_4\left(K_{34} - K_{35}\right) \\[6pt]
w_{4_A} &= \Gamma_1\left(K_{41} - K_{48}\right) + \Gamma_2\left(K_{42} - K_{47}\right) + \Gamma_3\left(K_{43} - K_{46}\right) + \\
&\quad \Gamma_4\left(K_{44} - K_{45}\right)
\end{aligned}
\right\} \tag{A14}
$$

From equation (A1), which expresses the relationship that must exist between the downwash angle $w/V$ at each control point, the wing angle of attack $\alpha_f$, and the section lift-curve slope $m_o$ for the wing station at the control point, the following series of equations result, where, typically, $w_1$ represents either $w_{1_S}$ or $w_{1_A}$:

$$\left.\begin{aligned}
\frac{w_1}{V} &= \frac{m_1\alpha_1}{2\pi} & \frac{w_3}{V} &= \frac{m_3\alpha_3}{2\pi} \\[2em]
\frac{w_2}{V} &= \frac{m_2\alpha_2}{2\pi} & \frac{w_4}{V} &= \frac{m_4\alpha_4}{2\pi}
\end{aligned}\right\} \qquad (A15).$$

If

$$k_{11} = 4\pi\left(K_{11} \pm K_{18}\right)$$

$$k_{12} = 4\pi\left(K_{12} \pm K_{17}\right)$$

$$\cdot \quad \cdot \quad \cdot \quad \cdot \quad \cdot$$

$$k_{44} = 4\pi\left(K_{44} \pm K_{45}\right)$$

or

$$k = 4\pi\left(K_L \pm K_R\right) \qquad (A16)$$

where the upper sign is used for symmetrical airloads, the lower sign is used for antisymmetrical airloads, and the subscripts $L$ and $R$ in equation (A16) mean left and right wing, respectively, then substitution of equation (A16) into equations (A14) gives

$$\left.\begin{aligned}
4\pi w_1 &= k_{11}\Gamma_1 + k_{12}\Gamma_2 + k_{13}\Gamma_3 + k_{14}\Gamma_4 \\[1em]
4\pi w_2 &= k_{21}\Gamma_1 + k_{22}\Gamma_2 + k_{23}\Gamma_3 + k_{24}\Gamma_4 \\[1em]
4\pi w_3 &= k_{31}\Gamma_1 + k_{32}\Gamma_2 + k_{33}\Gamma_3 + k_{34}\Gamma_4 \\[1em]
4\pi w_4 &= k_{41}\Gamma_1 + k_{42}\Gamma_2 + k_{43}\Gamma_3 + k_{44}\Gamma_4
\end{aligned}\right\} \qquad (A17)$$

The relation between the running load $l$ and the circulation is

$$\left.\begin{array}{l} l_1 = \rho V \Gamma_1 \\[20pt] l_2 = \rho V \Gamma_2 \\[20pt] l_3 = \rho V \Gamma_3 \\[20pt] l_4 = \rho V \Gamma_4 \end{array}\right\} \qquad\qquad \text{(A18)}$$

and the equation relating dynamic pressure to mass density and true airspeed is

$$q = \rho V^2/2 \qquad\qquad \text{(A19)}$$

Equations (A15), (A17), (A18), and (A19) may be combined to give the following final system of linear equations:

$$\left.\begin{array}{l} k_{11}l_1 + k_{12}l_2 + k_{13}l_3 + k_{14}l_4 = 4qm_1\alpha_1 \\[24pt] k_{21}l_1 + k_{22}l_2 + k_{23}l_3 + k_{24}l_4 = 4qm_2\alpha_2 \\[24pt] k_{31}l_1 + k_{32}l_2 + k_{33}l_3 + k_{34}l_4 = 4qm_3\alpha_3 \\[24pt] k_{41}l_1 + k_{42}l_2 + k_{43}l_3 + k_{44}l_4 = 4qm_4\alpha_4 \end{array}\right\} \qquad \text{(A20)}$$

Equations (A20) can now be written in matrix form.  The equation for each station can be written as

$$
\left.
\begin{aligned}
\sum_{j=1}^{4} k_{1j} l_j &= 4qm_1\alpha_1 \\[2em]
\sum_{j=1}^{4} k_{2j} l_j &= 4qm_2\alpha_2 \\[2em]
\sum_{j=1}^{4} k_{3j} l_j &= 4qm_3\alpha_3 \\[2em]
\sum_{j=1}^{4} k_{4j} l_j &= 4qm_4\alpha_4
\end{aligned}
\right\} \tag{A21}
$$

Equations (A21) and therefore equations (A20) can be expressed in the general form

$$
\sum_{j=1}^{n} k_{ij} l_j = 4qm_i\alpha_i \qquad (i = 1, 2, 3, \ldots n) \tag{A22}
$$

In matrix notation equation (A22) becomes

$$
\left[ S_1 \right] \{ l \} = \left[ \overset{\circ}{4qm_0} \right] \{ \alpha_f \} \tag{A23}
$$

where

$$
\left[ S_1 \right] =
\begin{bmatrix}
k_{11} & k_{12} & k_{13} & k_{14} \\
k_{21} & k_{22} & k_{23} & k_{24} \\
k_{31} & k_{32} & k_{33} & k_{34} \\
k_{41} & k_{42} & k_{43} & k_{44}
\end{bmatrix}
\tag{A24}
$$

$$\{\imath\} = \begin{Bmatrix} \imath_1 \\ \imath_2 \\ \imath_3 \\ \imath_4 \end{Bmatrix} \tag{A25}$$

and

$$\left[4qm_0\right]\overset{o}{}\{\alpha_f\} = \begin{Bmatrix} 4qm_1\alpha_1 \\ 4qm_2\alpha_2 \\ 4qm_3\alpha_3 \\ 4qm_4\alpha_4 \end{Bmatrix} \tag{A26}$$

The development of the steps necessary to compute the $k_{ij}$ elements in the $\left[S_1\right]$ or "downwash" matrix follow. As a first step the relation which exists between the strength of a segment of a straight-line vortex and the induced velocity at a nearby point should be found. If the strength of the vortex (whose sense is given by the right-hand rule for moments) is $\Gamma$, the velocity induced at the point $P$ can be written as

$$w_P = \frac{\Gamma(\cos \alpha - \cos \beta)}{4\pi R} \tag{A27}$$

where $\alpha$ and $\beta$ are the angles between the direction of the vortex segment and lines joining the ends of the segment to the point as shown in the sketch
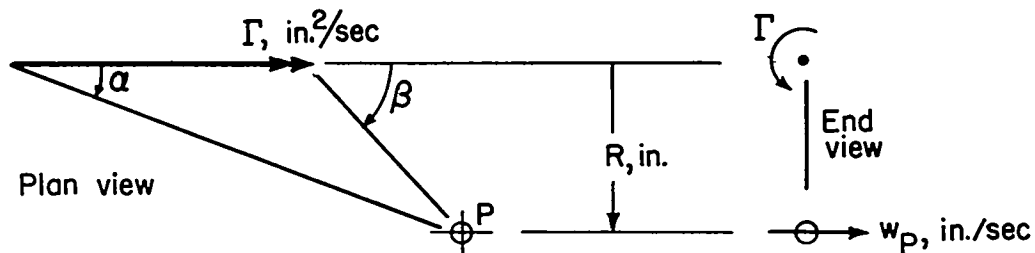


Equation (A27) is used in the subsequent derivation of the $\left[S_1\right]$ matrix.

A plan view of the geometry of a typical horseshoe vortex on the left-hand wing is given in the following sketch, in which distances and angles are considered positive as indicated and the sense of the circulation of the elements of the horseshoe vortex is given by the right-hand moment rule:



The points V and D are a typical horseshoe reference point and a typical control point, respectively.

The incremental downwash velocities induced by a single horseshoe vortex, if downwash velocities are considered as positive, are:

(1) For the left-hand trailing vortex the relations

$$R = -\left(s_y - h\right)$$

$$\alpha = 0^\circ \qquad\qquad \cos \alpha = 1$$

$$\beta = 270^\circ - \theta \qquad \cos \beta = -\sin \theta$$

are substituted into the general relation

$$w_L = \frac{\Gamma(\cos \alpha - \cos \beta)}{4\pi R} \qquad\qquad (A28)$$

to obtain the incremental downwash velocity

$$w_L = -\frac{\Gamma(1 + \sin \theta)}{4\pi \left(s_y - h\right)} \qquad\qquad (A29)$$

(2) From the right-hand trailing vortex where

$$R = s_y + h$$

$$\alpha = 90^\circ - \phi \qquad \cos \alpha = \sin \phi$$

$$\beta = 180^\circ \qquad\qquad \cos \beta = -1$$

the incremental downwash velocity is

$$w_R = \frac{\Gamma(\sin \phi + 1)}{4\pi \left(s_y + h\right)} \qquad\qquad (A30)$$

(3) From the bound vortex where

$$R = s_x$$

$$\alpha = 180° - \theta \qquad \cos \alpha = -\cos \theta$$

$$\beta = 180° - \phi \qquad \cos \beta = -\cos \phi$$

the incremental downwash velocity is

$$w_B = \frac{\Gamma(\cos \phi - \cos \theta)}{4\pi s_x} \tag{A31}$$

The total downwash velocity at a typical control point due to a complete single horseshoe is then

$$w = w_L + w_R + w_B$$

$$= \frac{\Gamma}{4\pi}\left(- \frac{1 + \sin \theta}{s_y - h} + \frac{1 + \sin \phi}{s_y + h} + \frac{\cos \phi - \cos \theta}{s_x}\right) \tag{A32}$$

Substitution of the identities

$$\left.\begin{array}{c} s_y - h \equiv \dfrac{s_x \cos \theta}{\sin \theta} \\[2ex] s_y + h \equiv \dfrac{s_x \cos \phi}{\sin \phi} \end{array}\right\} \tag{A33}$$
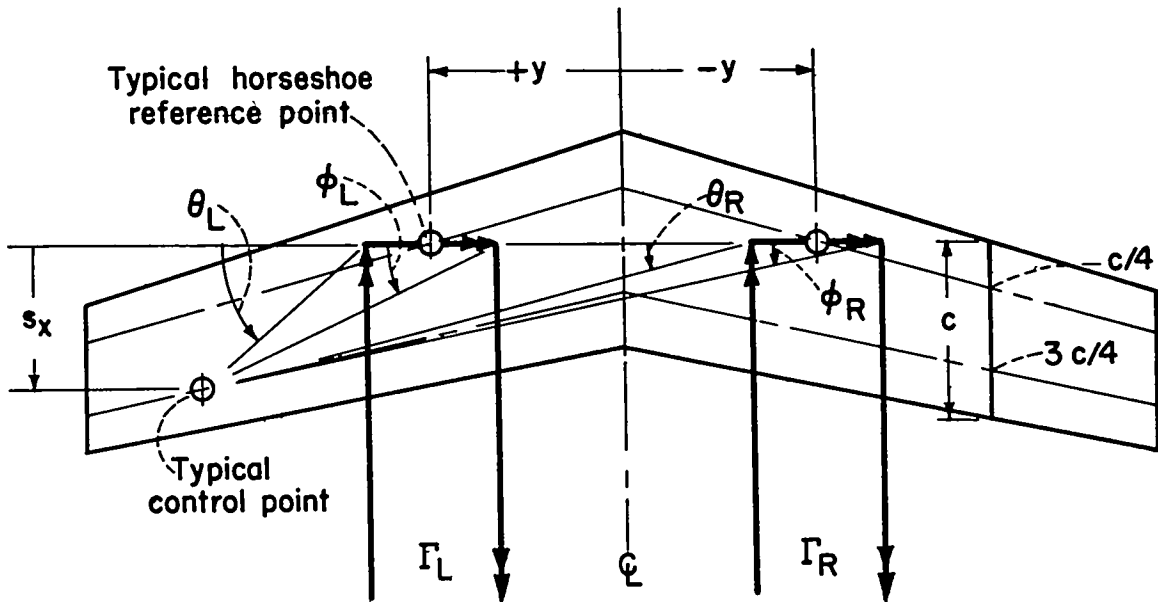
into equation (A32) yields

$$w = \frac{\Gamma}{4\pi s_x}\left(\frac{1 + \sin \phi}{\cos \phi} - \frac{1 + \sin \theta}{\cos \theta}\right) \tag{A34}$$

Equations (A34) and (A2) are identical; therefore,

$$K_{ij} = \frac{1}{4\pi s_{x_{ij}}}\left(\frac{1 + \sin \phi_{ij}}{\cos \phi_{ij}} - \frac{1 + \sin \theta_{ij}}{\cos \theta_{ij}}\right) \tag{A35}$$

If, as indicated in the sketch



the control points are assumed to be located on the left semispan of the wing so that $\theta_L$ and $\phi_L$ represent the pertinent angles for a horseshoe located on the left semispan and $\theta_R$ and $\phi_R$ represent the pertinent angles for the corresponding horseshoe on the right semispan, then for a typical control point

$$\left.\begin{aligned} K_L &= \frac{1}{4\pi s_x}\left(\frac{1 + \sin \phi_L}{\cos \phi_L} - \frac{1 + \sin \theta_L}{\cos \theta_L}\right) \\[2em] K_R &= \frac{1}{4\pi s_x}\left(\frac{1 + \sin \phi_R}{\cos \phi_R} - \frac{1 + \sin \theta_R}{\cos \theta_R}\right) \end{aligned}\right\} \tag{A36}$$

From equation (A16),

$$k = 4\pi\left(K_L \pm K_R\right)$$

so that in the $\left[S_1\right]$ or downwash matrix each element $k$ is computed from the equation

$$k = \frac{1}{s_x}\left(\frac{1 + \sin\phi_L}{\cos\phi_L} - \frac{1 + \sin\theta_L}{\cos\theta_L} \pm \frac{1 + \sin\phi_R}{\cos\phi_R} \mp \frac{1 + \sin\theta_R}{\cos\theta_R}\right) \tag{A37}$$

As in equation (A16), the upper sign is to be used for symmetrical spanwise airload distributions, and the lower sign is to be used for antisymmetrical spanwise airload distributions. Note that in equation (A34)

$$\sin\phi = \frac{x_D - x_V}{\sqrt{\left(x_D - x_V\right)^2 + \left(y_D - y_V + h\right)^2}}$$

$$\cos\phi = \frac{y_D - y_V + h}{\sqrt{\left(x_D - x_V\right)^2 + \left(y_D - y_V + h\right)^2}}$$

$$\sin\theta = \frac{x_D - x_V}{\sqrt{\left(x_D - x_V\right)^2 + \left(y_D - y_V - h\right)^2}}$$

$$\cos\theta = \frac{y_D - y_V - h}{\sqrt{\left(x_D - x_V\right)^2 + \left(y_D - y_V - h\right)^2}}$$

The $\left[S_1\right]$ matrix therefore is computed from the matrix equation

$$\left[S_1\right] = \left[\frac{1}{s_x}\left(\frac{1 + \sin \phi_L}{\cos \phi_L} - \frac{1 + \sin \theta_L}{\cos \theta_L} \pm \frac{1 + \sin \phi_R}{\cos \phi_R} \mp \frac{1 + \sin \theta_R}{\cos \theta_R}\right)\right] \qquad \text{(A38)}$$

where the upper sign is used for symmetric flight conditions and the lower sign is used for antisymmetrical conditions.

Since the $\left[S_1\right]$ matrix is used in equation (A23), which is

$$\left[S_1\right]\{l\} = \left[4qm_0\right]\{\alpha_f^0\}$$

the elements of the $\left[S_1\right]$ matrix are seen to be influence coefficients relating the incremental downwash angle at each control point to the intensity of the running lift over each increment of the semispan of the wing. In general, all the elements in the principal diagonal of the $\left[S_1\right]$ matrix will always be positive and those elements not in the principal diagonal will always be negative because the velocities were considered as positive downward and wash velocities from a horseshoe vortex are downward only in the region behind the bound vortex and between the trailing vortices of that horseshoe.

## Compressibility Corrections

The method by which compressibility effects are handled in this report is based on simple sweep theory. This theory is presented in references 6 to 8 and substantiated in references 9 to 12. Summarized briefly, infinite-aspect-ratio sweep theory indicates that compressibility effects are functions of the effective Mach number $M_e$, which in this case is the Mach number of the stream velocity component that is normal to the leading edge, so that the lift-curve slope in compressible flow is given by

$$m_0 = \frac{m}{\sqrt{1 - M^2 \cos^2 \Lambda_M}} \qquad \text{(A39)}$$

where

m           section lift-curve slope at  $M = 0$

M           stream Mach number

$\Lambda_M$           effective sweep angle for compressibility effects or yaw
            angle of infinite wing, radians

The same relationship exists for the effects of Mach number on
section pitching-moment coefficient

$$c_{m_0} = \frac{c_m}{\sqrt{1 - M^2 \cos^2 \Lambda_M}} \tag{A40}$$

Compressibility effects on a finite-aspect-ratio swept wing can be
handled in a similar fashion.  For the finite-aspect-ratio swept wing,
however, recognition should be given to the fact that compressibility
effects will vary across the span of the wing.  In general, smaller
values of the effective sweep angle are indicated for the wing root and
tip sections than for the midsemispan region.  Even in the midsemispan
region the effective sweep angles for compressibility effects are not
functions of the wing plan-form geometry alone; the spanwise variations
of camber, thickness ratio, chordwise thickness distribution, and angle
of attack are likewise involved in the determination of the value for
the local effective sweep angles.

Consider equation (7) for the downwash angle induced at a distance  $r$
rearward of the lifting line which was derived from two-dimensional
considerations

$$\frac{w_r}{V} = \frac{m_0}{2\pi} \frac{c}{2r} \alpha_f$$

This equation expresses the relation between the downwash angle at the
three-quarter-chord point (i.e., at  $r = c/2$) and the geometric angle
of attack  $\alpha_f$  when the section lift-curve slope is equal to its theo-
retical value  $2\pi$.

Several approaches can now be made to the compressibility problem
regarding the values of lift-curve slope, the angles of attack, and the
location of control points to be utilized for equating downwash angle
to geometric angle of attack.  In the method used in this paper the

distance $r$ is always equal to one-half of the local streamwise chord, so that in matrix notation equation (7) reduces to (see eq. (9))

$$\left\{\frac{w}{V}\right\}_{3c/4} = \left[\frac{\overset{o}{m_0}}{2\pi}\right]\left\{\alpha_f\right\}$$

The applicable values of $m_0$ to be used in this equation are those at the effective Mach number $M_e = M \cos \Lambda_M$, and thus each wing station is permitted to have its own compressibility corrections. In the absence of test data reduced according to the method of appendix G, a value of $m_0$ can be calculated from equation (A39) for a value of $\Lambda_M$ equal to the geometric sweep angle of the plan-form streamwise quarter-chord line. Although, in general, this procedure will yield only an approximation to the correct theoretical value, this value will usually be sufficiently accurate for preliminary design purposes when $A/\cos \Lambda$ is large (where $A$ is the aspect ratio) or $M \cos \Lambda$ is small, or both.

This "modified angle of attack" method is characteristically different from the "plan form distortion" methods of handling compressibility effects (refs. 13 and 14); the former distorts the angle at the original three-quarter-chord point, whereas the latter stretches the half-chord distance.

An important advantage in the compressibility-correction method presented in this paper is that only one $[S_1]$ matrix need be computed, whereas a different $[S_1]$ matrix for each Mach number is required in the plan-form-distortion method.

The following developments show the equivalence of these two methods of accounting for compressibility effects. The first comparison is for the case of an infinite wing in yaw.

If $\Lambda_M$ is the sweep or yaw angle for this infinite wing, then according to the plan-form-distortion procedure (indicated by the subscript pd) the equivalent wing in incompressible flow (M = 0) is to be at a yaw angle such that

$$\tan \bar{\Lambda}_M = \frac{\tan \Lambda_M}{\sqrt{1 - M^2}}$$

Further, the lift-curve slope of this equivalent wing in incompressible flow, multiplied by the factor $1/\sqrt{1 - M^2}$, is equal to the lift-curve slope of the original wing in compressible flow.

The lift equation for the equivalent Mach number method of this paper (indicated by the subscript $M_e$) is

$$L_{M_e} = qc\alpha \frac{2\pi \cos \Lambda_M}{\sqrt{1 - M^2\cos^2\Lambda_M}}$$

and that according to the plan-form-distortion theory is

$$L_{pd} = qc\alpha \frac{2\pi \cos \overline{\Lambda}_M}{\sqrt{1 - M^2}}$$

In order for the two lifts to be equal, the following equality must be true for any value of $M$:

$$\frac{\cos \overline{\Lambda}_M}{\sqrt{1 - M^2}} = \frac{\cos \Lambda_M}{\sqrt{1 - M^2\cos^2\Lambda_M}}$$

It can be shown that such is the case by the use of elementary trigonometric identities.

The next comparison is for the case with zero sweepback. The plan-form-distortion method stretches the half-chord distance as a function of Mach number to

$$\frac{c'}{2} = \frac{c}{2} \frac{1}{\sqrt{1 - M^2}}$$

which when substituted for $r$ in equation (3) gives

$$w = \frac{\Gamma\sqrt{1 - M^2}}{\pi c}$$

Equating the downwash angle at the stretched control point to the section angle of attack gives

$$\frac{w}{V} = \frac{\Gamma\sqrt{1 - M^2}}{\pi cV} = \alpha_f \tag{A41}$$

The compressible lift-curve slope (ref. 14) is

$$m_o = \frac{2\pi}{\sqrt{1 - M^2}} \tag{A42}$$

Equations (A41) and (A42) may be substituted into equation (2) to give

$$l = \frac{2\pi}{\sqrt{1 - M^2}} \frac{\Gamma\sqrt{1 - M^2}}{\pi cV} \frac{\rho V^2 c}{2}$$

or

$$l = \rho V \Gamma$$

For the compressibility-effects method of this paper the downwash angle at the three-quarter-chord point equated to the angle of attack corrected for effects of section lift-curve slope is (see eq. (8))

$$\left(\frac{w}{V}\right)_{3c/4} = \frac{\Gamma}{\pi cV} = \frac{m_o}{2\pi} \alpha_f$$

from which

$$\alpha_f = \frac{2\Gamma}{m_o cV} \tag{A43}$$

When equation (A43) is substituted into equation (2) the same final answer is obtained:

$$l = \rho V \Gamma$$

The identities of compressibility corrections in the case of either the unyawed ($\Lambda_M = 0$) infinite wing or the yawed ($\Lambda_M \neq 0$) infinite wing substantiates, at least qualitatively, the use of the compressibility correction methods as presented in this paper.

## APPENDIX B

## THE ELASTICITY MATRICES $[S_2]$ AND $[S_2{}']$

The purpose of this appendix is to explain, in brief form, the structural theory involved in and the steps necessary for the computation of the elasticity matrices $[S_2]$ and $[S_2{}']$.

### Development of the $[S_2]$ Matrix

In the development of the downwash matrix $[S_1]$ in appendix A, a continuously varying spanwise airload distribution was replaced by a series of constant-intensity running loads, each of which covers an increment of the wing semispan. This concept of an equivalent system of loads is also used in this appendix.

Consider the geometry of the structural skeleton of the wing to be as represented in figure 3, in which double arrows indicate that the right-hand rule of moments applies. The notation in figure 3 is defined as follows:

$L_1, L_2, \ldots L_n$      total lift of increment of wing having span of $2h_1$, $2h_2, \ldots 2h_n$, respectively, numbered inboard from the left wing tip, lb (see eq. (B1))

$e_1, e_2, \ldots e_n$      streamwise distance from horseshoe reference point at a wing station to elastic axis at the same station, positive when elastic-axis point is to rear of horseshoe reference point, in.

$f_1, f_2, \ldots f_n$      streamwise distance from elastic-axis reference point at a station to elastic-axis reference point at the next inboard station, positive when inboard elastic-axis point is forward of outboard elastic-axis point

$d_1, d_2, \ldots d_n$      lateral distance between elastic-axis point at a station and elastic-axis point at the next station inboard

$\Lambda_1, \Lambda_2, \ldots \Lambda_n$      local sweepback angle of elastic axis

$M_{X_1}$, $M_{X_2}$, . . . $M_{X_n}$     rolling moment at elastic-axis point around longi-
tudinal axis through local elastic-axis reference
point due to total lift of all the vortices out-
board of this point, positive when it raises left
wing tip, in-lb

$M_{Y_1}$, $M_{Y_2}$, . . . $M_{Y_n}$     pitching moment at elastic-axis point around lateral
axis through local elastic-axis reference point
due to total lift of all the vortices outboard of
this point, positive when nose up, in-lb

$M_1$, $M_2$, . . . $M_n$     beam bending moment at elastic-axis point about an
axis perpendicular to local elastic axis, positive
when it puts compression in wing upper surface,
in-lb (see eq. (B2))

$T_1$, $T_2$, . . . $T_n$     torsional moment around elastic axis at local
elastic-axis point, positive when it is in direc-
tion of leading edge up, in-lb (see eq. (B3))

The general form for the wing lift is

$$L_n = 2h_n l_n \tag{B1}$$

where $l_n$ is the intensity of the running lift at station $\eta_n$ measured
in pounds per inch and $2h_n$ is the span of the horseshoe vortex at
station $\eta_n$; the general form for the bending moment is

$$M_n = M_{X_n} \cos \Lambda_n - M_{Y_n} \sin \Lambda_n \tag{B2}$$

and the general form for the torsional moment is

$$T_n = M_{Y_n} \cos \Lambda_n + M_{X_n} \sin \Lambda_n \tag{B3}$$

At station 1, on the center line of the horseshoe vortex nearest the left wing tip (see figs. 3 and 4), the following equations apply:

$$M_{X_1} = \frac{L_1}{2} \frac{h_1}{2} = \frac{L_1 h_1}{4} \tag{B4}$$

$$M_{Y_1} = \frac{L_1}{2}\left(e_1 - \frac{h_1 \tan \Lambda_1}{2}\right) \tag{B5}$$

which, when substituted into equations (B2) and (B3), yield

$$M_1 = L_1\left(\frac{h_1}{4 \cos \Lambda_1} - \frac{e_1 \sin \Lambda_1}{2}\right) \tag{B6}$$

$$T_1 = L_1 \frac{e_1 \cos \Lambda_1}{2} \tag{B7}$$

At station 2, on the center line of the second horseshoe vortex inboard of the left wing tip,

$$M_{X_2} = L_1 d_1 + \frac{L_2 h_2}{4} \tag{B8}$$

$$M_{Y_2} = L_1\left(e_1 - f_1\right) + \frac{L_2}{2}\left(e_2 - \frac{h_2 \tan \Lambda_2}{2}\right) \tag{B9}$$

and equations (B2) and (B3) become

$$M_2 = L_1 d_1 \cos \Lambda_2 - L_1 (e_1 - f_1) \sin \Lambda_2 + L_2 \left( \frac{h_2}{4 \cos \Lambda_2} - \frac{e_2 \sin \Lambda_2}{2} \right) \quad \text{(B10)}$$

$$T_2 = L_1 d_1 \sin \Lambda_2 + L_1 (e_1 - f_1) \cos \Lambda_2 + L_2 \left( \frac{e_2 \cos \Lambda_2}{2} \right) \quad \text{(B11)}$$

At station 3,

$$M_{X_3} = L_1 (d_1 + d_2) + L_2 d_2 + \frac{L_3 h_3}{4} \quad \text{(B12)}$$

and, similarly,

$$M_{Y_3} = L_1 (e_1 - f_1 - f_2) + L_2 (e_2 - f_2) + \frac{L_3}{2} \left( e_3 - \frac{h_3 \tan \Lambda_3}{2} \right) \quad \text{(B13)}$$

and, similarly,

$$M_3 = \left[ L_1 (d_1 + d_2) + L_2 d_2 \right] \cos \Lambda_3 - \left[ L_1 (e_1 - f_1 - f_2) + \right.$$

$$\left. L_2 (e_2 - f_2) \right] \sin \Lambda_3 + L_3 \left( \frac{h_3}{4 \cos \Lambda_3} - \frac{e_3 \sin \Lambda_3}{2} \right) \quad \text{(B14)}$$

$$T_3 = \left[ L_1 (d_1 + d_2) + L_2 d_2 \right] \sin \Lambda_3 + \left[ L_1 (e_1 - f_1 - f_2) + \right.$$

$$\left. L_2 (e_2 - f_2) \right] \cos \Lambda_3 + L_3 \frac{e_3 \cos \Lambda_3}{2} \quad \text{(B15)}$$

Equations similar to these can be developed for M and T for the remaining stations on the left semispan of the wing.

In algebraic form, the equations for $M_n$ and $T_n$ are

$$M_n = \cos \Lambda_n \sum_{k=1}^{n-1} \left( L_k \sum_{l=k}^{n-1} d_l \right) - \sin \Lambda_n \sum_{k=1}^{n-1} \left[ L_k \left( e_k - \sum_{l=k}^{n-1} f_l \right) \right] +$$

$$L_n \left( \frac{h_n}{4 \cos \Lambda_n} - \frac{e_n \sin \Lambda_n}{2} \right) \qquad\qquad (B16)$$

$$T_n = \sin \Lambda_n \sum_{k=1}^{n-1} \left( L_k \sum_{l=k}^{n-1} d_l \right) + \cos \Lambda_n \sum_{k=1}^{n-1} \left[ L_k \left( e_k - \sum_{l=k}^{n-1} f_l \right) \right] +$$

$$L_n \frac{e_n \cos \Lambda_n}{2} \qquad\qquad (B17)$$

Notice that the first two terms in each of these equations are equal to zero when $n = 1$, that is, for the tip station.

In matrix notation, equations (B16) and (B17) become

$$\{M\} = \left[ \left[ \overset{o}{\cos \Lambda} \right] \left[ r_1 \right] - \left[ \overset{o}{\sin \Lambda} \right] \left[ u \right] \right] \{L\} \qquad\qquad (B18)$$

$$\{T\} = \left[ \left[ \overset{o}{\sin \Lambda} \right] \left[ r_2 \right] + \left[ \overset{o}{\cos \Lambda} \right] \left[ u \right] \right] \{L\} \qquad\qquad (B19)$$

where

$$\{M\} = \begin{Bmatrix} M_1 \\ M_2 \\ M_3 \\ \cdot \\ M_n \end{Bmatrix} \qquad \text{(B20)}$$

$$\{T\} = \begin{Bmatrix} T_1 \\ T_2 \\ T_3 \\ \cdot \\ T_n \end{Bmatrix} \qquad \text{(B21)}$$

$$\{L\} = \begin{Bmatrix} L_1 \\ L_2 \\ L_3 \\ \cdot \\ L_n \end{Bmatrix} \qquad \text{(B22)}$$

$$\begin{bmatrix} \overset{o}{\cos \Lambda} \end{bmatrix} = \begin{bmatrix} \cos \Lambda_1 & 0 & 0 & 0 & \cdot & \cdot \\ 0 & \cos \Lambda_2 & 0 & 0 & \cdot & \cdot \\ 0 & 0 & \cos \Lambda_3 & 0 & \cdot & \cdot \\ 0 & 0 & 0 & \cos \Lambda_4 & \cdot & \cdot \\ \cdot & \cdot & \cdot & \cdot & \cdot & \cdot \\ \cdot & \cdot & \cdot & \cdot & \cdot & \cdot \end{bmatrix} \qquad \text{(B23)}$$

$$\begin{bmatrix} \overset{o}{\sin \Lambda} \end{bmatrix} = \begin{bmatrix} \sin \Lambda_1 & 0 & 0 & 0 & \cdot & \cdot \\ 0 & \sin \Lambda_2 & 0 & 0 & \cdot & \cdot \\ 0 & 0 & \sin \Lambda_3 & 0 & \cdot & \cdot \\ 0 & 0 & 0 & \sin \Lambda_4 & \cdot & \cdot \\ \cdot & \cdot & \cdot & \cdot & \cdot & \cdot \\ \cdot & \cdot & \cdot & \cdot & \cdot & \cdot \end{bmatrix} \qquad \text{(B24)}$$

$$[u] = \begin{bmatrix}
0 & 0 & 0 & 0 & 0 & \cdot & \cdot \\
e_1 - f_1 & 0 & 0 & 0 & 0 & \cdot & \cdot \\
e_1 - f_1 - f_2 & e_2 - f_2 & 0 & 0 & 0 & \cdot & \cdot \\
e_1 - f_1 - f_2 - f_3 & e_2 - f_2 - f_3 & e_3 - f_3 & 0 & 0 & \cdot & \cdot \\
e_1 - f_1 - f_2 - f_3 - f_4 & e_2 - f_2 - f_3 - f_4 & e_3 - f_3 - f_4 & e_4 - f_4 & 0 & \cdot & \cdot \\
\cdot & \cdot & \cdot & \cdot & \cdot & \cdot & \cdot \\
\cdot & \cdot & \cdot & \cdot & \cdot & \cdot & \cdot
\end{bmatrix} \quad (B25)$$

$$[r_1] = \begin{bmatrix}
\dfrac{h_1}{4\cos^2\Lambda_1} - \dfrac{e_1 \tan\Lambda_1}{2} & 0 & 0 & 0 & 0 & \cdot & \cdot \\[2ex]
d_1 & \dfrac{h_2}{4\cos^2\Lambda_2} - \dfrac{e_2 \tan\Lambda_2}{2} & 0 & 0 & 0 & \cdot & \cdot \\[2ex]
d_1 + d_2 & d_2 & \dfrac{h_3}{4\cos^2\Lambda_3} - \dfrac{e_3 \tan\Lambda_3}{2} & 0 & 0 & \cdot & \cdot \\[2ex]
d_1 + d_2 + d_3 & d_2 + d_3 & d_3 & \dfrac{h_4}{4\cos^2\Lambda_4} - \dfrac{e_4 \tan\Lambda_4}{2} & 0 & \cdot & \cdot \\[2ex]
d_1 + d_2 + d_3 + d_4 & d_2 + d_3 + d_4 & d_3 + d_4 & d_4 & \dfrac{h_5}{4\cos^2\Lambda_5} - \dfrac{e_5 \tan\Lambda_5}{2} & \cdot & \cdot \\[2ex]
\cdot & \cdot & \cdot & \cdot & \cdot & \cdot & \cdot \\
\cdot & \cdot & \cdot & \cdot & \cdot & \cdot & \cdot
\end{bmatrix} \quad (B26)$$

$$
[r_2] =
\begin{bmatrix}
\dfrac{e_1}{2 \tan \Lambda_1} & 0 & 0 & 0 & 0 & \cdot & \cdot \\
d_1 & \dfrac{e_2}{2 \tan \Lambda_2} & 0 & 0 & 0 & \cdot & \cdot \\
d_1 + d_2 & d_2 & \dfrac{e_3}{2 \tan \Lambda_3} & 0 & 0 & \cdot & \cdot \\
d_1 + d_2 + d_3 & d_2 + d_3 & d_3 & \dfrac{e_4}{2 \tan \Lambda_4} & 0 & \cdot & \cdot \\
d_1 + d_2 + d_3 + d_4 & d_2 + d_3 + d_4 & d_3 + d_4 & d_4 & \dfrac{e_5}{2 \tan \Lambda_5} & \cdot & \cdot \\
\cdot & \cdot & \cdot & \cdot & \cdot & \cdot & \cdot \\
\cdot & \cdot & \cdot & \cdot & \cdot & \cdot & \cdot
\end{bmatrix}
\quad (B27)
$$

Equations (B18) and (B19) provide the means for computing the bending and torsional moments along the span of the wing due to the loads $L$ as given by equation (B1).

Each of the loads $l$ or $L$, however, is affected by the variation in angle of attack from root to tip. This problem is handled by computing the streamwise angle-of-attack change $\alpha_s$ due to the structural deformations caused by the series of loads $\{L\}$. Since a streamwise angle-of-attack change is required, assume that a unit positive pitching moment $m_Y$ (nose-up moment) is applied in turn at each of the points $1, 2, \ldots n$ on the elastic axis. The unit pitching moment is in the plane in which $\alpha_s$ is to be measured and its direction agrees with the positive sense of $\alpha_s$.

The streamwise angle-of-attack change can then be obtained by applying the general relation (see ref. 15)

$$\alpha_{s_\sigma} = \int_0^\sigma \frac{mM \, ds}{EI} + \int_0^\sigma \frac{tT \, ds}{GJ} \tag{B28}$$

where

$\alpha_{s_\sigma}$      desired streamwise angle-of-attack change due to values of bending moments $M$ and torsional moments $T$ along elastic axis of wing resulting from the series of loads $\{L\}$

$m$      beam bending moment per unit pitching moment applied at station at which $\alpha_{s_\sigma}$ is to be determined

$t$      torsional moment around elastic axis per unit pitching moment

$ds$      increment along elastic axis

$EI$      effective beam bending stiffness around the axis of the bending moments $M$ and $m$

$GJ$      effective torsional stiffness around the axis of the torsional moments $T$ and $t$

The stations on the wing for which the angle-of-attack changes $\alpha_s$ are to be computed are those on the center line of each horseshoe vortex.

It is assumed that sufficient accuracy in the results will be obtained by using the values of bending moment $M$ and torsional moment $T$ obtained by means of equations (B18) and (B19) and that these values of $M$ and $T$ may be considered to be constant over the increments of the wing span corresponding to the span (2h) of each horseshoe vortex.

Values of $EI$ and $GJ$ are also assumed to be constant over each such increment in wing span, and the values to be used are the effective values which correspond to the wing station $\eta$ at the midpoint of each horseshoe vortex.

The general relation (eq. (B28)) can be used to express $\alpha_s$ in matrix form by letting

$\Lambda_n$          sweepback angle of elastic axis at station $\eta_n$, radians

$M_n$          beam bending moment at station $\eta_n$ due to loads $\{L\}$ on wing

$T_n$          torsional moment around elastic axis at station $\eta_n$ due to loads $\{L\}$ on wing

$m_{ij}$          beam bending moment at station $i$ per unit pitching moment applied at station $j$

$t_{ij}$          torsional moment around elastic axis at station $i$ per unit pitching moment applied at station $j$

$$(ds)_n = \frac{2h_n}{\cos \Lambda_n}$$

$2h_n$          horseshoe span at station $\eta_n$

$\alpha_{s_n}$          angle-of-attack change at station $\eta_n$ due to all the loads $\{L\}$ on wing

Then, for station 1,

$$\alpha_{s_1} = \left[ \frac{m_{11}M_1h_1}{(EI)_1 \cos \Lambda_1} + \frac{2m_{21}M_2h_2}{(EI)_2 \cos \Lambda_2} + \ldots + \frac{2m_{n1}M_nh_n}{(EI)_n \cos \Lambda_n} \right] +$$

$$\left[ \frac{t_{11}T_1h_1}{(GJ)_1 \cos \Lambda_1} + \frac{2t_{21}T_2h_2}{(GJ)_2 \cos \Lambda_2} + \ldots + \frac{2t_{n1}T_nh_n}{(GJ)_n \cos \Lambda_n} \right] \quad (B29)$$

for station 2,

$$\alpha_{s_2} = \left[ \frac{2m_{12}M_1h_1}{(EI)_1 \cos \Lambda_1} + \frac{m_{22}M_2h_2}{(EI)_2 \cos \Lambda_2} + \ldots + \frac{2m_{n2}M_nh_n}{(EI)_n \cos \Lambda_n} \right] +$$

$$\left[ \frac{2t_{12}T_1h_1}{(GJ)_1 \cos \Lambda_1} + \frac{t_{22}T_2h_2}{(GJ)_2 \cos \Lambda_2} + \ldots + \frac{2t_{n2}T_nh_n}{(GJ)_n \cos \Lambda_n} \right] \quad (B30)$$

and so forth.

From the geometry of the problem, when point $i$ is at or inboard of point $j$, the bending moment due to a unit pitching moment applied at point $j$ is

$$m_{ij} = -\sin \Lambda_i \tag{B31a}$$

when point $i$ is outboard of point $j$, the bending moment is

$$m_{ij} = 0 \tag{B31b}$$

when point $i$ is at or inboard of point $j$, the torsional moment due to a unit pitching moment applied at point $j$ is

$$t_{ij} = \cos \Lambda_i \tag{B32a}$$

and when point $i$ is outboard of point $j$, the torsional moment is

$$t_{ij} = 0 \tag{B32b}$$

and the complete series of equations for $\alpha_s$, of which equations (B29) and (B30) are representative examples, can be written in matrix form as

$$\{\alpha_s\} = [m]\left[\frac{2h}{\cos \Lambda}\right]^{\circ}\left[\frac{1}{EI}\right]^{\circ}\{M\} + [t]\left[\frac{2h}{\cos \Lambda}\right]^{\circ}\left[\frac{1}{GJ}\right]^{\circ}\{T\} \tag{B33}$$

Typical elements in $[m]$ and $[t]$ are

$$[m] = \begin{bmatrix} -\sin \Lambda_1/2 & -\sin \Lambda_2 & -\sin \Lambda_3 & -\sin \Lambda_4 & \cdot & \cdot \\ 0 & -\sin \Lambda_2/2 & -\sin \Lambda_3 & -\sin \Lambda_4 & \cdot & \cdot \\ 0 & 0 & -\sin \Lambda_3/2 & -\sin \Lambda_4 & \cdot & \cdot \\ 0 & 0 & 0 & -\sin \Lambda_4/2 & \cdot & \cdot \\ \cdot & \cdot & \cdot & \cdot & \cdot & \cdot \\ \cdot & \cdot & \cdot & \cdot & \cdot & \cdot \end{bmatrix} \quad (B34)$$

$$[t] = \begin{bmatrix} \cos \Lambda_1/2 & \cos \Lambda_2 & \cos \Lambda_3 & \cos \Lambda_4 & \cdot & \cdot \\ 0 & \cos \Lambda_2/2 & \cos \Lambda_3 & \cos \Lambda_4 & \cdot & \cdot \\ 0 & 0 & \cos \Lambda_3/2 & \cos \Lambda_4 & \cdot & \cdot \\ 0 & 0 & 0 & \cos \Lambda_4/2 & \cdot & \cdot \\ \cdot & \cdot & \cdot & \cdot & \cdot & \cdot \\ \cdot & \cdot & \cdot & \cdot & \cdot & \cdot \end{bmatrix} \quad (B35)$$

Substituting equations (B1), (B18), and (B19) into equation (B33) gives

$$\{\alpha_s\} = \left[ [m]\left[\frac{2h}{\cos \Lambda}\right]\left[\frac{1}{EI}\right]\left[ [\cos \Lambda][r_1] - [\sin \Lambda][u] \right] + \right.$$

$$\left. [t]\left[\frac{2h}{\cos \Lambda}\right]\left[\frac{1}{GJ}\right]\left[ [\sin \Lambda][r_2] + [\cos \Lambda][u] \right] \right][2h]\{l\} \quad (B36)$$

If

$$\left[S_2\right] = \left[\left[m\right]\left[\frac{2h}{\cos \Lambda}\right]\left[\frac{1}{EI}\right]\left[\left[\cos \Lambda\right]\left[r_1\right] - \left[\sin \Lambda\right]\left[u\right]\right] + \right.$$

$$\left.\left[t\right]\left[\frac{2h}{\cos \Lambda}\right]\left[\frac{1}{GJ}\right]\left[\left[\sin \Lambda\right]\left[r_2\right] + \left[\cos \Lambda\right]\left[u\right]\right]\right]\left[2h\right] \qquad (B37)$$

then

$$\left\{\alpha_s\right\} = \left[S_2\right]\left\{l\right\} \qquad (B38)$$

Equation (B37) represents the most general form for the $\left[S_2\right]$ matrix, and each element $a_{ij}$ of this matrix represents the angle-of-attack change in radians at station $i$ due to the structural deflection of the wing caused by a unit loading at station $j$. In effect, the $\left[S_2\right]$ matrix is an array of influence coefficients, and the elements of this matrix may be computed according to equation (B37), or, when an actual wing is available, they may be obtained by load-deflection tests of that wing.

Development of the Auxiliary Elasticity Matrix $\left[S_2'\right]$

The $\left[S_2\right]$ matrix as defined in the previous section considers air-loads outboard of each specified station, as defined by a streamwise cut through the wing box. Inasmuch as ribs are conventionally installed in a plane essentially normal to the elastic axis, the spar-box loads are more correctly determined by considering the airloads outboard of a plane

normal to the elastic axis.  These loadings are represented in the fol-
lowing sketch:
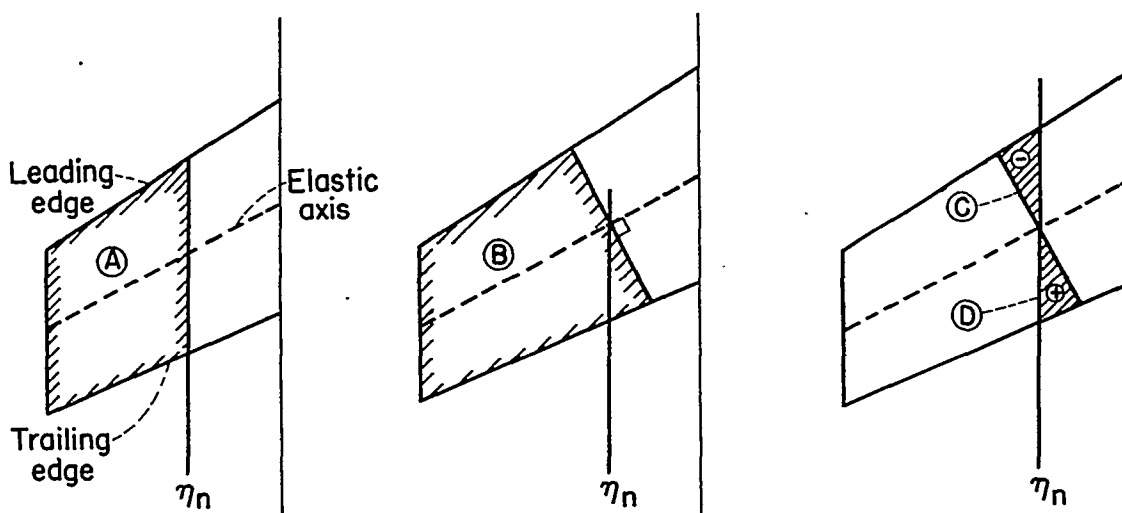


The corrective loading is then the loading obtained by subtracting
the loading of Ⓐ from that of Ⓑ .  The triangular areas Ⓒ and Ⓓ
represent the corrective loading.  It will be noticed that the loading
over the area Ⓒ is the negative of the loading of the corresponding
area in Ⓐ and the loading over Ⓓ is the positive of the corresponding
area in Ⓑ .  In order to obtain these corrective loadings, it will be
necessary to assume a distribution of pressure over the corrective areas.

The equations are now developed that represent the shear, wing
moment, and wing torsion due to the corrective loadings, and the
$\left[S_2\right]$ matrix is modified to include these effects.  A plan view of the
left wing is shown in figure 5, where

E                local angle between elastic axis and lateral axis equal
                 to $\Lambda$, the sweep angle of the elastic axis

L                local angle between leading edge and lateral axis

T                local angle between trailing edge and lateral axis

The correction terms for moment, shear, and torsion due to wing
airload in the $\left[S_2\right]$ matrix are

$\Delta M_{X_1}$, $\Delta M_{X_2}$, $\ldots \Delta M_{X_n}$  correction to rolling moment at elastic-axis point around longitudinal axis through local elastic-axis reference point, positive when it raises left wing tip, in-lb

$\Delta M_{Y_1}$, $\Delta M_{Y_2}$, $\ldots \Delta M_{Y_n}$  correction to pitching moment at elastic-axis point around lateral axis through local elastic-axis reference point, positive when nose up, in-lb

$\Delta M_1$, $\Delta M_2$, $\ldots \Delta M_n$  correction to wing bending moment at elastic-axis point about an axis perpendicular to local elastic axis, positive when it puts compression in wing upper surface, in-lb (see eq. (B39))

$\Delta T_1$, $\Delta T_2$, $\ldots \Delta T_n$  correction to torsional moment around elastic axis at local elastic-axis point, positive when it is in direction of leading edge up, in-lb (see eq. (B40))

$\Delta S_1$, $\Delta S_2$, $\ldots \Delta S_n$  correction to local shear, positive up, lb

The wing bending moment $M_n$ is

$$M_n = M_{X_n} \cos E_n - M_{Y_n} \sin E_n \tag{B39}$$

and the wing torsional moment $T_n$ is

$$T_n = M_{Y_n} \cos E_n + M_{X_n} \sin E_n \tag{B40}$$

Assumed pressure distribution.- The distribution of pressure $p$ over the corrective areas is assumed to be given by the two-dimensional equation for a thin flat plate

$$p = 4q\alpha \sqrt{\frac{1 - \dfrac{x}{c}}{x/c}} \tag{B41}$$

and modified to account for the actual value of local running lift. In the modified form, the distribution of pressure (measured in pounds per square inch) along a streamwise chord becomes

$$p = \frac{2}{\pi} \frac{l}{c} \sqrt{\frac{1 - \dfrac{x}{c}}{x/c}} \tag{B42}$$

where $x/c$ is the fraction of the streamwise chord to the rear of the leading edge. The ratio $l/c$ is assumed to be constant so that the lines of constant pressure radiate from the origin O in figure 5. In accordance with the assumptions previously given concerning the corrective loadings, the pressures are negative (downward) over area FDG and positive (upward) over area ABG.

A polar coordinate system $(\rho, \theta)$ is selected, and the shear, moment, and torsion due to the pressures on area OFB will be subtracted from the shear, moment, and torsion due to the pressures on area ODA. Lines of $\theta = \text{Constant}$ are lines of constant pressure and $p$ will be a function of $\theta$ only.

From the geometry of figure 5, $p$ may be expressed as a function of $\theta$ by writing

$$c + \overline{OM} \tan T - x = \overline{OM} \tan(L - \theta)$$

Hence

$$x = c + \overline{OM}\left[\tan T - \tan(L - \theta)\right] \tag{B43}$$

and

$$c + \overline{OM} \tan T = \overline{OM} \tan L$$

or

$$\overline{OM} = \frac{c}{\tan L - \tan T} \tag{B44}$$

Combining equations (B43) and (B44) yields

$$x = c\left[1 + \frac{\tan T - \tan(L - \theta)}{\tan L - \tan T}\right] \tag{B45}$$

If equation (B45) is substituted into equation (B42),

$$p = K\sqrt{\frac{\tan(L - \theta) - \tan T}{\tan L - \tan(L - \theta)}} \tag{B46}$$

where

$$K = \frac{2l}{\pi c} \tag{B47}$$

Rolling-moment correction at station $n$, $\Delta M_{X_n}$.- The rolling-moment correction at station $n$, $\Delta M_{X_n}$, is obtained by adding the rolling moment $\Delta M_{X_A}$ due to area OFB to the rolling moment $\Delta M_{X_B}$ due to area ODA (fig. 5).

The rolling moment $\Delta M_{X_A}$ due to area OFB may be found by writing the equation for the elementary moment about $\overline{FM}$ for any value of $\rho$ between O and that at the line $\overline{FM}$ as:

$$d\Delta M_{X_A} = p\left[\overline{OM} - \rho \cos(L - \theta)\right] \rho \, d\rho \, d\theta$$

The equation of the line $\overline{FM}$ is

$$\rho \cos(L - \theta) = \overline{OM}$$

or the value of $\rho$ at the line $\overline{FM}$ is

$$\rho = \frac{\overline{OM}}{\cos(L - \theta)}$$

Over area OFB the moment is negative; hence,

$$\Delta M_{X_A} = -K\overline{OM} \int_0^{L-T} \sqrt{\frac{\tan(L - \theta) - \tan T}{\tan L - \tan(L - \theta)}} \, d\theta \int_0^{\frac{\overline{OM}}{\cos(L-\theta)}} \rho \, d\rho \, +$$

$$K \int_0^{L-T} \sqrt{\frac{\tan(L - \theta) - \tan T}{\tan L - \tan(L - \theta)}} \cos(L - \theta) d\theta \int_0^{\frac{\overline{OM}}{\cos(L-\theta)}} \rho^2 d\rho$$

Since $\theta$ varies between O and $L - T$, the integrals can be evaluated by letting

$$\left. \begin{array}{l} \dfrac{\tan L - \tan(L - \theta)}{\tan L - \tan T} = \sin^2 U \\[3ex] \dfrac{\tan(L - \theta) - \tan T}{\tan L - \tan(L - \theta)} = \cot^2 U \end{array} \right\} \qquad \text{(B48)}$$

It follows that

$$d(L - \theta) = -2(\tan L - \tan T)\cos^2(L - \theta)\sin U \cos U \, dU$$

Consequently,

$$\Delta M_{X_A} = -K\overline{OM}^3(\tan L - \tan T)\int_0^{\pi/2}\cos^2 U \, dU +$$

$$\frac{2K}{3}\overline{OM}^3(\tan L - \tan T)\int_0^{\pi/2}\cos^2 U \, dU$$

$$= \frac{-\pi}{12}K\overline{OM}^3(\tan L - \tan T)$$

$$= -\frac{l c^2}{6(\tan L - \tan T)^2} \tag{B49}$$

The rolling moment $\Delta M_{X_B}$ due to area ODA may be derived in a similar manner to get

$$\Delta M_{X_B} = K\overline{OM}\int_0^{L-T}\sqrt{\frac{\tan(L - \theta) - \tan T}{\tan L - \tan(L - \theta)}}\, d\theta\int_0^{\frac{R}{\cos(L-\theta-E)}}\rho \, d\rho \, -$$

$$K\int_0^{L-T}\sqrt{\frac{\tan(L - \theta) - \tan T}{\tan L - \tan(L - \theta)}}\cos(L - \theta)d\theta\int_0^{\frac{R}{\cos(L-\theta-E)}}\rho^2 d\rho \tag{B50}$$

where

$$R = \frac{\overline{OM}\cos(E - T)}{\cos T} + c(1 - \epsilon)\sin E \tag{B51}$$

After integration this equation simplified to

$$\Delta M_{X_B} = \frac{\pi K \overline{OM} R^2 (\tan L - \tan T)}{4(\tan L + \cot E)^2 \sin^2 E \sqrt{1 - Q^2}} -$$

$$\frac{\pi K R^3 (\tan L - \tan T)(4 - 3Q^2)}{24(\tan L + \cot E)^3 \sin^3 E \sqrt{(1 - Q^2)^3}} \qquad (B52)$$

where

$$Q^2 = \frac{\tan L - \tan T}{\tan L + \cot E} \qquad (0 \leqq Q^2 < 1)$$

Equations (B49) and (B52) may now be combined to give the rolling-moment correction $\Delta M_{X_n}$ at station n:

$$\Delta M_{X_n} = \Delta M_{X_A} + \Delta M_{X_B}$$

$$= \frac{\pi K}{24} \left[ \frac{6cR^2(1 - Q^2)(\tan L + \cot E)\sin E - R^3(4 - 3Q^2)(\tan L - \tan T)}{\sqrt{(1 - Q^2)^3}(\tan L + \cot E)^3 \sin^3 E} - \right.$$

$$\left. \frac{2c^3}{(\tan L - \tan T)^2} \right] \qquad (B53)$$

If U defined in equations (B48) is written as

$$U = 1 + \frac{\cos(E - T)\cos L}{\sin E \sin(L - T)} \qquad (B54)$$

and if

$$V = \tan L + \cot E \tag{B55}$$

then $R$ (see eq. (B51)) becomes

$$R = c(U - \epsilon)\sin E \tag{B56}$$

and

$$\Delta M_{X_n} = \frac{lc^2}{12}\left[\frac{6(U - \epsilon)^2(1 - Q^2) - (U - \epsilon)^3(4 - 3Q^2)Q^2}{V^2(1 - Q^2)^{3/2}} - \frac{2}{V^2Q^4}\right] \tag{B57}$$

For the special case of the untapered wing where the leading edge is parallel to the trailing edge or $T = L$,

$$\Delta M_{X_n} = - \frac{lc^2}{16} \frac{\sin^2 E \cos^2 L}{\cos^2(E - L)} (8\epsilon^2 - 4\epsilon + 1) \tag{B58}$$

Pitching-moment correction at station $n$, $\Delta M_{Y_n}$.- The incremental pitching-moment corrections due to the areas OFB and ODA may be derived and combined in a manner similar to that for the rolling-moment corrections and the equation for $\Delta M_{Y_n}$ becomes

$$\Delta M_{Y_n} = \frac{lc^2}{12}\left\{\frac{Q^2(U - \epsilon)^3\left[(4 - 3Q^2)\tan L - Q^2 V\right] + 6(1 - Q^2)(U - \epsilon)^2(\epsilon Q^2 V - \tan L)}{V^2(1 - Q^2)^{3/2}} - \right.$$

$$\left. \frac{(6\epsilon - 1)VQ^2 - 2\tan L}{V^2Q^4}\right\} \tag{B59}$$

For the special case of the untapered wing where the leading edge is parallel to the trailing edge or $T = L$,

$$\Delta M_{Y_n} = - \frac{lc^2}{16} (8\epsilon^2 - 4\epsilon + 1) \frac{\sin E \cos L}{\cos(E - L)}\left[2 - \frac{\sin E \cos L \tan L}{\cos(E - L)}\right] \tag{B60}$$

Shear correction at station $n$, $\Delta S_n$.- The elementary shear is

$$d\Delta S_n = p\rho \, d\rho \, d\theta \tag{B61}$$

From this equation the incremental shears over the areas OFB and ODA may also be derived and combined in a manner similar to that for the rolling moment to give

$$\Delta S_n = \frac{lc}{2}\left[\frac{Q^2(U - \epsilon)^2}{v\sqrt{1 - Q^2}} - \frac{1}{Q^2 v}\right] \tag{B62}$$

For the special case of the untapered wing where the leading edge is parallel to the trailing edge or $T = L$,

$$\Delta S_n = -\frac{lc}{4}\frac{\sin E \cos L}{\cos(E - L)}(4\epsilon - 1) \tag{B63}$$

Modification of $\left[S_2\right]$ matrix.- The $\left[S_2\right]$ matrix is modified by using the corrective rolling and pitching equations. Using the equations

$$\Delta M_n = \Delta M_{X_n} \cos E_n - \Delta M_{Y_n} \sin E_n \tag{B64}$$

$$\Delta T_n = \Delta M_{X_n} \sin E_n + \Delta M_{X_n} \cos E_n \tag{B65}$$

and letting (from eqs. (B57) and (B59))

$$\mu = -\Delta M_{X_n}\big/l \tag{B66}$$

$$J = -\Delta M_{Y_n}\big/l \tag{B67}$$

results in

$$\Delta M_n = (-\mu \cos E_n + J \sin E_n)l$$

$$\Delta T_n = -(\mu \sin E_n + J \cos E_n)l$$

or, in matrix form (with $\Lambda_n \equiv E_n$),

$$\{\Delta M\} = \left[ -\left[\cos \overset{o}{\Lambda}\right]\left[\overset{o}{\mu}\right] + \left[\sin \overset{o}{\Lambda}\right]\left[\overset{o}{J}\right] \right]\{l\} \qquad (B68)$$

$$\{\Delta T\} = -\left[ \left[\sin \overset{o}{\Lambda}\right]\left[\overset{o}{\mu}\right] + \left[\cos \overset{o}{\Lambda}\right]\left[\overset{o}{J}\right] \right]\{l\} \qquad (B69)$$

Equation (B18) thus becomes

$$\{M\} = \left[ \left[\cos \overset{o}{\Lambda}\right]\left[ \left[\overset{o}{r_1}\right]\left[\overset{o}{2h}\right] - \left[\overset{o}{\mu}\right] \right] - \left[\sin \overset{o}{\Lambda}\right]\left[ \left[\overset{o}{u}\right]\left[\overset{o}{2h}\right] - \left[\overset{o}{J}\right] \right] \right]\{l\} \quad (B70)$$

and equation (B19) becomes

$$\{T\} = \left[ \left[\sin \overset{o}{\Lambda}\right]\left[ \left[\overset{o}{r_2}\right]\left[\overset{o}{2h}\right] - \left[\overset{o}{\mu}\right] \right] + \left[\cos \overset{o}{\Lambda}\right]\left[ \left[\overset{o}{u}\right]\left[\overset{o}{2h}\right] - \left[\overset{o}{J}\right] \right] \right]\{l\} \quad (B71)$$

The corrected form of the $\left[S_2\right]$ matrix thus becomes

$$\left[S_2{}'\right] = \left[ [m]\left[\frac{\overset{o}{2h}}{\cos \Lambda}\right]\left[\frac{\overset{o}{1}}{EI}\right]\left[ \left[\cos \overset{o}{\Lambda}\right]\left[ \left[\overset{o}{r_1}\right]\left[\overset{o}{2h}\right] - \left[\overset{o}{\mu}\right] \right] - \left[\sin \overset{o}{\Lambda}\right]\left[ \left[\overset{o}{u}\right]\left[\overset{o}{2h}\right] - \left[\overset{o}{J}\right] \right] \right] +$$

$$[t]\left[\frac{\overset{o}{2h}}{\cos \Lambda}\right]\left[\frac{\overset{o}{1}}{GJ}\right]\left[ \left[\sin \overset{o}{\Lambda}\right]\left[ \left[\overset{o}{r_2}\right]\left[\overset{o}{2h}\right] - \left[\overset{o}{\mu}\right] \right] + \left[\cos \overset{o}{\Lambda}\right]\left[ \left[\overset{o}{\mu}\right]\left[\overset{o}{2h}\right] - \left[\overset{o}{J}\right] \right] \right] \right]$$

$$(B72)$$

where, as in equation (B38),

$$\{\alpha_s\} = \left[S_2{}'\right]\{l\} \qquad\qquad (B73)$$

It should be noted that, because of the assumed pressure distribution given by equation (B41), this correction does not correctly handle conditions involving deflected flaps and roll-control devices.

APPENDIX C

COMPUTATION OF $\{\alpha_g\}$ MATRICES

This appendix outlines the method by which the component parts of the $\{\alpha_g\}$ matrices may be determined. The $\{\alpha_g\}$ matrices comprise two classes of twist: (I) those which would be present even if the wing were rigid and (II) those due to inertia effects, thrust or drag, and section pitching moments on the flexible wing. A given airplane design condition may obviously require any combination of the twists listed under classes I and II, that is,

$$\{\alpha_g\} = \{\alpha_g\}_I + \{\alpha_g\}_{II} \tag{C1}$$

For simplicity, the sources of $\{\alpha_g\}$ may be summarized as follows:

Class I - aerodynamic twists (i.e., zero-lift-line shifts due to effects other than wing structural deflections)

(a) Built-in twist due to camber or construction, or both.

(b) Interference twist due to fuselage, external stores, and so forth.

(c) Twist due to flap deflection.

(d) Twist due to aileron deflection.

(e) Twist due to spoiler deflection.

(f) Apparent twist due to airplane rolling velocity.

(g) Apparent twist due to airplane pitching velocity. Angles of attack due to airplane pitching velocity should be measured at $3c/4$.

Class II - structural twists due to wing deflections caused by the following inertia and aerodynamic loadings which are independent of the wing lift distribution:

(a) Vertical acceleration acting upon dry-wing dead weight, wing internal-fuel dead weight, and external-stores dead weight.

(b) Effect of airplane rolling acceleration upon dry-wing dead weight, wing internal-fuel dead weight, and external-stores dead weight.

(c) Effect of airplane pitching acceleration upon dry-wing dead weight, wing internal-fuel dead weight, and external-stores dead weight.

(d) External-stores thrust or drag.

(e) Section pitching-moment coefficient with flaps, ailerons, spoilers, and so forth in neutral position.

(f) Incremental section pitching-moment coefficient due to flap deflection, aileron deflection, or spoiler deflection, or in various combinations.

Of the class I twists, the aerodynamic built-in twist is known from the wing geometry and the characteristics of the profiles used, and the interference twist may be obtained from actual tests of the complete airplane configuration, either model or full-scale, by using the procedure of appendix G or from other calculation methods. Twists due to control deflection are determinable from the same type of tests as were used to evaluate the interference twist. Apparent twists due to airplane rolling and pitching velocities are completely determined when the airplane flight condition to be investigated is specified.

The type of twists due to the effects of wing deflections arising from loads which are independent of wing angle of attack, such as those listed under class II, may be computed with the aid of equation (B33) since, in this case, $\left\{\alpha_s\right\} \equiv \left\{\alpha_g\right\}$

$$\left\{\alpha_g\right\} = \left[m\right]\left[\frac{2h}{\cos \Lambda}\right]\left[\frac{1}{EI}\right]\left\{M\right\} + \left[t\right]\left[\frac{2h}{\cos \Lambda}\right]\left[\frac{1}{GJ}\right]\left\{T\right\} \qquad (C2)$$

where $\left\{M\right\}$ and $\left\{T\right\}$ are the wing bending moments and the torsions along the wing elastic axis due to the loadings of class II or to any combination of them.

Although the $\left\{\alpha_g\right\}$ twists do not all explicitly require the calculation of loadings, they do influence the equilibrium airload and must be accounted for in determining the net wing loads from equations (21), (22), and (23).

# APPENDIX D

## DERIVATION OF EXTERNAL-STORE MATRICES

The term external stores as used in this report is intended to apply to such items as nacelles, external fuel tanks, bombs, rockets, and similar items commonly attached to the wings of airplanes.

In this appendix the lift coefficients and pitching-moment coefficients for each external store in the presence of the rest of the airplane configuration are assumed to be known and to vary linearly with angle of attack. On this basis a set of linear equations is developed in which the airloads on each external store are accounted for in computing the deflections of and airloads on the elastic wing or airplane. The coefficients used are based on the airplane wing area and the wing mean aerodynamic chord. There is a specific lateral reference axis for each external-store pitching-moment coefficient, and the angle of attack of the external store is taken to be the angle of attack of that wing station within the span of whose horseshoe vortex the station of the external store lies. Special symbols used in this appendix are as follows:

$C_{L_E}$, $C_{m_E}$      lift and pitching-moment coefficients, respectively, of an external store measured at its aerodynamic center (see eqs. (D1))

$C_{L_{E_0}}$, $C_{m_{E_0}}$      lift and pitching-moment coefficients, respectively, of an external store at zero angle of attack measured at its aerodynamic center

$L_{EO}$, $M_{EO}$      lift and pitching moment, respectively, of an external store measured at its aerodynamic center (see eqs. (D2))

$M_{X_\epsilon}$, $M_{X_{\epsilon+1}}$,      rolling moment at elastic-axis point around longitudinal axis through local elastic-axis point due to loads on a . . . $M_{X_n}$      particular store outboard of this point, positive when it tends to raise left wing tip, in-lb

$M_{Y_\epsilon}$, $M_{Y_{\epsilon+1}}$,      pitching moment at elastic-axis reference point around lateral axis through this reference point and due to . . . $M_{Y_n}$      loads on a particular store outboard of this point, positive when it tends to raise nose, in-lb

Additional symbols required are shown in the following sketch:
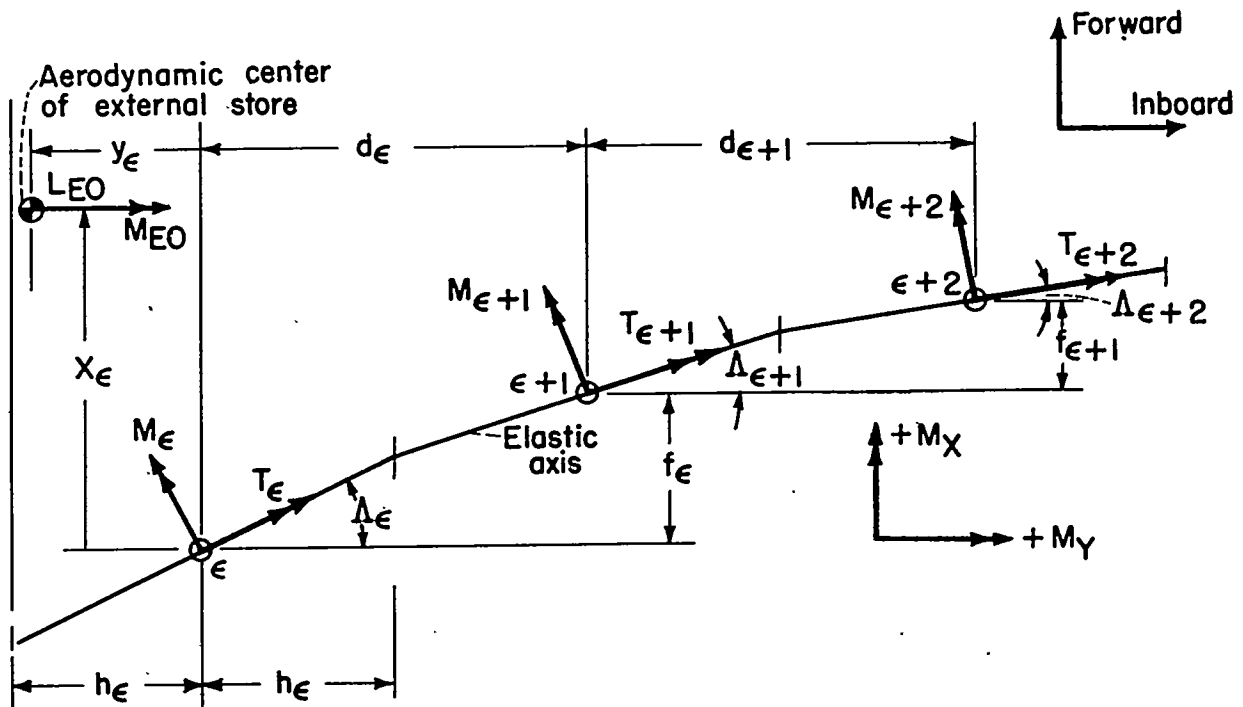
Consider one external store whose characteristics are

$$
\left.
\begin{aligned}
C_{L_E} &= C_{L_{E_0}} + \left(C_{L_E}\right)_\alpha \alpha_{f_E} \\[2ex]
C_{m_E} &= C_{m_{E_0}} + \left(C_{m_E}\right)_\alpha \alpha_{f_E}
\end{aligned}
\right\}
\qquad (\text{D1})
$$

so that

$$
\left.
\begin{aligned}
L_{EO} &= qS \left[ C_{L_{E_0}} + \left(C_{L_E}\right)_\alpha \alpha_{f_E} \right] \\[2ex]
M_{EO} &= qS\bar{c} \left[ C_{m_{E_0}} + \left(C_{m_E}\right)_\alpha \alpha_{f_E} \right]
\end{aligned}
\right\}
\qquad (\text{D2})
$$

The lift and moment on the external store $L_{EO}$ and $M_{EO}$ are located with respect to point $\epsilon$ by the dimensions $y_\epsilon$ and $x_\epsilon$ as shown in the sketch.

At the first station inboard of the external store $\epsilon$,

$$M_{X_\epsilon} = L_{EO} y_\epsilon$$

$$M_{Y_\epsilon} = M_{EO} + L_{EO} x_\epsilon$$

$$M_\epsilon = M_{X_\epsilon} \cos \Lambda_\epsilon - M_{Y_\epsilon} \sin \Lambda_\epsilon$$

$$= L_{EO}(y_\epsilon \cos \Lambda_\epsilon - x_\epsilon \sin \Lambda_\epsilon) - M_{EO} \sin \Lambda_\epsilon \qquad (D3)$$

$$T_\epsilon = M_{X_\epsilon} \sin \Lambda_\epsilon + M_{Y_\epsilon} \cos \Lambda_\epsilon$$

$$= L_{EO}(y_\epsilon \sin \Lambda_\epsilon + x_\epsilon \cos \Lambda_\epsilon) + M_{EO} \cos \Lambda_\epsilon \qquad (D4)$$

At the next inboard station $\epsilon + 1$,

$$M_{X_{\epsilon+1}} = L_{EO}(y_\epsilon + d_\epsilon)$$

$$M_{Y_{\epsilon+1}} = M_{EO} + L_{EO}(x_\epsilon - f_\epsilon)$$

$$M_{\epsilon+1} = L_{EO}\left[(y_\epsilon + d_\epsilon)\cos \Lambda_{\epsilon+1} - (x_\epsilon - f_\epsilon)\sin \Lambda_{\epsilon+1}\right] - M_{EO} \sin \Lambda_{\epsilon+1} \quad (D5)$$

$$T_{\epsilon+1} = L_{EO}\left[(y_\epsilon + d_\epsilon)\sin \Lambda_{\epsilon+1} + (x_\epsilon - f_\epsilon)\cos \Lambda_{\epsilon+1}\right] + M_{EO} \cos \Lambda_{\epsilon+1} \quad (D6)$$

At station $\epsilon + 2$,

$$M_{X_{\epsilon+2}} = L_{EO}(y_\epsilon + d_\epsilon + d_{\epsilon+1})$$

$$M_{Y_{\epsilon+2}} = M_{EO} + L_{EO}(x_\epsilon - f_\epsilon - f_{\epsilon+1})$$

$$M_{\epsilon+2} = L_{EO}\left[(y_\epsilon + d_\epsilon + d_{\epsilon+1})\cos \Lambda_{\epsilon+2} - (x_\epsilon - f_\epsilon - f_{\epsilon+1})\sin \Lambda_{\epsilon+2}\right] -$$

$$M_{EO} \sin \Lambda_{\epsilon+2} \qquad\qquad\qquad (D7)$$

$$T_{\epsilon+2} = L_{EO}\left[(y_\epsilon + d_\epsilon + d_{\epsilon+1})\sin \Lambda_{\epsilon+2} + (x_\epsilon - f_\epsilon - f_{\epsilon+1})\cos \Lambda_{\epsilon+2}\right] +$$

$$M_{EO} \cos \Lambda_{\epsilon+2} \qquad\qquad\qquad (D8)$$

At station $n$, the most inboard station considered,

$$M_{X_n} = L_{EO}\left(y_\epsilon + \sum_{m=\epsilon}^{n-1} d_m\right)$$

$$M_{Y_n} = M_{EO} + L_{EO}\left(x_\epsilon - \sum_{m=\epsilon}^{n-1} f_m\right)$$

Since

$$M_n = M_{X_n} \cos \Lambda_n - M_{Y_n} \sin \Lambda_n$$

$$T_n = M_{X_n} \sin \Lambda_n + M_{Y_n} \cos \Lambda_n$$

then,

$$M_n = L_{EO}\left[\cos \Lambda_n\left(y_\epsilon + \sum_{m=\epsilon}^{n-1} d_m\right) - \sin \Lambda_n\left(x_\epsilon - \sum_{m=\epsilon}^{n-1} f_m\right)\right] - M_{EO} \sin \Lambda_n$$

(D9)

and

$$T_n = L_{EO}\left[\sin \Lambda_n\left(y_\epsilon + \sum_{m=\epsilon}^{n-1} d_m\right) + \cos \Lambda_n\left(x_\epsilon - \sum_{m=\epsilon}^{n-1} f_m\right)\right] + M_{EO} \cos \Lambda_n$$

(D10)

In matrix notation, the following equations, typical for each external store on the semispan, are equivalent to the algebraic equations (D9) and (D10):

$$\{M_E\} = \left\{\left[\overset{o}{\cos} \Lambda\right]\{R\} - \left[\overset{o}{\sin} \Lambda\right]\{U\}\right\}L_{EO} - \left[\overset{o}{\sin} \Lambda\right]\{I_E\}M_{EO} \quad \text{(D11)}$$

$$\{T_E\} = \left\{\left[\overset{o}{\sin} \Lambda\right]\{R\} - \left[\overset{o}{\cos} \Lambda\right]\{U\}\right\}L_{EO} + \left[\overset{o}{\cos} \Lambda\right]\{I_E\}M_{EO} \quad \text{(D12)}$$

where, if the value at the top of the column is for the tip and the other values are for the successive stations inboard to the root and $\epsilon$ is the station within whose horseshoe span the external store is located,

$$\{R\} = \begin{Bmatrix} 0 \\ 0 \\ 0 \\ y_\epsilon \\ y_\epsilon + d_\epsilon \\ y_\epsilon + d_\epsilon + d_{\epsilon+1} \\ y_\epsilon + d_\epsilon + d_{\epsilon+1} + d_{\epsilon+2} \\ \cdot \end{Bmatrix}$$

(D13)

$$\{U\} = \begin{Bmatrix} 0 \\ 0 \\ 0 \\ x_\epsilon \\ x_\epsilon - f_\epsilon \\ x_\epsilon - f_\epsilon - f_{\epsilon+1} \\ x_\epsilon - f_\epsilon - f_{\epsilon+1} - f_{\epsilon+2} \\ . \end{Bmatrix} \tag{D14}$$

$$\{I_E\} = \begin{Bmatrix} 0 \\ 0 \\ 0 \\ 1 \\ 1 \\ 1 \\ . \end{Bmatrix} \tag{D15}$$

$$\{M_E\} = \begin{Bmatrix} 0 \\ 0 \\ 0 \\ M_\epsilon \\ M_{\epsilon+1} \\ M_{\epsilon+2} \\ . \end{Bmatrix} \tag{D16}$$

$$\{T_E\} = \begin{Bmatrix} 0 \\ 0 \\ 0 \\ T_\epsilon \\ T_{\epsilon+1} \\ T_{\epsilon+2} \\ . \end{Bmatrix} \tag{D17}$$

From equation (B33)

$$\{\alpha_s\}_E = [m] \begin{bmatrix} \overset{0}{\frac{2h}{\cos \Lambda}} \end{bmatrix} \begin{bmatrix} \overset{0}{\frac{1}{EI}} \end{bmatrix} \{M_E\} + [t] \begin{bmatrix} \overset{0}{\frac{2h}{\cos \Lambda}} \end{bmatrix} \begin{bmatrix} \overset{0}{\frac{1}{GJ}} \end{bmatrix} \{T_E\} \tag{D18}$$

where the external-store bending moment and torsion are given by equations (D11) and (D12), respectively.

Substitution of equations (D2) into equations (D11) and (D12) leads to:

$$\{M_E\} = \left\{ \left[\overset{o}{\cos}\,\Lambda\right]\{R\} - \left[\overset{o}{\sin}\,\Lambda\right]\{U\} \right\} qSC_{L_{E_0}} + \left\{ \left[\overset{o}{\cos}\,\Lambda\right]\{R\} - \right.$$

$$\left. \left[\overset{o}{\sin}\,\Lambda\right]\{U\} \right\} qS\left(C_{L_E}\right)_\alpha \alpha_{f_E} - \left[\overset{o}{\sin}\,\Lambda\right]\{I_E\} qS\bar{c}\,C_{m_{E_0}} -$$

$$\left[\overset{o}{\sin}\,\Lambda\right]\{I_E\} qS\bar{c}\left(C_{m_E}\right)_\alpha \alpha_{f_E} \qquad \text{(D19)}$$

and

$$\{T_E\} = \left\{ \left[\overset{o}{\sin}\,\Lambda\right]\{R\} + \left[\overset{o}{\cos}\,\Lambda\right]\{U\} \right\} qSC_{L_{E_0}} + \left\{ \left[\overset{o}{\sin}\,\Lambda\right]\{R\} + \right.$$

$$\left. \left[\overset{o}{\cos}\,\Lambda\right]\{U\} \right\} qS\left(C_{L_E}\right)_\alpha \alpha_{f_E} + \left[\overset{o}{\cos}\,\Lambda\right]\{I_E\} qS\bar{c}\,C_{m_{E_0}} +$$

$$\left[\overset{o}{\cos}\,\Lambda\right]\{I_E\} qS\bar{c}\left(C_{m_E}\right)_\alpha \alpha_{f_E} \qquad \text{(D20)}$$

For convenience, let

$$\{X_{2M}\} = \left\{ \left[\overset{o}{\cos}\,\Lambda\right]\{R\} - \left[\overset{o}{\sin}\,\Lambda\right]\{U\} \right\} \qquad \text{(D21)}$$

$$\{X_{2T}\} = \left\{ \left[\overset{o}{\sin}\,\Lambda\right]\{R\} + \left[\overset{o}{\cos}\,\Lambda\right]\{U\} \right\} \qquad \text{(D22)}$$

then equations (D19) and (D20) become

$$\{M_E\} = qS\left\{ \{X_{2M}\}C_{L_{E_0}} + \{X_{2M}\}\left(C_{L_E}\right)_\alpha \alpha_{f_E} - \left[\overset{o}{\sin}\,\Lambda\right]\{I_E\}\bar{c}\,C_{m_{E_0}} - \right.$$

$$\left. \left[\overset{o}{\sin}\,\Lambda\right]\{I_E\}\bar{c}\left(C_{m_E}\right)_\alpha \alpha_{f_E} \right\} \qquad \text{(D23)}$$

$$\{T_E\} = qS\left\{\{X_{2T}\}C_{L_{E_0}} + \{X_{2T}\}(C_{L_E})_\alpha \alpha_{f_E} + [\overset{o}{\cos} \Lambda]\{I_E\}\bar{c}C_{m_{E_0}} + \right.$$

$$\left. [\overset{o}{\cos} \Lambda]\{I_E\}\bar{c}(C_{m_E})_\alpha \alpha_{f_E}\right\} \tag{D24}$$

Now let

$$\{K_{1M}\} = \{X_{2M}\}C_{L_{E_0}} - [\overset{o}{\sin} \Lambda]\{I_E\}\bar{c}C_{m_{E_0}} \tag{D25}$$

$$\{K_{2M}\} = \{X_{2M}\}(C_{L_E})_\alpha - [\overset{o}{\sin} \Lambda]\{I_E\}\bar{c}(C_{m_E})_\alpha \tag{D26}$$

and

$$\{K_{1T}\} = \{X_{2T}\}C_{L_{E_0}} + [\overset{o}{\cos} \Lambda]\{I_E\}\bar{c}C_{m_{E_0}} \tag{D27}$$

$$\{K_{2T}\} = \{X_{2T}\}(C_{L_E})_\alpha + [\overset{o}{\cos} \Lambda]\{I_E\}\bar{c}(C_{m_E})_\alpha \tag{D28}$$

then

$$\{M_E\} = qS\left\{\{K_{1M}\} + \{K_{2M}\}\alpha_{f_E}\right\} \tag{D29}$$

$$\{T_E\} = qS\left\{\{K_{1T}\} + \{K_{2T}\}\alpha_{f_E}\right\} \tag{D30}$$

Equation (D18) relating $\{\alpha_s\}_E$ with $\{M_E\}$ and $\{T_E\}$ can now be written as

$$\{\alpha_s\}_E = qS\left\{\{K_1\} + \{K_2\}\alpha_{f_E}\right\} \tag{D31}$$

where

$$\{K_1\} = [m]\left[\overset{\circ}{\frac{2h}{\cos\Lambda}}\right]\left[\overset{\circ}{\frac{1}{EI}}\right]\{K_{1M}\} + [t]\left[\overset{\circ}{\frac{2h}{\cos\Lambda}}\right]\left[\overset{\circ}{\frac{1}{GJ}}\right]\{K_{1T}\}$$

$$\{K_2\} = [m]\left[\overset{\circ}{\frac{2h}{\cos\Lambda}}\right]\left[\overset{\circ}{\frac{1}{EI}}\right]\{K_{2M}\} + [t]\left[\overset{\circ}{\frac{2h}{\cos\Lambda}}\right]\left[\overset{\circ}{\frac{1}{GJ}}\right]\{K_{2T}\}$$

$$(D32)$$

The equations just derived are typical for a single external store on the semispan. Each additional external store on the semispan requires a similar set of equations.

The total angle-of-attack change due to the wing airloads shear and the airload on the external store is

$$\{\alpha_s\} = \{\alpha_s\}_W + \{\alpha_s\}_E \tag{D33}$$

where the subscript $W$ denotes wing and $E$ denotes external store.

Here there is an $\{\alpha_s\}_E$ term on the right-hand side for each external store; that is,

$$\{\alpha_s\} = \{\alpha_s\}_W + \{\alpha_s\}_{E_1} + \{\alpha_s\}_{E_2} + \cdots \tag{D34}$$

Equations (12), (13), and (B38) for $\{l\}$, $\{\alpha_f\}$, and $\{\alpha_s\}_W$, respectively, repeated for convenience are

$$\left[\overset{\circ}{\frac{1}{4qm_0}}\right][S_1]\{l\} = \{\alpha_f\}$$

$$\{\alpha_f\} = \{\alpha_r\} + \{\alpha_g\} + \{\alpha_s\}$$

$$[S_2]\{l\} = \{\alpha_s\}_W$$

Including the effects of external stores on $\{\alpha_s\}$ according to equations (D34) yields

$$\left[\frac{1}{4qm_o}\right]\left[S_1\right]\{\overset{o}{l}\} = \{\alpha_r\} + \{\alpha_g\} + \{\alpha_s\}_W + \{\alpha_s\}_{E_1} + \{\alpha_s\}_{E_2} + \cdots \qquad (D35)$$

From equation (D31)

$$\left.\begin{array}{l} \{\alpha_s\}_{E_1} = \{K_1\}_1 qS + \{K_2\}_1 qS\alpha_{f_{E_1}} \\[2em] \{\alpha_s\}_{E_2} = \{K_1\}_2 qS + \{K_2\}_2 qS\alpha_{f_{E_2}} \end{array}\right\} \qquad (D36)$$

However, $\alpha_{f_E}$ can be found from

$$\alpha_{f_{E_n}} = \lfloor E_n \rfloor \{\alpha_f\} \qquad (D37)$$

where a typical value for $\lfloor E_n \rfloor$ is given by

$$\lfloor E_n \rfloor = \lfloor 0 \quad 0 \quad 0 \quad 1 \quad 0 \quad 0 \quad 0 \quad 0 \quad 0 \quad 0 \rfloor \qquad (D38)$$

The row matrix $\lfloor E_n \rfloor$ has as many columns as there are horseshoe vortices on the semispan and has a value of unity entered in the column which corresponds to that horseshoe within whose span the external store is located. (In the example implied in eq. (D38) there are ten stations and the external store $n$ is within the span of the fourth horseshoe from the left wing tip.)

Combining equations (12) and (D37) results in

$$\alpha_{f_{E_n}} = \lfloor E_n \rfloor \left[\frac{1}{4qm_o}\right]\left[S_1\right]\{\overset{o}{l}\} \qquad (D39)$$

Combining equations (D35), (D36), (D39), and (B38) yields

$$\left[\frac{1}{4qm_0}\right]\left[S_1\right]\{\overset{o}{l}\} = \{\alpha_r\} + \{\alpha_g\} + \left[S_2\right]\{l\} +$$

$$qS\left\{\{K_1\}_1 + \left[\{K_2\}_1\lfloor E_1\rfloor\right]\left[\frac{1}{4qm_0}\right]\left[S_1\right]\{\overset{o}{l}\}\right\} +$$

$$qS'\left\{\{K_1\}_2 + \left[\{K_2\}_2\lfloor E_2\rfloor\right]\left[\frac{1}{4qm_0}\right]\left[S_1\right]\{\overset{o}{l}\}\right\} + \dots \qquad \text{(D40)}$$

Let

$$\left[A_n\right] = \{K_2\}_n\lfloor E_n\rfloor \qquad \{B_n\} = \{K_1\}_n \qquad \text{(D41)}$$

and

$$\left[A\right] = \sum\left[A_n\right] \qquad \{B\} = \sum\{B_n\} \qquad \text{(D42)}$$

If equations (D41) and (D42) are substituted into equation (D40), the following matrix equation is obtained for an elastic wing having a number of external stores on the semispan:

$$\left[\left[\left[I\right] - qS\left[A\right]\right]\left[\frac{1}{4qm_0}\right]\left[S_1\right] - \left[S_2\right]\right]\{\overset{o}{l}\} = \{\alpha_r\} + \{\alpha_g\} + qS\{B\} \qquad \text{(D43)}$$

This equation is similar in importance and usefulness to equation (16) except that the aeroelastic effects of the airloads upon the external stores are now included. It reduces to equation (16) if all the $\left[A\right]$ and $\{B\}$ matrices are set equal to zero, since $\left[I\right] = \left[\overset{o}{1.0}\right]$.

## APPENDIX E

## WING-FUSELAGE INTERFERENCE

In this appendix an approximate method of calculating the effect of a fuselage on the spanwise airload distribution on the wing is developed. The primary sources of this interference are considered (ref. 16) to be as follows:

(1) The effects of the image vortex system inside the fuselage on the downwash angles at the various control points over the wing semispan. This image vortex system induces a flow which is a first approximation to that necessary to satisfy the condition that there be zero velocity normal to the fuselage.

(2) The effects of the vertical "overvelocities" resulting from the fuselage angle of attack. These velocity increments affect the local angle of attack at the various control points on the wing.

This method of analysis can be used when applicable data of the type described in appendix G are not available.

Item (1) may be considered as the effects of wing airloads upon themselves due to the presence of the fuselage; whereas item (2) accounts for the effects resulting from the fuselage having an angle of attack.

In the development that follows the fuselage is assumed to be of circular cross section, of constant diameter, and infinitely long.

For the image vortex system mentioned in item (1), the individual images of the wing trailing vortices can be shown to be located on a straight line joining the axis of the fuselage with the axis of the particular wing trailing vortex at a distance from the fuselage center line such that

$$R_2 = \frac{a^2}{R_1} \tag{E1}$$

where $a$ is the fuselage radius and $R_1$ is the distance from the fuselage axis to the trailing vortex (see fig. 6).

In similar fashion the bound vortex is assumed to have an image within the fuselage cross section. The image of the bound vortex is

assumed to lie on a straight line joining the forward ends of the image
trailing vortices.  The forward ends of these image trailing vortices
are assumed to lie in the same transverse plane (perpendicular to the
airplane center line) that contains the particular bound vortex being
represented.  Figure 6(a) shows a transverse section for the high-midwing
configuration and figure 6(b) shows a plan view for the midwing
configuration.

This system of real and image vortices is only an approximation.
It satisfies the condition of no flow across the fuselage boundary only
at the transverse plane containing a bound vortex and its image and the
transverse plane infinitely far behind the wing.  In general, some flow
will occur across the fuselage boundaries, and hence, to some degree at
least, the corrective downwash velocities induced at the wing control
points by the image vortices will be in error.

Within these limitations it is therefore considered that wing-
fuselage interference effects upon the wing spanwise airload distribu-
tion can be obtained by:

(1) Adding to the elements of the $\left[S_1\right]$ matrix for the exposed wing
a corrective matrix $\left[S_i\right]$ whose elements represent the vertical downwash
velocities induced at the various wing horseshoe control points by the
image vortex system within the fuselage boundaries.

Each image vortex within the fuselage is of the same strength and
sense of circulation as its real counterpart and there are as many image
horseshoe vortices within the fuselage as are used to represent the wing.

(2) Adding to the twist of the wing $\left(\text{i.e., } \left\{\alpha_g\right\}\right)$ a correction due
to the vertical overvelocity field arising from the effects of fuselage
angle of attack.  The correction applied to $\left\{\alpha_g\right\}$ is proportional to
the quantity $(\alpha_r - \alpha_i)$ where $\alpha_r$ is the angle of attack of the wing
root-section zero-lift line and $\alpha_i$ is the incidence angle between the
wing root-section zero-lift line and the fuselage center line.

The above corrections are developed as follows.

The elements of the corrective matrix $\left[S_i\right]$ may be derived by considering the geometry of the following sketch:



Ogie is a horizontal plane
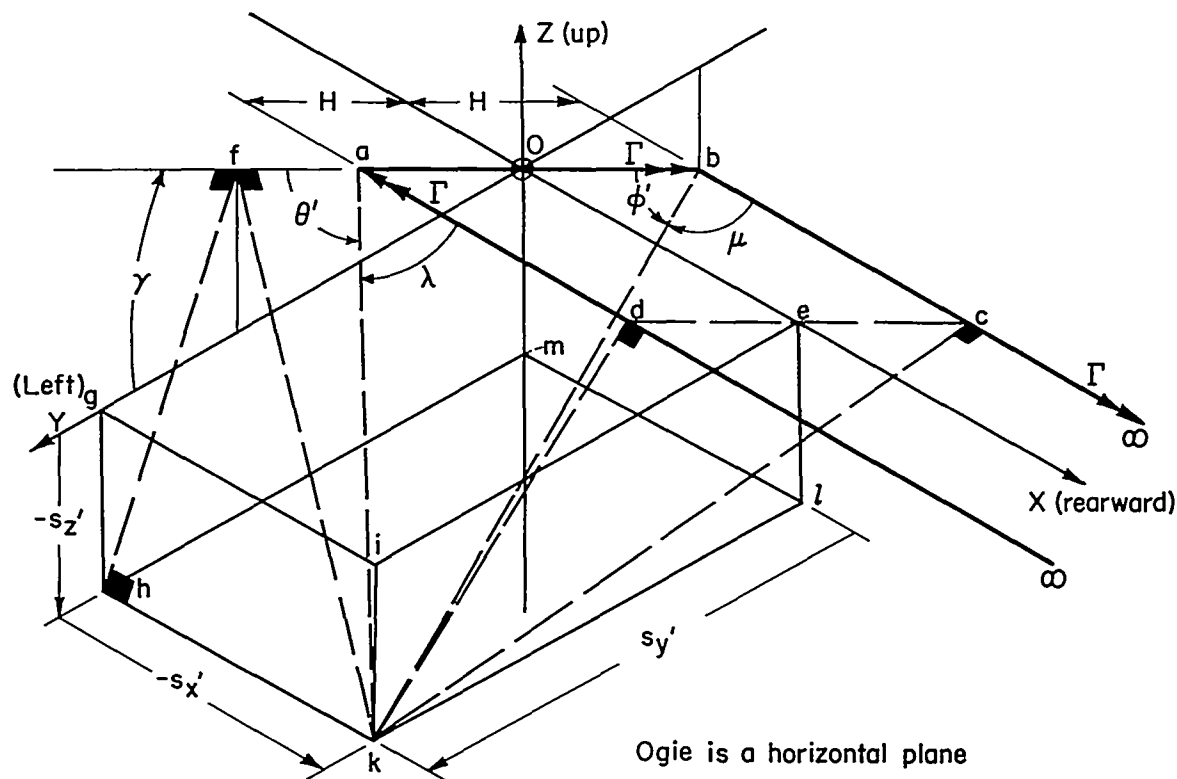
The horseshoe vortex shown in this sketch is considered to be one of the image vortices, the location of which is given by equation (E1). The strength of circulation $\Gamma$ of this image vortex is equal to that of its real counterpart. The plane of the horseshoe $\infty ab\infty$ is at an angle $\gamma$ to the horizontal plane Ogie and the bound vortex $\overline{ab}$ lies in the plane Omhg. The point $k$ may be considered to be one of the downwash control points as described in appendix A.

The total vertical downwash $w_k$ at the point $k$ due to this image horseshoe vortex is the sum of the contributions due to each segment. By means of equation (A27) the contribution of the trailing vortex $\overline{a\infty}$ is

$$w_{\overline{a\infty}} = \frac{-\Gamma}{4\pi}\left(\frac{1 + \cos\lambda}{B}\right)\left(\frac{s_y' - H\cos\gamma}{B}\right) \tag{E2}$$

that due to the trailing vortex $\overline{b\infty}$ is

$$w_{\overline{b\infty}} = \frac{\Gamma}{4\pi}\left(\frac{1 + \cos \mu}{A}\right)\left(\frac{s_y{}' + H \cos \gamma}{A}\right) \tag{E3}$$

and that due to the bound vortex $\overline{ab}$ is

$$w_{\overline{ab}} = \frac{\Gamma}{4\pi}\left(\frac{\cos \phi' - \cos \theta'}{D}\right)\left(\frac{s_x{}'}{D}\right) \tag{E4}$$

where

$$\left.\begin{array}{l} A = \overline{ck} \\[6pt] B = \overline{dk} \\[6pt] D = \overline{fk} \end{array}\right\} \tag{E5}$$

From the geometry of the sketch the distances $A$, $B$, and $D$ are found from

$$\left.\begin{array}{l} A^2 = \left(s_y{}' + H \cos \gamma\right)^2 + \left(s_z{}' + H \sin \gamma\right)^2 \\[8pt] B^2 = \left(s_y{}' - H \cos \gamma\right)^2 + \left(s_z{}' + H \sin \gamma\right)^2 \\[8pt] D^2 = s_x{}'^2 + \left(s_y{}' \sin \gamma - s_z{}' \cos \gamma\right)^2 \end{array}\right\} \tag{E6}$$

and the angles are obtained from

$$\left.\begin{array}{l} \theta' = \tan^{-1}\dfrac{\overline{fk}}{\overline{fa}} = \tan^{-1}\dfrac{D}{s_y{}' \cos \gamma + s_z{}' \sin \gamma - H} \\[14pt] \phi' = \tan^{-1}\dfrac{\overline{fk}}{\overline{fb}} = \tan^{-1}\dfrac{D}{s_y{}' \cos \gamma + s_z{}' \sin \gamma + H} \\[14pt] \lambda = \tan^{-1}\dfrac{\overline{dk}}{\overline{ad}} = \tan^{-1}\dfrac{B}{s_x{}'} \\[14pt] \mu = \tan^{-1}\dfrac{\overline{ck}}{\overline{bc}} = \tan^{-1}\dfrac{A}{s_x{}'} \end{array}\right\} \tag{E7}$$

Summing the individual downwash contributions (eqs. (E2), (E3), and (E4)) gives the total downwash at $k$ due to one image horseshoe

$$w_k = \frac{\Gamma}{4\pi}\left[\frac{\left(s_y{}' + H\cos\gamma\right)\left(1 + \cos\mu\right)}{A^2} + \frac{\left(\cos\phi' - \cos\theta'\right)s_x{}'}{D^2} - \right.$$

$$\left.\frac{\left(s_y{}' - H\cos\gamma\right)\left(1 + \cos\lambda\right)}{B^2}\right] \tag{E8}$$

The downwash angles at the control points on the wing due to the fuselage images may then be written in matrix notation as

$$\left\{\frac{w}{V}\right\}_i = \frac{1}{4\pi V}\left[S_i\right]\left\{\Gamma\right\} = \frac{1}{8\pi q}\left[S_i\right]\left\{\ell\right\} \tag{E9}$$

in which the desired correction matrix for image vortex effects is $\left[S_i\right]$, the elements of which are the locally applicable values of the function inside the brackets of equation (E8). The development for antisymmetrical conditions would be analogous to that for symmetrical conditions, the only change being that the sense of the vortices (and their images) on the left-hand side of the plane of symmetry in figure 6 would be reversed.

The second interference effect, that due to vertical overvelocity, may be taken into account as shown in the following analysis: With respect to the fuselage center line there is a transverse component of the free-stream velocity $V_z$, given by (see sketch)

$$V_z = V\left(\alpha_r - \alpha_i\right)$$
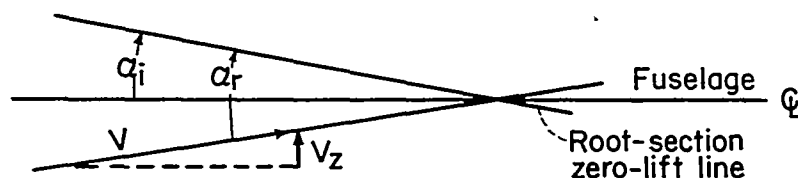


Since the fuselage displaces the air in this transverse flow field, there are local changes in this vertical flow velocity.

If $V_z{}'$ is equal to the total local vertical velocity in the presence of the fuselage, then the overvelocity $\Delta V_z$ is

$$\Delta V_z = V_z{}' - V_z \tag{E10}$$

This vertical overvelocity can be expressed as

$$\Delta V_z = \frac{\Delta V_z}{V_z} V\left(\alpha_r - \alpha_i\right) \tag{E11}$$

Contour maps from which the value of $\Delta V_z/V_z$ can be obtained as a function of vertical and lateral distances from the body center line are shown in figure 7.

These contours were developed from the equations for uniform flow past an infinitely long circular cylinder from reference 17 as follows:

$$V_z' = V_z\left(1 + \frac{\Delta V_z}{V_z}\right) \tag{E12}$$

$$\frac{V_z'}{V_z} = 1 + \frac{a^2 \cos 2\theta}{R^2} \tag{E13}$$

where $a$ is the cylinder radius, $R$ is the radial distance from the axis, and $\theta$ is measured from a line normal to the axis and $V_z$. Thus

$$\frac{\Delta V_z}{V_z} = \frac{a^2 \cos 2\theta}{R^2} \tag{E14}$$

From equation (E11) the angle-of-attack increment $\Delta\alpha_g$ at a control point due to the local overvelocity becomes

$$\Delta\alpha_g = \frac{\Delta V_z}{V_z}\left(\alpha_r - \alpha_i\right) \tag{E15}$$

Equation (E15) in matrix notation is

$$\left\{\Delta\alpha_g\right\} = \left[\overset{o}{S}_o\right]\left\{\alpha_r - \alpha_i\right\} \tag{E16}$$

where $\left[\overset{o}{S}_o\right]$ is a diagonal matrix whose elements are the locally applicable values of $\Delta V_z/V_z$; that is,

$$\left[\overset{o}{S}_o\right] = \left[\frac{\overset{o}{\Delta V_z}}{V_z}\right] \tag{E17}$$

By use of the matrices

$\left[S_1\right]$    downwash matrix given by equation (A38) for the wing alone
(the portion of the wing outboard of the fuselage)

$\left[S_2\right]$    wing elasticity matrix given by equation (B37)

$\left[S_{\mathbf{i}}\right]$    image-vortex matrix given by equation (E9)

$\left[\overset{o}{S_o}\right]$    overvelocity matrix given by equation (E17)

and the equation

$$\{\alpha_s\} = \left[S_2\right]\{l\}$$

the equation for wing equilibrium including fuselage-interference effects
can be written as

$$\left[\left[S_1\right] + \left[S_{\mathbf{i}}\right]\right]\{l\} = \left[\overset{o}{4qm_o}\right]\left\{\{\alpha_r + \alpha_g + \alpha_s\} + \left[\overset{o}{S_o}\right]\{\alpha_r - \alpha_{\mathbf{i}}\}\right\} \quad (E18)$$

or, in a more convenient form,

$$\left[\left[\overset{o}{\frac{1}{4qm_o}}\right]\left[\left[S_1\right] + \left[S_{\mathbf{i}}\right]\right] - \left[S_2\right]\right]\{l\} - \alpha_r\left[\left[I\right] + \left[\overset{o}{S_o}\right]\right]\{1\} = \{\alpha_g\} - \alpha_{\mathbf{i}}\left[\overset{o}{S_o}\right]\{1\}$$

$$(E19)$$

Equation (E19) may be substituted without change for equation (21) for
the wing load distribution.

APPENDIX F

EQUATIONS FOR TAILLESS AND TAIL-BOOM AIRPLANE CONFIGURATIONS

This appendix develops equations which, when properly inserted into the basic equations, allow solution for (1) a tailless airplane and (2) an airplane with the tail load entering the wing structure through tail booms. The equations are left in general form. Constant sweep angles and equal vortex spacing simplify the equations considerably.

### Tailless Airplane

For the case of a tailless airplane longitudinal balance is usually accomplished by the deflection of controls on the wing. These control deflections alter the span load distribution over the wing while contributing to the balance of the airplane, and therefore terms expressed as functions of the control deflection $\delta$ will appear in the lift-distribution equation (eq. (21)) and the pitching-moment balance equation (eq. (23)) in place of the $P_T$ terms. Since the lift produced by the control deflection is part of the wing lift, $P_T$ in the lift balance equation (eq. (22)) will be zero.

The development of expressions in terms of the control deflection follows.

The required expression for $\delta$ to be substituted into equation (21) consists of two $\alpha_g$ components; $\alpha_{g_I}$, which is the apparent twist due to control deflection, and $\alpha_{g_{II}}$, which is the twist due to section pitching moment with control deflected. From equation (C2)

$$\left\{\alpha_{g_{II}}\right\}_{c_m} = \left[m\right]\left[\frac{2h}{\cos \Lambda}\right]^{\circ}\left[\frac{1}{EI}\right]^{\circ}\left\{M\right\}_{c_m} + \left[t\right]\left[\frac{2h}{\cos \Lambda}\right]^{\circ}\left[\frac{1}{GJ}\right]^{\circ}\left\{T\right\}_{c_m} \tag{F1}$$

For class II twists due to section pitching-moment coefficient (type (f) in appendix C), the following equations may be written for $\left\{M\right\}_{c_m}$ and $\left\{T\right\}_{c_m}$ in equation (F1):

$$\left\{M\right\}_{c_m} = -q\left[\sin \Lambda\right]^{\circ}\left[I_3\right]\left[2hc^2\right]^{\circ}\left\{c_{m_o}\right\} \tag{F2}$$

$$\left\{T\right\}_{c_m} = q\left[\cos \Lambda\right]^{\circ}\left[I_3\right]\left[2hc^2\right]^{\circ}\left\{c_{m_o}\right\} \tag{F3}$$

where

$$
I_3 = \begin{bmatrix}
1/2 & 0 & 0 & 0 & \cdot & \cdot \\
1 & 1/2 & 0 & 0 & \cdot & \cdot \\
1 & 1 & 1/2 & 0 & \cdot & \cdot \\
1 & 1 & 1 & 1/2 & \cdot & \cdot \\
\cdot & \cdot & \cdot & \cdot & \cdot & \cdot \\
\cdot & \cdot & \cdot & \cdot & \cdot & \cdot
\end{bmatrix}
$$

For $[m]$ and $[t]$ in equation (F1), equations (B34) and (B35) may be written as

$$
[m] = -\left[I_0\right]\left[\overset{o}{\sin} \Lambda\right] \tag{F4}
$$

$$
[t] = \left[I_0\right]\left[\overset{o}{\cos} \Lambda\right] \tag{F5}
$$

where

$$
I_0 = \begin{bmatrix}
1/2 & 1 & 1 & 1 & \cdot & \cdot \\
0 & 1/2 & 1 & 1 & \cdot & \cdot \\
0 & 0 & 1/2 & 1 & \cdot & \cdot \\
0 & 0 & 0 & 1/2 & \cdot & \cdot \\
\cdot & \cdot & \cdot & \cdot & \cdot & \cdot \\
\cdot & \cdot & \cdot & \cdot & \cdot & \cdot
\end{bmatrix}
$$

Substituting equations (F2), (F3), (F4), and (F5) into equation (F1) yields

$$
\left\{\alpha_{g_{II}}\right\}_{c_m} = \left[I_0\right]\left[\overset{o}{2h}\right]\left[\left[\overset{o}{\tan} \Lambda\right]\left[\overset{o}{\frac{1}{EI}}\right]q\left[\overset{o}{\sin} \Lambda\right]\left[I_3\right]\left[\overset{o}{2hc^2}\right] + \right.
$$

$$
\left. \left[\frac{1}{GJ}\right]q\left[\overset{o}{\cos} \Lambda\right]\left[I_3\right]\left[\overset{o}{2hc^2}\right]\right]\left\{c_{m_0}\right\}
$$

or

$$\left\{\alpha_{g_{II}}\right\}_{c_m} = q\left[I_0\right]\left[2h\right]\left[\left[\tan^2\Lambda\right]\left[\frac{1}{EI}\right] + \left[\frac{1}{GJ}\right]\right]\left[\cos\Lambda\right]\left[I_3\right]\left[2hc^2\right]\left\{c_{m_0}\right\} \quad (F6)$$

Equation (F6) gives the structural twist due to control deflection. If wind-tunnel data are not available, theoretical expressions for $\left\{c_{m_0}\right\}$ in terms of the deflection $\delta$ may be used. From reference 18,

$$\left\{c_{m_0}\right\}_\delta = -\frac{1}{2}\left[\sin\theta_0 - \frac{1}{2}\sin 2\theta_0\right]\left\{\delta\right\}$$

where

$$\theta_0 = \sin^{-1}\left[2\sqrt{\xi(1-\xi)}\right]$$

$$\theta_0 = \cos^{-1}(2\xi - 1)$$

$$\xi = \frac{c_f}{c}$$

and $c_f$ is the flap chord. Substituting these values for $\theta_0$ results in

$$\left\{c_{m_0}\right\}_\delta = -\frac{1}{2}\left[2\sqrt{\xi(1-\xi)} - 2\sqrt{\xi(1-\xi)}(2\xi - 1)\right]\left\{\delta\right\}$$

$$= -2\left[\sqrt{\xi(1-\xi)^3}\right]\left\{\delta\right\} \quad (F7)$$

The $\alpha_{g_I}$ term required can be obtained from the following expression for the lift produced by control deflection (ref. 18):

$$\left\{c_l\right\}_\delta = 2\left[\pi - \theta_0 + \sin\theta_0\right]\left\{\delta\right\}$$

for a two-dimensional lift-curve slope of $2\pi$. For a two-dimensional lift-curve slope of $m_0$, this equation can be written as

$$\left\{c_l\right\}_\delta = \left[m_0\right]\left[1 - \frac{\theta_0}{\pi} + \frac{\sin\theta_0}{\pi}\right]\left\{\delta\right\}$$

Substituting the values for $\theta_0$ results in

$$\{c_l\}_\delta = \overset{\text{o}}{[m_0]}\left[1 - \frac{1}{\pi}\cos^{-1}(2\xi - 1) + \frac{1}{\pi}2\overset{\text{o}}{\sqrt{\xi(1-\xi)}}\right]\{\delta\} \tag{F8}$$

Dividing both sides by $\overset{\text{o}}{[m_0]}$ yields

$$\{\alpha_{g_I}\}_{c_m} = \left[1 - \frac{1}{\pi}\cos^{-1}(2\xi - 1) + \frac{1}{\pi}2\overset{\text{o}}{\sqrt{\xi(1-\xi)}}\right]\{\delta\} \tag{F9}$$

The total $\alpha_g$ term to be substituted for the $P_T$ term in the lift-distribution equation is obtained by combining equations (F6), (F7), and (F9), to give

$$\{\alpha_g\}_{c_m} = \{\alpha_{g_{II}}\}_{c_m} + \{\alpha_{g_I}\}_{c_m}$$

$$= 2q[I_0]\overset{\text{o}}{[2h]}\left[\overset{\text{o}}{[\tan^2\Lambda]}\overset{\text{o}}{\left[\frac{1}{EI}\right]} + \overset{\text{o}}{\left[\frac{1}{GJ}\right]}\right]\overset{\text{o}}{[\cos\Lambda]}\overset{\text{o}}{[I_3]}\overset{\text{o}}{[2hc^2]}\overset{\text{o}}{\left[\sqrt{\xi(1-\xi)^3}\right]}\{\delta\} -$$

$$\left[1 - \frac{1}{\pi}\cos^{-1}(2\xi - 1) + \frac{1}{\pi}2\overset{\text{o}}{\sqrt{\xi(1-\xi)}}\right]\{\delta\} \tag{F10}$$

For the pitching-moment balance equation (23) the expression required to replace $P_T$ may be obtained from the theoretical expression for flap pitching-moment coefficient (eq. (F7)) as

$$P_T = 2q\left[\frac{2hc^2}{x_T}\right]\left[\sqrt{\overset{\text{o}}{\xi(1-\xi)^3}}\right]\{\delta\} \tag{F11}$$

Since in the system of equations given in matrix form (eqs. (21), (22), and (23)) there are two unknowns other than $P_T$, it would not be

possible to have more than one unknown in the expression to be substituted for $P_T$; in other words, the $\{\delta\}$ matrix in equations (F10) and (F11) must have a known distribution shape. Let $\delta_r$ be the unknown reference deflection; the $\{\delta\}$ matrix may then be written as $\{\delta\} = \delta_r \left\{ \dfrac{\delta}{\delta_r} \right\}$ where

$\left\{ \dfrac{\delta}{\delta_r} \right\}$ is any chosen distribution shape. For the reference deflection at the second station from the tip this equation becomes

$$\{\delta\} = \delta_r \begin{Bmatrix} \delta_1/\delta_r \\ 1.0 \\ \delta_3/\delta_r \\ \cdot \\ \delta_{root}/\delta_r \end{Bmatrix}$$

For a constant deflection across the span, the distribution matrix becomes $\{1\}$.

### Balancing Tail Load Entering Wing Through Tail Boom

For the case where the tail load enters the wing structure through a tail boom, the distribution of load over the wing will be affected when the tail load changes and will vary in a different way depending on where the tail boom enters the wing. An expression to be substituted into the lift-distribution equation (21) for $P_T\{0\}$ is developed in this section of the appendix.

From figure 8, the beamwise moment produced at the point $P$ by the tail load entering the wing through the tail boom can be written as

$$M_{P_{T_{\epsilon_n}}} = \frac{P_T}{2} e_T \sin \Lambda_T + \frac{P_T}{2} y_P \cos \Lambda_T + \frac{P_T}{2} \sum_{m=\epsilon+1}^{n} \frac{d_m}{\cos \Lambda_m}$$

where $\Lambda_T$ is the sweep angle of the elastic axis at the entry section of the tail boom.

In matrix form

$$\{M\}_{P_T} = \frac{P_T}{2}\left[I_2\right]\left[\overset{o}{d}\right]\left[\frac{1}{\cos \Lambda}\right]\{I_T\} + \frac{P_T}{2}\left(e_T \sin \Lambda_T + y_P \cos \Lambda_T\right)\{I_T\} \quad (F12)$$

where $\left[I_2\right]$, $\{I_T\}$, and $\left[\overset{o}{d}\right]$ for six reference stations are defined as

$$\left[I_2\right] = \begin{bmatrix} 0 & 0 & 0 & 0 & 0 & 0 \\ 1 & 0 & 0 & 0 & 0 & 0 \\ 1 & 1 & 0 & 0 & 0 & 0 \\ 1 & 1 & 1 & 0 & 0 & 0 \\ 1 & 1 & 1 & 1 & 0 & 0 \\ 1 & 1 & 1 & 1 & 1 & 0 \end{bmatrix}$$

$$\{I_T\} = \begin{Bmatrix} 0 \\ 0 \\ 0 \\ 1 \\ 1 \\ 1 \end{Bmatrix} \begin{matrix} \text{Tip} \\ \\ \\ \leftarrow\text{Tail-boom entry point} \\ \\ \text{Root} \end{matrix}$$

$$\left[\overset{o}{d}\right] = \begin{bmatrix} 0 & 0 & 0 & 0 & 0 & 0 \\ 0 & 0 & 0 & 0 & 0 & 0 \\ 0 & 0 & 0 & 0 & 0 & 0 \\ 0 & 0 & 0 & 0 & 0 & 0 \\ 0 & 0 & 0 & 0 & d_{\epsilon+1} & 0 \\ 0 & 0 & 0 & 0 & 0 & d_{\epsilon+2} \end{bmatrix}$$

The equation for torque is

$$\{T\}_{P_T} = -\frac{P_T}{2}\left(e_T \cos \Lambda_T - y_P \sin \Lambda_T\right)\{I_T\} \tag{F13}$$

Substitution of equations (F4), (F5), (F12), and (F13) into equation (C2) gives an expression for the class II twist due to tail-boom entry:

$$\{\alpha_{g_{II}}\}_{P_T} = \left(\frac{P_T}{2}\right)\begin{bmatrix}I_0\end{bmatrix}\begin{bmatrix}\overset{o}{2h}\end{bmatrix}\left[-\begin{bmatrix}\overset{o}{\tan \Lambda}\end{bmatrix}\begin{bmatrix}\overset{o}{\frac{1}{EI}}\end{bmatrix}\begin{bmatrix}I_2\end{bmatrix}\begin{bmatrix}\overset{o}{d}\end{bmatrix}\begin{bmatrix}\overset{o}{\frac{1}{\cos \Lambda}}\end{bmatrix} + \right.$$

$$\left. \left(e_T \sin \Lambda_T + y_P \cos \Lambda_T\right)\begin{bmatrix}I\end{bmatrix}\right] - \begin{bmatrix}\overset{o}{\frac{1}{GJ}}\end{bmatrix}\left(e_T \cos \Lambda_T - y_P \sin \Lambda_T\right)\begin{bmatrix}I\end{bmatrix}\right]\{I_T\}$$

The column to be substituted into equation (21) is therefore

$$-\frac{1}{2}\begin{bmatrix}I_0\end{bmatrix}\begin{bmatrix}\overset{o}{2h}\end{bmatrix}\left[\begin{bmatrix}\overset{o}{\tan \Lambda}\end{bmatrix}\begin{bmatrix}\overset{o}{\frac{1}{EI}}\end{bmatrix}\begin{bmatrix}I_2\end{bmatrix}\begin{bmatrix}\overset{o}{d}\end{bmatrix}\begin{bmatrix}\overset{o}{\frac{1}{\cos \Lambda}}\end{bmatrix} + \right.$$

$$\left. \begin{bmatrix}\overset{o}{e_T \sin \Lambda_T + y_P \cos \Lambda_T}\end{bmatrix}\right] + \begin{bmatrix}\overset{o}{\frac{1}{GJ}}\end{bmatrix}\begin{bmatrix}\overset{o}{e_T \cos \Lambda_T - y_P \sin \Lambda_T}\end{bmatrix}\right]\{I_T\} \tag{F14}$$

This column will be multiplied by $P_T$ in equation (21). Equations (22) and (23) remain unchanged for this configuration.

## APPENDIX G

## METHOD OF REDUCING WIND-TUNNEL DATA

Difficulty is usually experienced in applying data obtained from wind-tunnel tests to the design of a full-scale airplane, especially in those cases where of necessity the stiffness of the model differs from that of the full-scale airplane.  The purpose of this appendix is to present a method of analysis by which model flexibility effects may be removed from the aerodynamic coefficients.

<u>Description of method</u>.- The method utilizes equation (12), which is

$$\left[S_1\right]\left\{l\right\} = \left[4qm_o^{\,o}\right]\left\{\alpha_f\right\}$$

where

$$\left\{\alpha_f\right\} = \left\{\left\{\alpha_r\right\} + \left\{\alpha_s\right\} + \left\{\alpha_g\right\}\right\}$$

When equation (12) is used for computing the lift distribution $\left\{l\right\}$ for a given full-scale airplane of any given flexibility, the $\left[S_1\right]$ and $\left\{\alpha_f\right\}$ matrices used depend only on the particular configuration and the given flight conditions, except for certain aerodynamic-twist components of the $\left\{\alpha_g\right\}$ matrix (see appendix C).  There remain to be selected, then, applicable values for these $\alpha_g$ components and for the $\left[m_o^{\,o}\right]$ matrix. These values may be determined with suitable data from wind-tunnel tests of a scaled model in conjunction with equation (12) as it applies to the model.

The approach taken is usually applicable and is based on the assumption that the following data are available from wind-tunnel tests of the model:  (a) the spanwise variation of the section normal-force coefficient obtained from integration of pressure data and (b) spanwise variation of section chord-line angle of attack with free-stream direction obtained from model deflection data.  These data should be available for each of several root-section angles of attack and at each of several Mach numbers over the essentially linear range of section lift coefficient.

A downwash matrix $\left[S_1\right]$ for the model should be computed according to procedures of appendix A. In general the horseshoe system should be identical with that which will be used in determination of the airload distribution on the full-scale airplane. The matrix for the model $\left[S_1\right]_M$ will then be equal to the reciprocal of the model scale factor times the $\left[S_1\right]$ matrix for the full-scale airplane, where the model scale factor is equal to the model span divided by the full-scale span.

The final angle-of-attack matrix for the model may be written as

$$\left\{\alpha_f\right\} = \left\{\left\{\alpha_r\right\} + \left\{\alpha_g\right\}_{I_a} + \left\{\alpha_s\right\}_M\right\} + \left\{\alpha_g\right\}_{I_b}$$

$$= \left\{\alpha\right\}_{meas} + \left\{\alpha_g\right\}_{I_b} \tag{G1}$$

where

$\left\{\alpha_r\right\}$     angle of attack of root section with undisturbed stream (measured)

$\left\{\alpha_g\right\}_{I_a}$     built-in twist (known)

$\left\{\alpha_s\right\}_M$     twist due to model flexibility (measured)

$\left\{\alpha_g\right\}_{I_b}$     interference twist due to aerodynamic interference effects of neighboring bodies (fuselage, nacelles, external stores, etc.) upon the wing (unknown)

$\left\{\alpha\right\}_{meas}$     sum of measured or known values

Equation (12) for the model then becomes

$$\left[\frac{1}{4q}\right]\left[S_1\right]_M\left\{l\right\} = \left[\overset{o}{m_o}\right]\left\{\left\{\alpha\right\}_{meas} + \left\{\alpha_g\right\}_{I_b}\right\} \tag{G2}$$

Since measured values of $\left\{l\right\}$ are used, equation (G2) represents a system of independent equations (one for each reference spanwise station of the model) which do not require a simultaneous solution.

If $\left\{\alpha_g\right\}_{I_b}$ is assumed to be invariant with change in wing angle of attack, the following matrices may be computed from data taken at two different root-section angles of attack:

$$\left\{\Delta\alpha_f\right\} = \left\{\alpha_2\right\}_{meas} - \left\{\alpha_1\right\}_{meas} \tag{G3}$$

$$\left\{\Delta l\right\} = \left\{l_2\right\} - \left\{l_1\right\} \tag{G4}$$

The matrices $\left\{\Delta\alpha_f\right\}$ and $\left\{\Delta l\right\}$ may be substituted for $\left\{\alpha\right\}_{meas}$ and $\left\{l\right\}$ in equation (G2), since the term $\left\{\alpha_g\right\}_{I_b}$ has been eliminated, and the applicable values of $\left\{m_o\right\}$ can be computed from

$$\left\{m_o\right\} = \left[\frac{1}{4q\,\Delta\alpha}\right]\left[S_1\right]_M\left\{\Delta l\right\} \tag{G5}$$

The interference twist $\left\{\alpha_g\right\}_{I_b}$ may now be computed from equation (G2) by using the values of $\left\{m_o\right\}$ computed from equation (G5) and the values of $\left\{l\right\}$ and $\left\{\alpha\right\}_{meas}$ measured at any root-section angle of attack, for example $\left\{l_2\right\}$ and $\left\{\alpha_2\right\}_{meas}$.

The foregoing procedure indicates the simplest solution for the constants in the straight-line equations given by equations (G2). If desired, equations (G2) may each be solved somewhat more accurately for $\left\{m_o\right\}$ and $\left\{\alpha_g\right\}_{I_b}$ by a least-squares procedure which utilizes values of $\left\{l\right\}$ and $\left\{\alpha\right\}_{meas}$ taken at several values of root-section angles of attack.

If the interference twist $\alpha_{g_{I_b}}$ at any section is assumed to include a component that varies with change in some section chord-line angle of attack, the method is still applicable to a close approximation. In this case the variable interference effects will appear implicitly in $\left\{m_o\right\}$.

The approximation arises from the assumption (implied in the above solution) that for a body at some spanwise station $j$ there exists an

interference twist at some other station $i$ which is proportional to the change in geometric angle at $i$; whereas in actuality the interference twist at station $i$ is proportional to change in geometric angle at the body station $j$.

Justification for the assumption can be shown as follows. Denote interference twist by $\alpha_I$, and the measured section chord-line angles at stations $i$ and $j$ by $\alpha_i$ and $\alpha_j$. Interference twist at station $i$ due to the body at station $j$ is written as the sum of a constant plus a variable twist

$$\left(\alpha_I\right)_i = \left(\alpha_{I_o}\right)_i + k_{ij}\alpha_j$$

where $k_{ij}$ is the proportionality constant. The final angle of attack at station $i$ then is

$$\left(\alpha_f\right)_i = \alpha_i + k_{ij}\alpha_j + \left(\alpha_{I_o}\right)_i$$

and equation (G2) for the spanwise station $i$ is

$$\frac{1}{4q}\lfloor S_1 \rfloor_i \{l\} = m_i\left(\alpha_i + k_{ij}\alpha_j + \left(\alpha_{I_o}\right)_i\right)$$

However,

$$\alpha_j = \alpha_i + \left(\alpha_j - \alpha_i\right)$$

therefore,

$$\frac{1}{4q}\lfloor S_1 \rfloor_i \{l\} = m_i\left(\left(1 + k_{ij}\right)\alpha_i + k_{ij}\left(\alpha_j - \alpha_i\right) + \left(\alpha_{I_o}\right)_i\right) \quad (G6)$$

The middle term is small compared to the first term and may be neglected since, for station $i$ close to station $j$, the difference $\alpha_j - \alpha_i$ is negligible, and for station $i$ far from station $j$ the interference

effect and therefore k is negligible. If the middle term is neglected, equation (G6) becomes equivalent to equation (G2) and the factor $1 + k_{ij}$ is apparent in the values of $m_0$ computed by equation (G5) even though it does not appear explicitly; that is, $m_0$ computed by equation (G5) is equal to the term $m_i(1 + k_{ij})$ in equation (G6).

Although only interference twist was considered in the foregoing description, the method is obviously applicable for determining other aerodynamic twists (see appendix C), for example, that due to flap deflection.

The foregoing method of analyzing data is relatively simple and straightforward and has the following advantages over other currently available methods:

(1) It provides a means by which data obtained from wind-tunnel tests of a properly instrumented elastic model wing can be evaluated for application to a full-scale wing of different elasticity distribution.

(2) It evaluates the variation of effective section lift-curve slope and of aerodynamic twist across the span as influenced by the presence of the fuselage, the nacelles, and other bodies on or near the wing (these obviously include spoilers, ailerons, and flaps).

(3) It determines the manner in which section lift-curve slope varies with Mach number.

Although the variation of lift-curve slope with Mach number can be obtained by the foregoing method by using wind-tunnel data at various Mach numbers, it is sometimes desired to determine the change (or changes) in lift distribution for section configurations for which suitable wind-tunnel data are not available, for example, variation of section lift with flap deflection $c_{l_\delta}$.

If the incompressible value of $c_{l_\delta}$ can be obtained or estimated by some means (e.g., from tests for the flap deflected at some other station) and if the effective sweep angle at the new flap station is known, then compressible values of $c_{l_\delta}$ can be obtained by substituting the $c_{l_\delta}$ values for the section lift-curve slopes in equation (A39)

$$m_0 = \frac{m}{\sqrt{1 - M^2 \cos^2 \Lambda_M}}$$

where $m_0$ and $m$ are the compressible and incompressible section lift-curve slopes, respectively.

It is therefore advantageous to evaluate the spanwise variation of $\Lambda_M$. The effective sweep angle for each section can be obtained from equation (A39) by using the previously measured variation of $m_0$ with Mach number. For example, equation (A39) can be rewritten as the linear equation (linear in squared terms)

$$\left(m^2\right)\left(\frac{1}{m_0{}^2}\right) + \left(\cos^2\Lambda_M\right)\left(M^2\right) = 1$$

This equation can be solved for $m$ and $\Lambda_M$ by a least-squares procedure if a series of equations are formed by substituting the values of $m_0$ and $M$ obtained for each of several Mach numbers.

Alternatively, a solution for $m$ and $\Lambda_M$ can be obtained by a graphical procedure (ref. 19). Plot the variation of $m_0$ with $M$ in a fashion such that the abscissa (M-scale) is proportional to the factor $1/\sqrt{1 - M^2\cos^2\Lambda_M}$. The plotted points will fall on a straight line which passes through the pole $\left(m_0 = 0, \ 1/\sqrt{1 - M^2\cos^2\Lambda_M} = 0\right)$, provided $\Lambda_M$ is correctly chosen and the law (eq. (A39)) applies. Note that $1/\sqrt{1 - M^2\cos^2\Lambda_M} = 1.0$ when $M = 0$. A form is presented in figure 9 by which the $m_0$ values can be conveniently plotted on such an abscissa scale for each of a number of values of $\Lambda_M$. For example, if a value of $\Lambda_M$ is tentatively chosen as $\Lambda_M = 30°$, draw a horizontal line intersecting the right-hand ordinate at $30°$. The intersections of this horizontal line with the Mach number lines are the abscissa locations for the indicated discrete values of $M$. Values of $m_0$ are then appropriately plotted vertically above or below these intersections. The intersection of this horizontal line with the pole-distance curve gives the pole location in scale units to the left of the abscissa point $M = 0$. The desired value of $\Lambda_M$ is then the one which gives the most nearly linear variation of the plotted data with consideration given to the pole point. The desired $m$ is the value of the intercept at $M$ equal to zero.

Illustrative example.- This section presents an analysis of wind-tunnel data obtained on a flexible model to determine the compressible section lift-curve slopes $\{m_0\}$.

The model was a wing-fuselage configuration with nacelles mounted below and forward of the wing on sweptforward struts attached to the wing semispan stations $\eta = 0.37$ and $0.65$. The wing had the following additional pertinent physical characteristics:

Aspect ratio . . . . . . . . . . . . . . . . . . . . . . . . . . . . . . . . 8.55
Taper ratio . . . . . . . . . . . . . . . . . . . . . . . . . . . . . . . . 0.40
Sweep at quarter-chord line, deg . . . . . . . . . . . . . . . . . . . . . . 35

and the locus of aerodynamic centers was assumed to coincide with the quarter-chord line.

The model wing was instrumented with strain gages cemented to the surface of the wing steel spar along one semispan and with pressure orifices located along streamwise chord sections on the opposite semi-span at stations $\eta$ = 0.155, 0.35, 0.56, 0.75, and 0.92.

Tests were made at root-section angles of attack of $0^\circ$ and $6^\circ$ for Mach numbers 0.30, 0.50, 0.70, 0.75, and 0.80.

The spanwise variation in section angle of attack for each test condition was obtained from the root-section angles of attack in conjunction with strain-gage readings. The spanwise variation in section normal-force coefficient for each test condition was obtained by a spanwise fairing of the various local integrated chordwise pressure distributions.

Elements of the $\begin{bmatrix} S_1 \end{bmatrix}$ matrix were computed for wing semispan stations $\eta$ = 0.10, 0.30, 0.50, 0.70, 0.85, 0.925, and 0.975. The resulting matrix is

$$
\begin{bmatrix} S_1 \end{bmatrix} =
\begin{bmatrix}
0.14869 & -0.04630 & -0.01249 & -0.00482 & -0.00149 & -0.00082 & -0.00063 \\
-0.04084 & 0.14811 & -0.05547 & -0.00793 & -0.00188 & -0.00094 & -0.00070 \\
-0.00287 & -0.01260 & 0.07827 & -0.02713 & -0.00285 & -0.00121 & -0.00084 \\
-0.00042 & -0.00068 & -0.00426 & 0.04382 & -0.01109 & -0.00229 & -0.00130 \\
-0.00013 & -0.00017 & -0.00053 & -0.00522 & 0.04153 & -0.01143 & -0.00287 \\
-0.00008 & -0.00009 & -0.00023 & -0.00093 & -0.00617 & 0.03969 & -0.01307 \\
-0.00006 & -0.00006 & -0.00015 & -0.00050 & -0.00124 & -0.00794 & 0.02917
\end{bmatrix}
$$

where the columns read down from the tip to the root and the rows read across from the tip to the root. For these same stations $\Delta c_n c/4$ and increments of section geometric angle of attack $\Delta\alpha$ due to the $6^\circ$ change in root angle of attack were computed from data at each test Mach number and tabulated in table I.

Substitution of $\{\Delta l\} = \{\Delta c_n qc\}$ for $\{l\}$ and $\{\Delta\alpha\}$ for $\{\alpha_f\}$ in equation (12) gives

$$
\begin{Bmatrix} S_1 \end{Bmatrix}_M \begin{Bmatrix} \dfrac{\Delta c_n c}{4} \end{Bmatrix} = \begin{bmatrix} \overset{o}{m_o} \end{bmatrix} \{\Delta\alpha\}
$$

from which the values $\left[\overset{o}{m_o}\right]$ were computed and tabulated in table I. Values of $m_o$ for $\eta = 0.975$ are not shown since $m_o$ is very sensitive to the manner in which the spanwise variation of $\Delta c_n$ is faired in the region of the wing tip. These values for each wing station are plotted against Mach number in figure 10(a).

Since the $\left[S_1\right]$ matrix is based upon the "wing alone" configuration, the body interference effects which vary with body angle of attack will be apparent in the values of lift-curve slope particularly for those stations near the wing root.

It was assumed that the Prandtl-Glauert relationship was applicable for these data. Accordingly the $\{m_o\}$ values were plotted (by using a form similar to that shown in fig. 9) for various selected values of $\Lambda_M$.

The plots which yielded the most nearly linear variation of the data are reproduced in figure (10(b)) for each span station. In selecting the plot which gave the most linear variation of $m_o$, consideration was given to the fact that at very low Mach numbers (approx. 0.30) the value of $m_o$ could be affected by Reynolds number; whereas those obtained for high Mach numbers would reflect the effects of shocks, and so forth. These points were therefore given less weight in determining the best fit.

Plots showing the spanwise variation of effective section sweep angle $\Lambda_M$ and lift-curve slope $m$ are given in figure 11.

APPENDIX H

CALCULATION OF THE DIVERGENCE DYNAMIC PRESSURE

Although the sweptback wing is usually considered to be divergence-free, it is conceivable that, with a large external diverging torque such as may be contributed by a tip tank, the wing could diverge. This appendix is concerned with the calculation of the dynamic pressure at which divergence will occur.

An expression for the static lift on a flexible swept wing with an external tank has been derived in appendix D and, for a divergence investigation, may be written as follows:

$$\left[\left[[I] - qS[A]\right]\left[\overset{o}{\frac{1}{4qm_o}}\right][S_1] - [S_2]\right]\{l\} = \{\alpha_r\} \qquad (H1)$$

This is a matrix equation in which the elements in the column represent the lifts on the various spanwise segments of the wing. The total lift can be found from equation (H1) by multiplying the lift per unit span by the row matrix $\lfloor 2h \rfloor$ where $2h$ defines the segment width in the spanwise direction. Then

$$L = 2\lfloor 2h \rfloor \{l\} = 2\lfloor 2h \rfloor\left[\left[[I] - qS[A]\right]\left[\overset{o}{\frac{1}{4qm_o}}\right][S_1] - [S_2]\right]^{-1}\{\alpha_r\}$$

or

$$L = 2\lfloor 2h \rfloor\left[\left[\frac{1}{q}[I] - S[A]\right]\left[\overset{o}{\frac{1}{4m_o}}\right][S_1] - [S_2]\right]^{-1}\{\alpha_r\} \qquad (H2)$$

Equation (H2) represents the lift on a wing in static equilibrium. Under the condition of wing divergence the equilibrium wing lift would be infinite.

The divergence speed is then represented by the lowest value of $q$ for which the lift in equation (H2) becomes infinite. For the right-hand side to be infinite, the determinant of the matrix whose inverse is given in equation (H2) must be zero, or

$$\left|\left[\frac{1}{q}[I] - S[A]\left[\frac{1}{4m_0}\right]^o[S_1]\right] - [S_2]\right| = 0$$

which can be written in the form

$$\left|\frac{1}{q}\left[\frac{1}{4m_0}\right]^o[S_1] - S[A]\left[\frac{1}{4m_0}\right]^o[S_1] - [S_2]\right| = 0 \qquad (H3)$$

The procedure is to solve for the lowest value of $q$ which satisfies equation (H3). From the Cayley-Hamilton theorem, the dominant or highest modulus root $\lambda$ in the equation

$$\lambda[I] - [D] = [O] \qquad (H4)$$

may be found by iterating the matrix $[D]$. In this case equation (H3) may be put in the form of equation (H4) by multiplying through by

$$\left[\left[\frac{1}{4m_0}\right]^o[S_1]\right]^{-1}$$

The result is

$$\frac{1}{q}[I] - \left[\left[\frac{1}{4m_0}\right]^o[S_1]\right]^{-1}\left[S[A]\left[\frac{1}{4m_0}\right]^o[S_1] + [S_2]\right] = [O] \qquad (H5)$$

Now $\lambda = \frac{1}{q}$; therefore, iteration of the matrix product

$$\left[\left[\begin{array}{c}\phantom{0}\\ \frac{1}{4m_0}\end{array}\right][S_1]\right]^{-1}\left[S[A]\left[\begin{array}{c}\phantom{0}\\ \frac{1}{4m_0}\end{array}\right][S_1] + [S_2]\right] \qquad (H6)$$

will yield the lowest value of  q,  which in this case is the desired divergence dynamic pressure.

The theory of matrix iteration may be found in reference 20; however, a simple outline of the steps required to iterate the matrix product (H6) to obtain the divergence dynamic pressure is given here.  First a trial column is chosen and this column is premultiplied by matrix (H6) to obtain a result column.  The elements of this result column are divided by the last element of the result column and then become the elements of a second trial column (the last element will be unity, having been divided by itself).  The second trial column is then premultiplied by matrix (H6) to yield a second result column.  This procedure is repeated until the same value is obtained for the last element in two successive result matrices.  The reciprocal of this value is the desired divergence dynamic pressure  q.

# REFERENCES

1. Diederich, Franklin W.:  Calculation of the Aerodynamic Loading of Swept and Unswept Flexible Wings of Arbitrary Stiffness.  NACA Rep. 1000, 1950.  (Supersedes NACA TN 1876.)

2. Weissinger, J.:  The Lift Distribution of Swept-Back Wings.  NACA TM 1120, 1947.

3. Falkner, V. M.:  The Calculation of Aerodynamic Loading on Surfaces of Any Shape.  R. & M. No. 1910, British A.R.C., 1943.

4. Mutterperl, William:  The Calculation of Span Load Distributions on Swept-Back Wings.  NACA TN 834, 1941.

5. Wieghardt, Karl:  Chordwise Load Distribution of a Simple Rectangular Wing.  NACA TM 963, 1940.

6. Krahn, E.:  Steady Subsonic Flows.  Reps. and Translations No. 994, British M.A.P. Völkenrode, Apr. 15, 1948.

7. Busemann, A.:  Swept-Back Wings at High Speeds.  Translation No. F-TS-629-RE, Air Materiel Command, U. S. Army Air Forces, Oct. 1946.

8. Jones, Robert T.:  Wing Plan Forms for High-Speed Flight.  NACA Rep. 863, 1947.  (Supersedes NACA TN 1033.)

9. Lippisch, A., and Beuschausen, W.:  Pressure Distribution Measurements at High Speed and Oblique Incidence of Flow.  NACA TM 1115, 1947.

10. Gothert, B.:  High-Speed Measurements on a Swept-Back Wing (Sweepback Angle $\varphi = 35^{\circ}$).  NACA TM 1102, 1947.

11. Dannenberg, Robert E.:  Measurements of Section Characteristics of a $45^{\circ}$ Swept Wing Spanning a Rectangular Low-Speed Wind Tunnel as Affected by the Tunnel Walls.  NACA TN 2160, 1950.

12. Murray, Harry E.:  Comparison With Experiment of Several Methods of Predicting the Lift of Wings in Subsonic Compressible Flow.  NACA TN 1739, 1948.

13. Göthert, B.:  Plane and Three-Dimensional Flow at High Subsonic Speeds.  NACA TM 1105, 1946.

14. DeYoung, John, and Harper, Charles W.:  Theoretical Symmetric Span
    Loading at Subsonic Speeds for Wings Having Arbitrary Plan Form.
    NACA Rep. 921, 1948.

15. Van den Broek, J. A.:  Elastic Energy Theory.  John Wiley and Sons,
    Inc., 1942.

16. Lennertz, J.:  On the Mutual Reaction of Wings and Body.  NACA
    TM 400, 1927.

17. Glauert, H.:  The Elements of Aerofoil and Airscrew Theory.  Second
    ed., Cambridge Univ. Press, 1948, p. 30.

18. Cahill, Jones R.:  Summary of Section Data on Trailing-Edge High-
    Lift Devices.  NACA Rep. 938, 1949.  (Supersedes NACA RM L8D09.)

19. Helmbold, Heinrich B.:  ATI Report 11-15 August 1945 (Heinkel
    Report).  Translation No. F-TS-679-RE, Air Materiel Command,
    U. S. Army Air Forces, Oct. 1946.

20. Frazer, R. A., Duncan, W. J., and Collar, A. R.:  Elementary Matrices
    and Some Applications to Dynamics and Differential Equations.  The
    Macmillan Co., 1946.

## TABLE I.- MEASURED DATA AND RESULTING SECTION LIFT-CURVE SLOPES FOR

## WIND-TUNNEL MODEL OF APPENDIX G

| $\eta$ | M = 0.30 | | | M = 0.50 | | | M = 0.70 | | |
|---|---|---|---|---|---|---|---|---|---|
| | $\Delta c_n c/4$ | $\Delta\alpha$, radians | $m_o$ | $\Delta c_n c/4$ | $\Delta\alpha$, radians | $m_o$ | $\Delta c_n c/4$ | $\Delta\alpha$, radians | $m_o$ |
| 0.975 | 13.897 | 0.10135 | ---- | 13.628 | 0.09665 | ---- | 14.358 | 0.09117 | ---- |
| .925 | 16.966 | .10140 | 4.75 | 17.460 | .09672 | 5.08 | 18.819 | .09132 | 6.20 |
| .85 | 20.775 | .10148 | 5.41 | 21.682 | .09710 | 5.54 | 22.998 | .09192 | 6.08 |
| .70 | 24.390 | .10217 | 4.83 | 27.023 | .09849 | 5.98 | 28.903 | .09422 | 6.71 |
| .50 | 30.490 | .10317 | 5.84 | 31.658 | .10097 | 6.25 | 33.669 | .09832 | 6.79 |
| .30 | 36.112 | .10401 | 6.97 | 36.112 | .10294 | 6.69 | 38.241 | .10177 | 6.93 |
| .10 | 37.485 | .10455 | 7.19 | 39.490 | .10424 | 7.74 | 43.587 | .10392 | 8.72 |

| $\eta$ | M = 0.75 | | | M = 0.80 | | |
|---|---|---|---|---|---|---|
| | $\Delta c_n c/4$ | $\Delta\alpha$, radians | $m_o$ | $\Delta c_n c/4$ | $\Delta\alpha$, radians | $m_o$ |
| 0.975 | 15.510 | 0.08972 | ---- | 15.433 | 0.08762 | ---- |
| .925 | 19.684 | .08997 | 6.59 | 20.631 | .08792 | 6.97 |
| .85 | 23.814 | .09066 | 6.46 | 25.492 | .08867 | 7.07 |
| .70 | 29.548 | .09316 | 6.86 | 31.804 | .09152 | 7.45 |
| .50 | 34.837 | .09772 | 7.15 | 37.886 | .09662 | 7.83 |
| .30 | 39.077 | .10137 | 7.00 | 42.650 | .10082 | 7.59 |
| .10 | 45.157 | .10382 | 9.09 | 50.126 | .10382 | 10.16 |
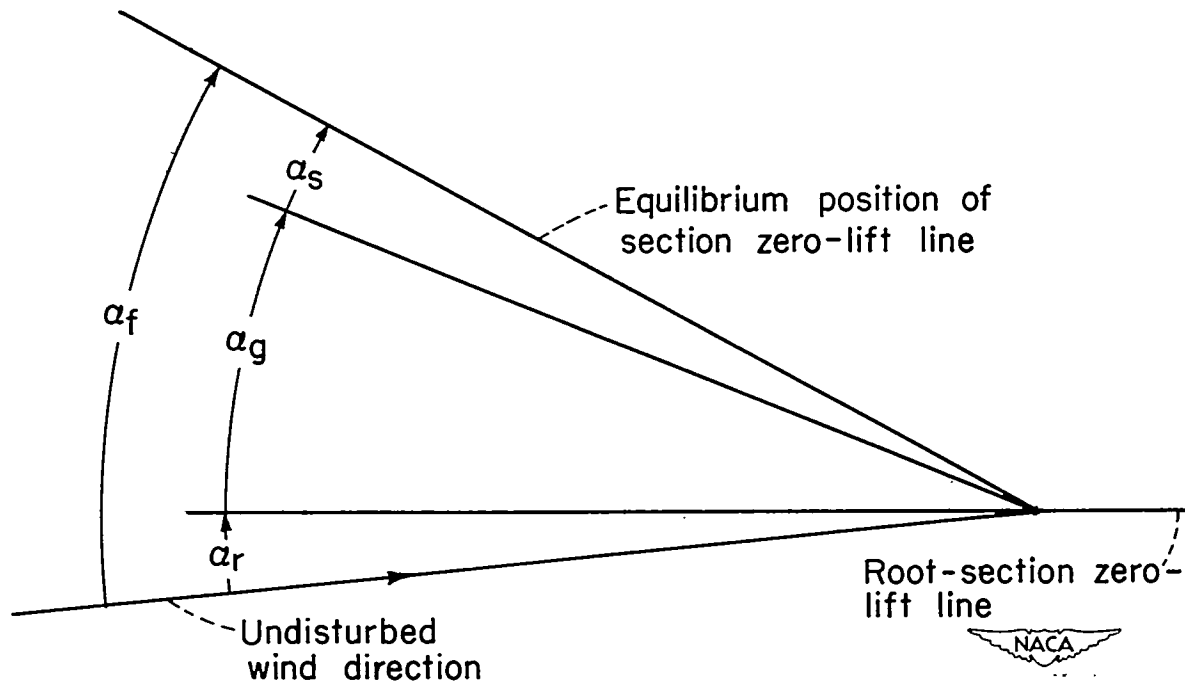
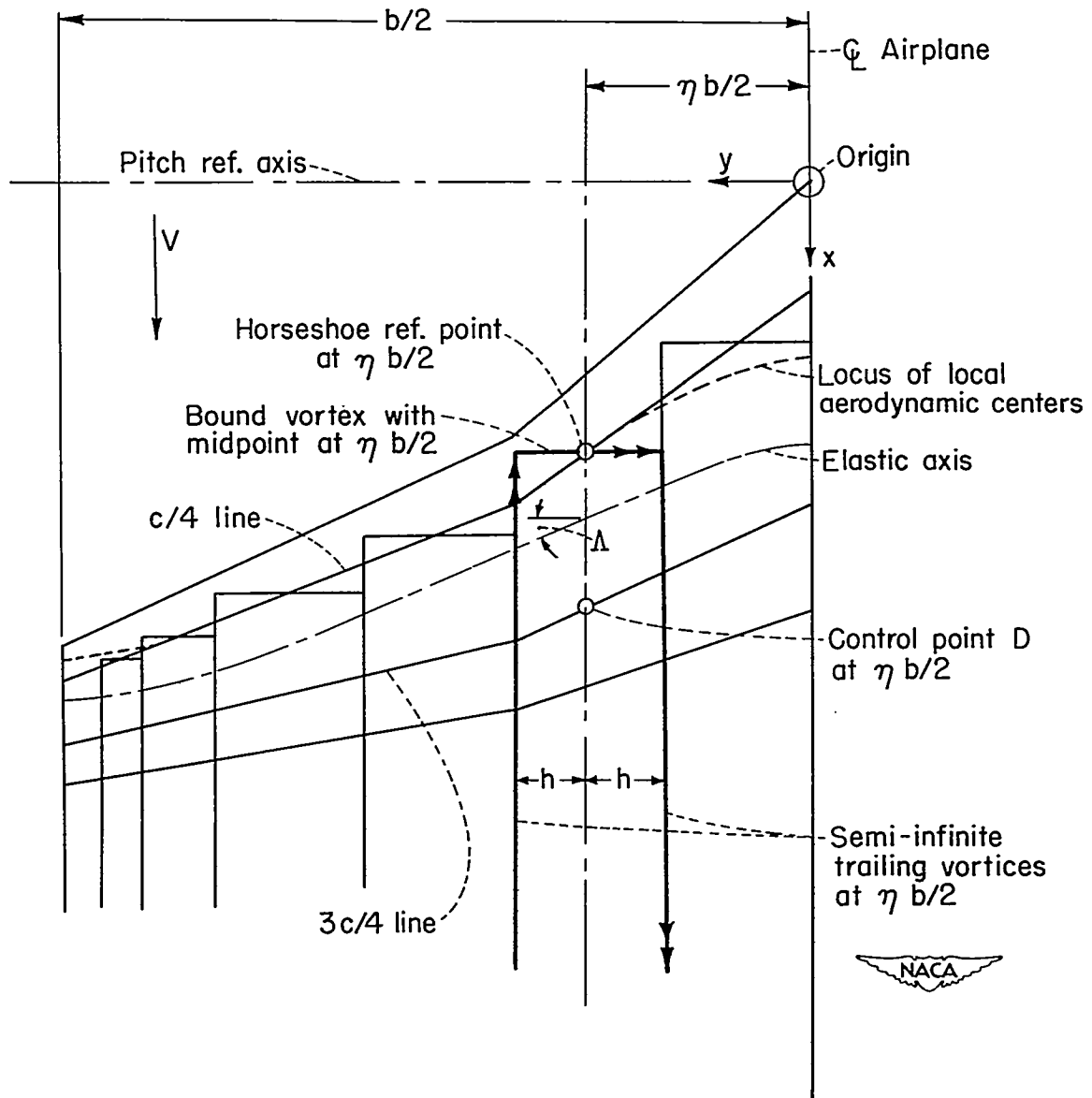Figure 1.- Angle-of-attack definitions and sign conventions.  Positive
angles shown.

Figure 2.- Typical vortex locations and location of pertinent points on an arbitrary wing plan form.
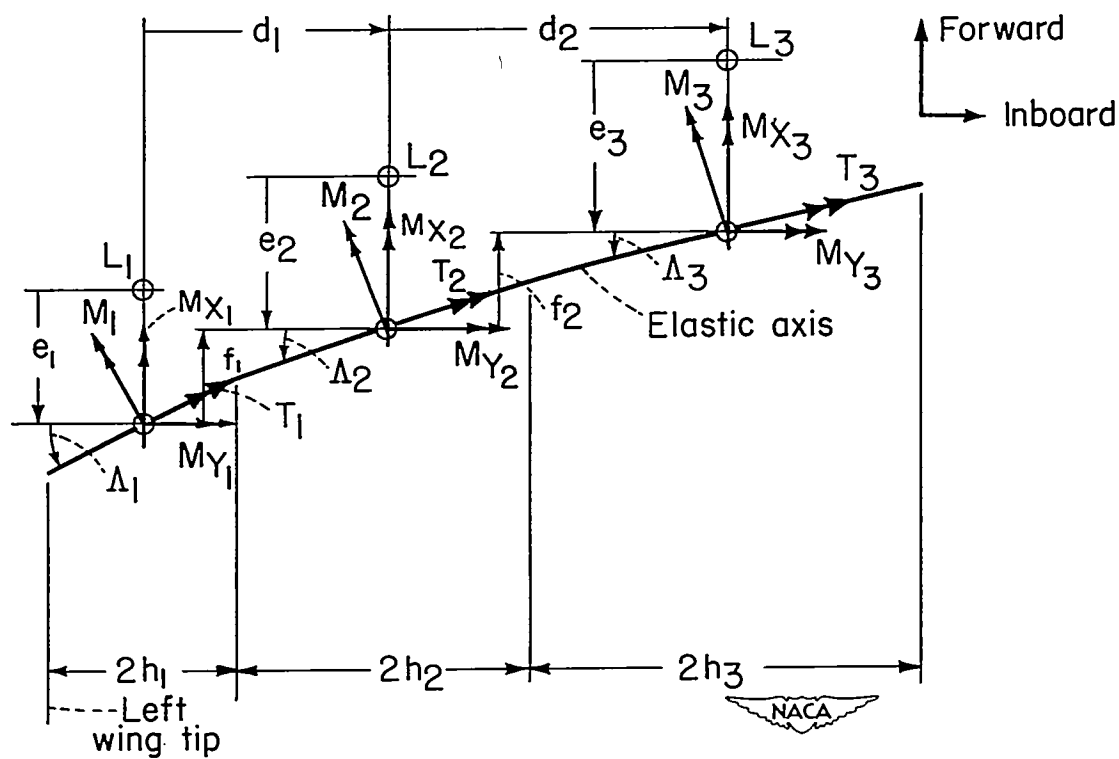
Figure 3.- Structural skeleton of outboard sections of left wing shown in plan view.
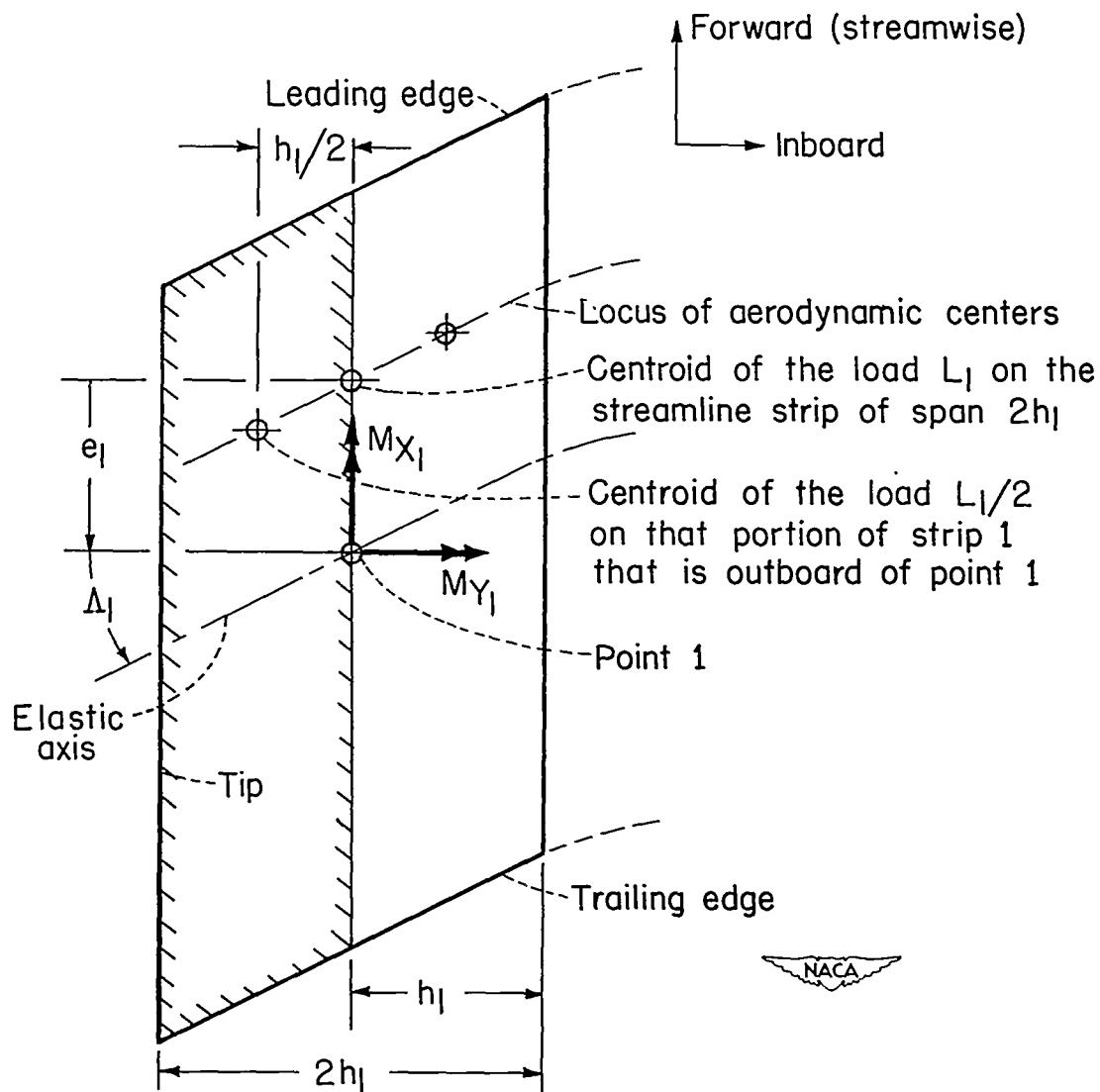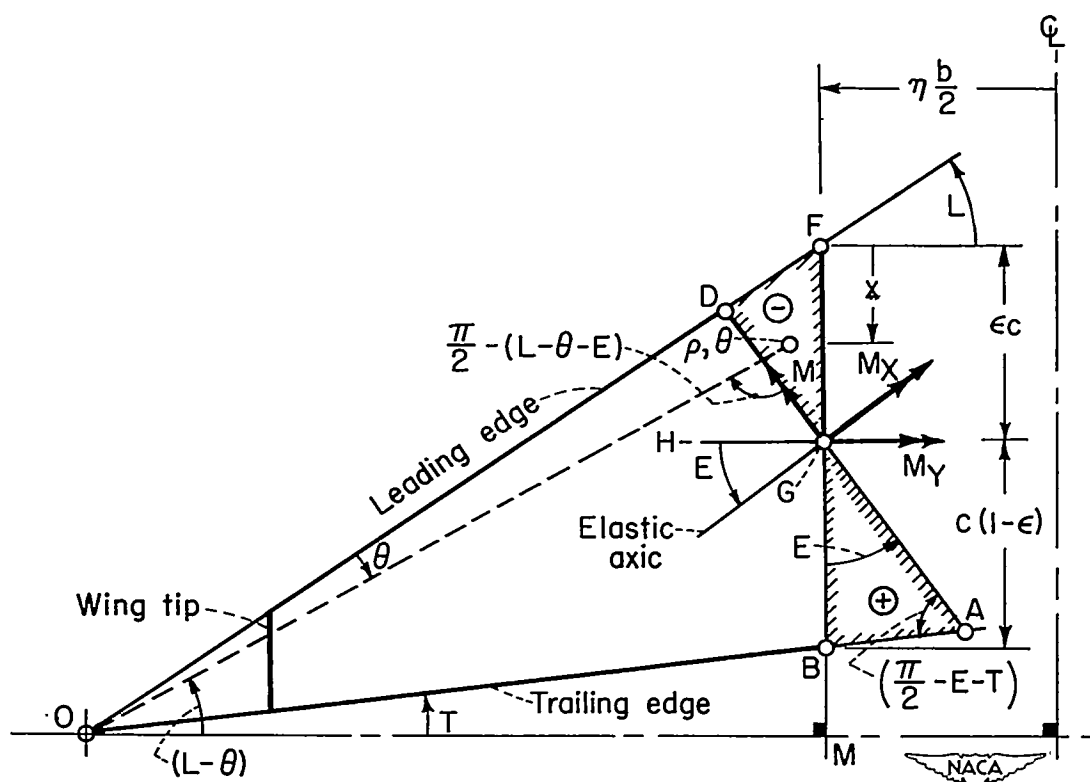
Figure 4.- Plan view of left wing tip section.

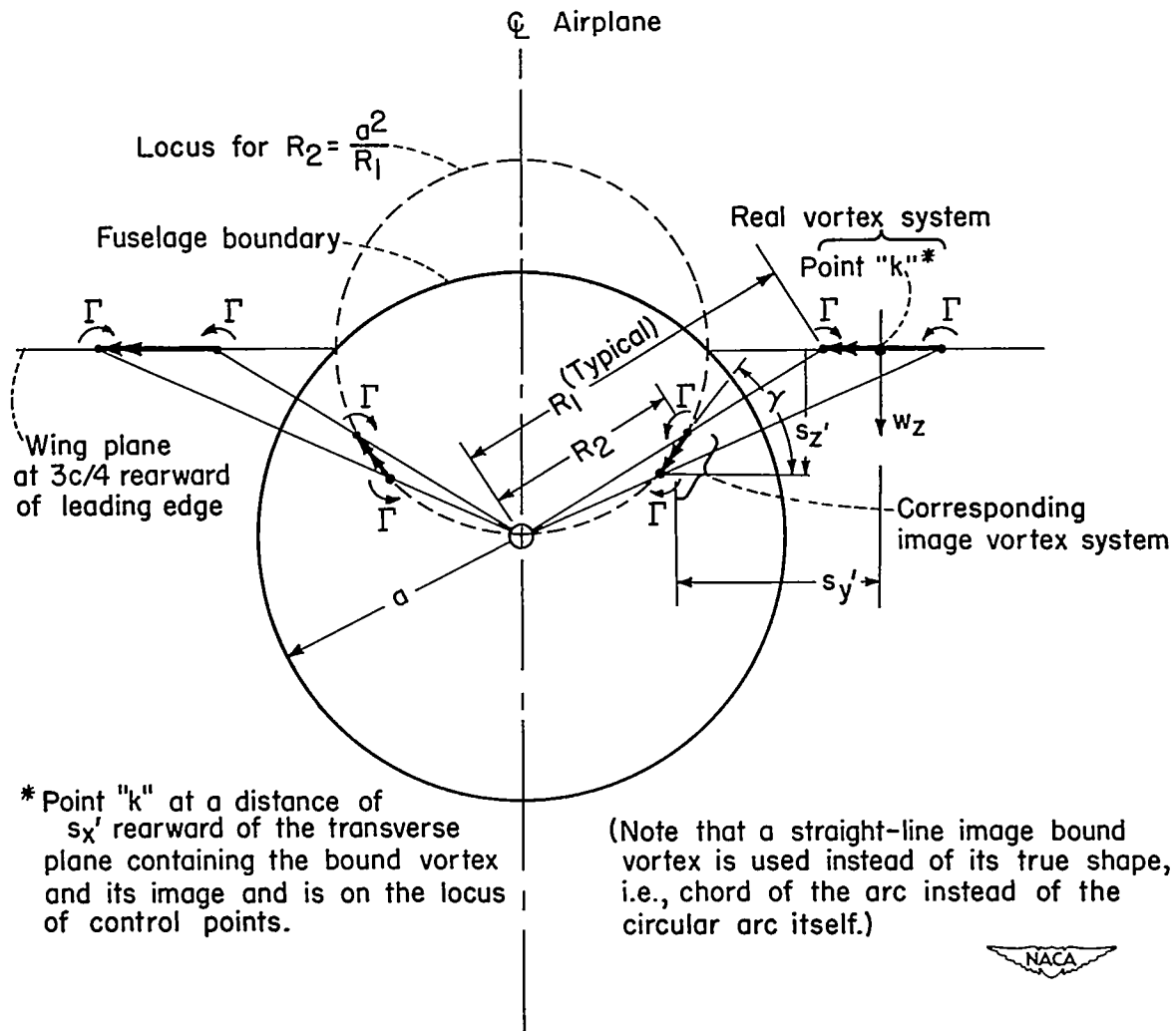Figure 5.- Polar representation of left wing used in development of the $\left[S_2{}'\right]$ matrix.

(a) Front view of typical vortex-image system (high-midwing configuration).

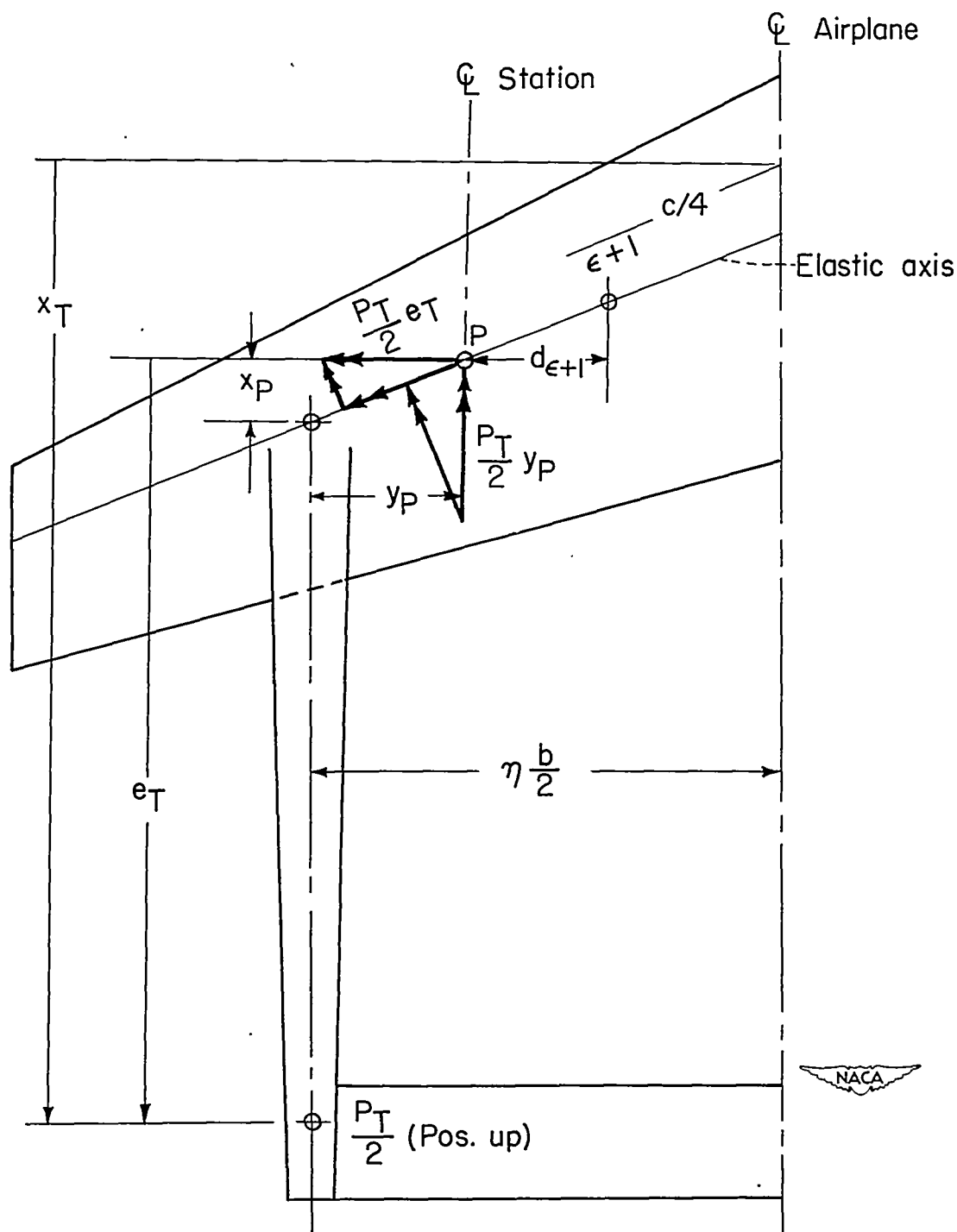Figure 6.- Diagram of vortex-image system for a wing-fuselage combination.

(b) Plan view of typical vortex-image system (midwing configuration).

Figure 6.- Concluded.

Figure 7.- Plot of overvelocity contours.
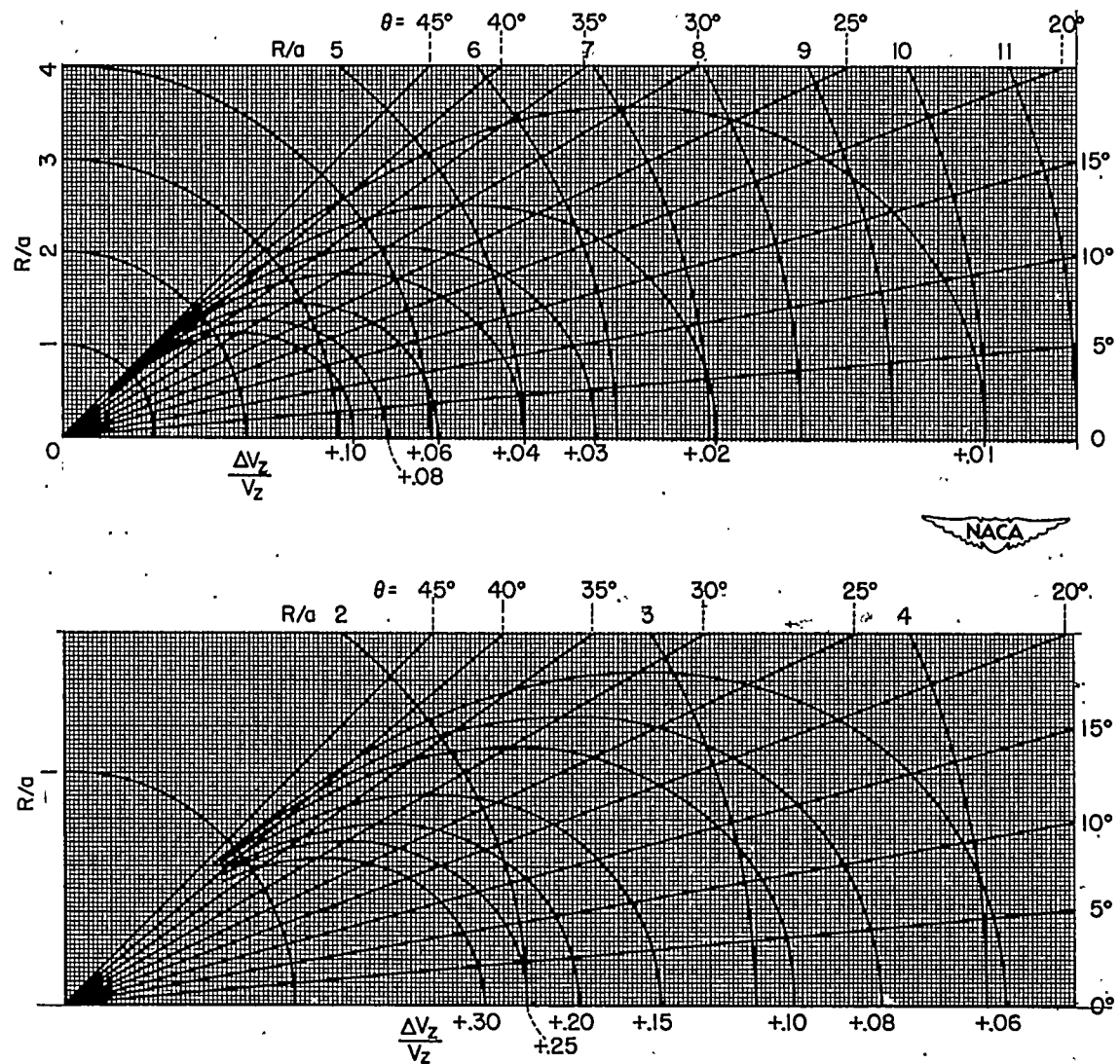
Figure 7.- Concluded.

Figure 8.- Diagram of a representative wing—tail-boom combination showing entry of tail load on to wing structure (d is distance between stations measured perpendicular to streamline).
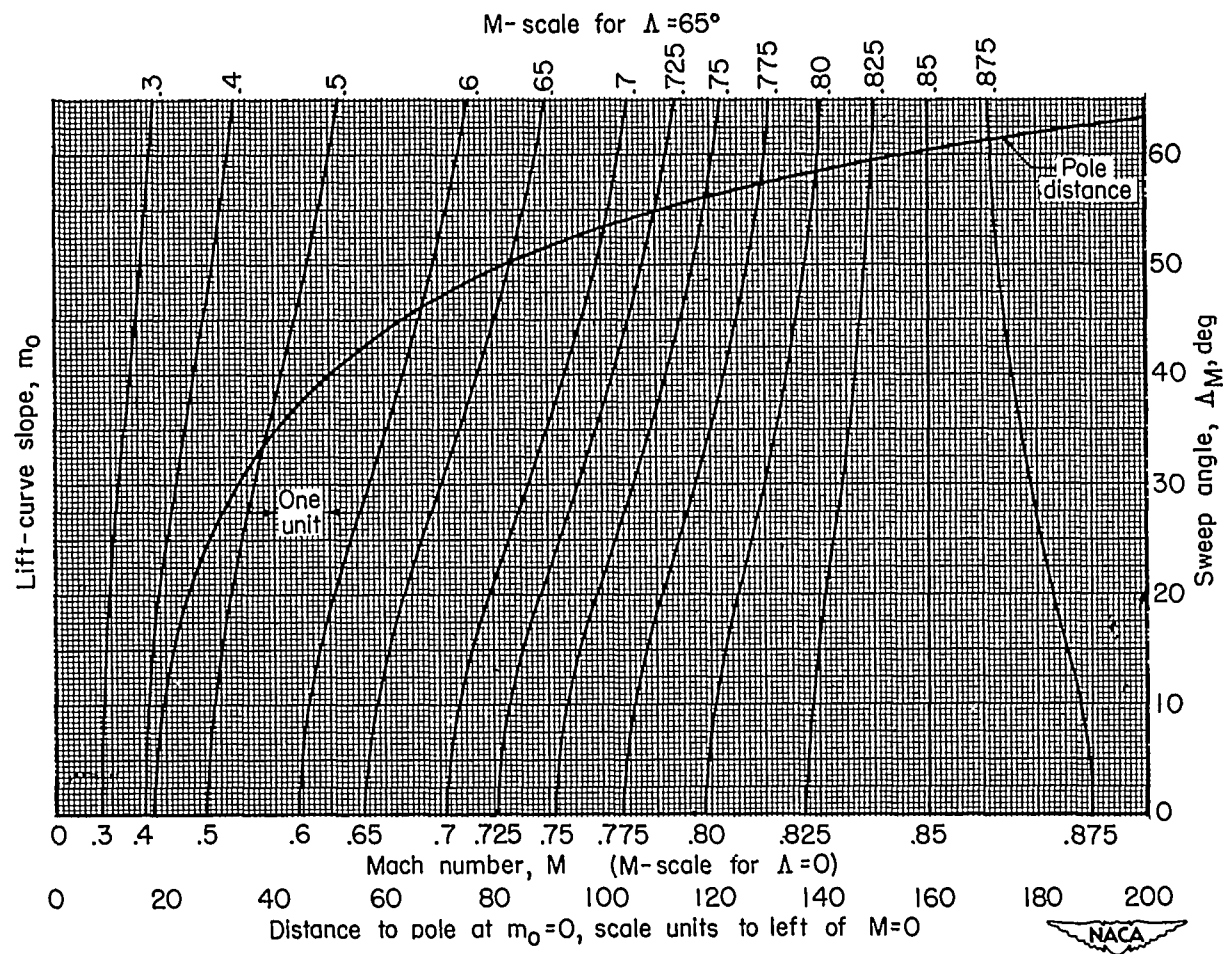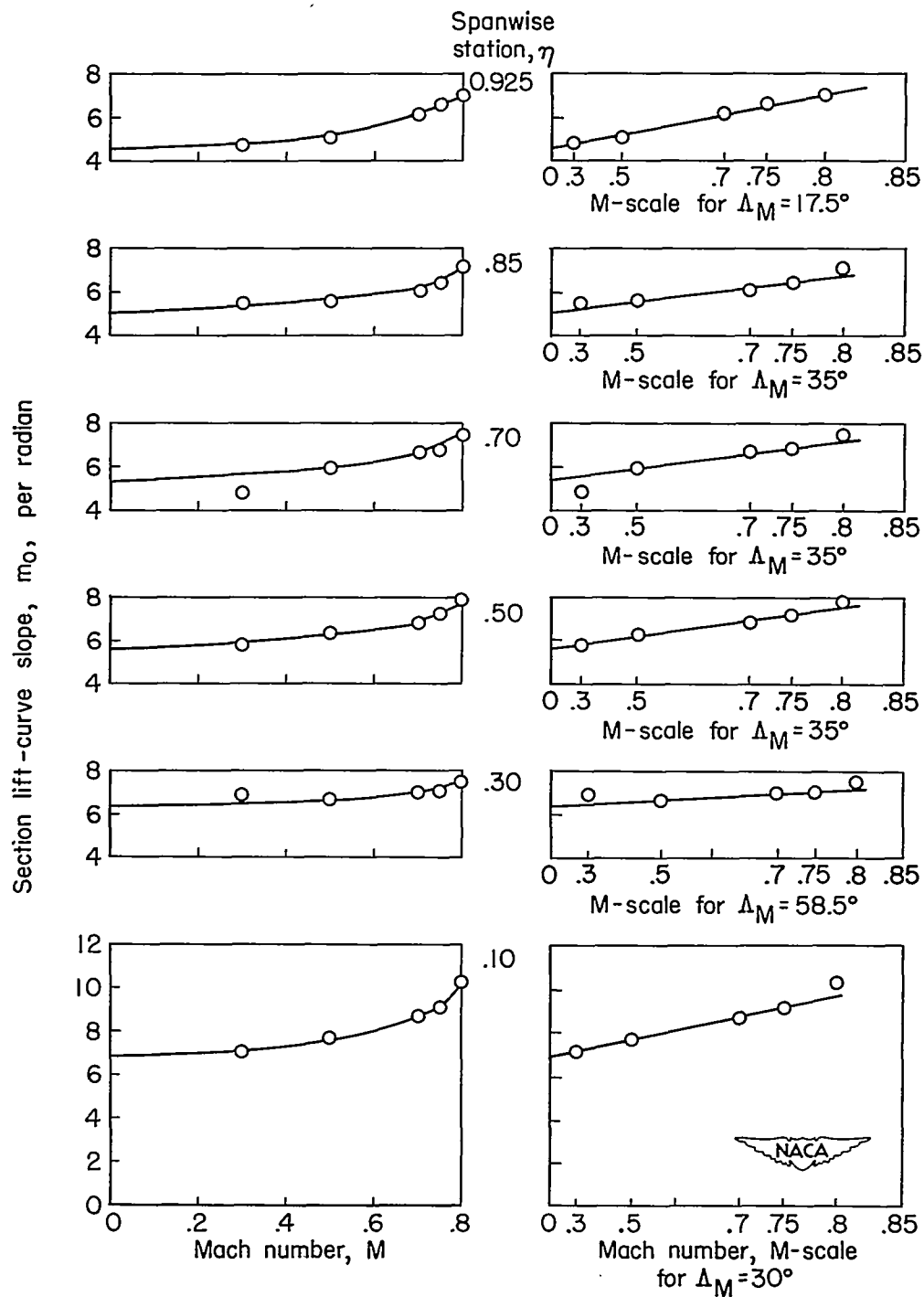
M-scale for $\Lambda = 65°$

Lift-curve slope, $m_0$

Sweep angle, $\Lambda_M$, deg

Pole distance

One unit

Mach number, M    (M-scale for $\Lambda = 0$)

Distance to pole at $m_0 = 0$, scale units to left of M=0

NACA

Figure 9.- Plotting form based on equation $m_0 = \dfrac{m}{\sqrt{1 - M^2\cos^2\Lambda_M}}$ for

graphical determination of effective section sweep angle $\Lambda_M$ for
a known variation of lift-curve slope with Mach number.

(a) Linear scale.                    (b) Expanded M-scale.

Figure 10.- Variation at several semispan stations of section lift-curve
   slope with Mach number for linear scale and expanded M-scale.  Wind-
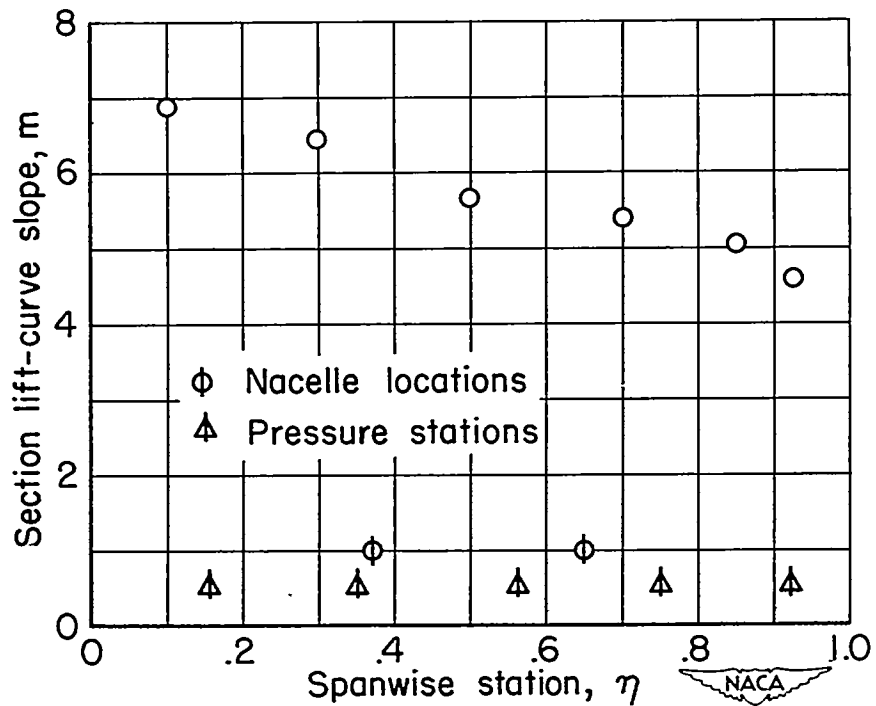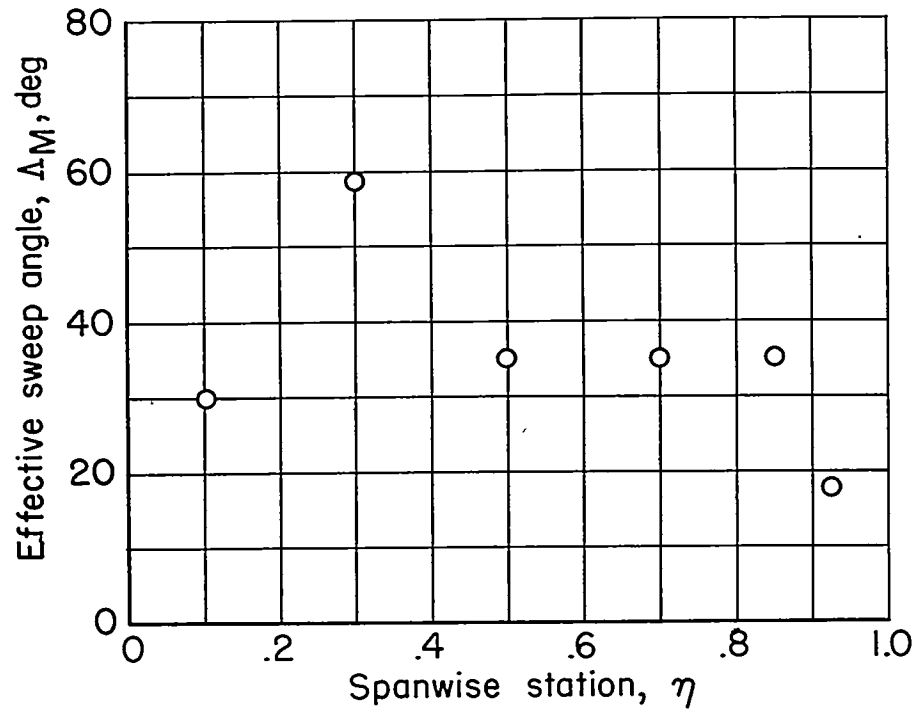   tunnel model of appendix G.

Figure 11.- Spanwise variation of effective sweep angle $\Lambda_M$ and section lift-curve slope $m$ for wind-tunnel model of appendix G.